PREVENTION OF DISUSE BONE LOSS BY USING IMPLANTABLE MICRO-ELECTRICAL STIMULATORS (IMES)

LAU YUEN CHI

Ph.D

The Hong Kong Polytechnic University

2015

The Hong Kong Polytechnic University

Department of Rehabilitation Sciences

Prevention of Disuse Bone Loss by Using Implantable Micro-Electrical Stimulators (IMES)

LAU YUEN CHI

A thesis submitted in partial fulfillment of the requirements for the Degree of Doctor of Philosophy

June 2014

CERTIFICATE OF ORIGINALITY

I hereby declare that this thesis is my own work and that, to the best of my knowledge and belief, it reproduces no material previously published or written, nor material that has been accepted for the award of any other degree or diploma, except where due acknowledgement as been made in the text.

_____

LAU YUEN CHI MMedSc, MPH

Abstract of thesis entitled "Prevention of disuse bone loss by using implantable micro-electrical stimulators" submitted by Lau Yuen Chi for the degree of Doctor of Philosophy at the Hong Kong Polytechnic University in May 2014

ABSTRACT

Osteoporosis is characterized by extensive decline in bone mass and deteriorated bone micro-architecture leading to increased risk of fracture. Primary osteoporosis refers to osteoporotic conditions associated with aging and decreased gonadal function while secondary osteoporosis is caused by other health problems. Disuse is one of the reasons inducing bone loss resulting in secondary osteoporosis and has been shown to be a regional phenomenon in the areas with tremendous decreases in weight bearing, like the lower limbs. Long term bed rest, spinal cord injuries (SCI), and other brain neurologic conditions leading to substantial reduction in ground force reaction and muscle contraction in the lower limbs as well as exposure to microgravity can lead to disuse osteoporosis. Disuse osteoporosis can be the result of an accelerated rate of bone resorption and slower bone formation, which are associated with the activities of osteoclasts and osteoblasts respectively. Although mechanical stimulation in the form of physical exercise has been reported to prevent bone loss effectively in both humans and animals, patients with physical disabilities and the elderly have difficulty performing exercises. Thus, a safe, easily applicable, and effective preventive treatment for prevention of disuse osteoporosis is needed.

The application of electrical stimulation on treating various physiological disorders has been widely reported. Former studies demonstrated that electrical stimulation could increase muscle strength and endurance, and reversed a certain level of osteoporosis in bones stressed by the stimulation in patients who had suffered from spinal cord injuries. However, previous findings on physiological effects of electrical stimulation on bone loss prevention were not consistent.

Calcitonin gene-related peptide (CGRP) is a neural peptide secreted by sensory neurons. Previous reports have suggested that CGRP might serve as a local regulator of bone cell function and probably affects bone metabolism via the nervous route as well as via an autocrine loop. Interestingly, CGRP secretion from the dorsal horn could be stimulated by electrical stimulation of a dorsal root. Hence, electrical stimulation of a sensory nerve at its dorsal root in order to trigger CGRP secretion would be a possible treatment for preventing bone loss. Thus, the aim of this study is to investigate the impact of electrical stimulation at dorsal root ganglia on disuse osteoporosis and the underlying mechanism.

Sixty male Sprague Dawley rats (male, 3-month-old, 400–420 g) were randomly allocated into six equal groups of 10 rats each. The animals were subjected to different treatments according to the following treatment groups: (1) cage control (CC); (2) hindlimb unloaded (HU); and, (3) hindlimb unloaded with electrical stimulation (ES), in which animals were implanted with the implantable micro-electrical stimulators (IMES) before the treatment period. In addition, the effects of treatments were evaluated at two different time points respectively at 2 weeks or 6

weeks. In the ES group, electrical stimuli (treatment parameters: 90μs, 150Hz, 61.3μA and 0.25V) with rectangular waveform and constant amplitude were generated by an implantable micro-electrical stimulator (IMES) and applied directly to the right dorsal root ganglion (DRG). After the treatment period, DRG tissues and tibias were harvested. The expression of CGRP at DRG as well as proximal tibial metaphysis was evaluated by immunohistochemistry whereas the activities of osteoclasts and osteoblasts in proximal tibial metaphysis were indicated by Tartrate-resistant acid phosphatase (TRAP) and alkaline phosphatase (ALP) staining respectively. The change in bone density was estimated by pre- and post-treatment peripheral quantitative computed tomography (pQCT) measurement whereas the bone micro-architecture was evaluated by micro-computed tomography (μCT). In addition, the biomechanical properties of tibias were measured by 3-point bending.

Immunohistochemistry results showed that reduced expression of CGRP+ neurons in DRG and proximal tibial metaphysis was observed in HU group whereas direct electrical stimulation at DRG via IMES was able to enhance the expression of CGRP+ neurons in DRG and this enhancement was expected to be associated with the increased expression of CGRP+ neurons at proximal metaphysis of unloaded tibias. The results of TRAP and ALP staining suggested that enhanced osteoclastic activities and suppressed osteoblastic activities would be induced upon unloading since significantly higher density of TRAP+ cells but a lower proportion of ALP active area were observed in the HU group compared to the CC group for both 2-week and 6-week samples. However, no difference in TRAP and ALP was found between CC and ES groups

suggesting that suppressed osteoclastic activity and enhanced osteoblastic activity were induced by the electrical stimulation treatment. Further, significant decline in bone mineral density (BMD) and bone mineral content (BMC) as well as deteriorated bone micro-structure were observed in proximal metaphysis of unloaded tibias in HU group as compared to CC after both 2-week and 6-week treatment. However, no significant difference in BMD and BMC as well as bone micro-structural parameters existed between ES and CC at week 2. In addition, after 6 weeks of treatment, no significant difference in BMD and BMC existed between ES and CC as well. However, significant deteriorated bone micro-structure was observed in ES compared to CC after 6 weeks, suggested that electrical stimulation at DRG would reduce decline in bone density by altering the activities of osteoclasts and osteoblasts but the micro-architecture of trabecular bone was possibly regulated by alternative mechanism such as hormonal control. In diaphysis, no significant difference in BMD and BMC as well as micro-structural parameters was found in diaphysis among all groups at week 2. At week 6, no difference in micro-structural parameters in diaphysis was observed between CC and HU but total volume and bone volume of ES were significantly lower than those of CC. The results of pQCT and μCT suggested that electrical stimulation would effectively reduce decline in BMD and BMC as well as preserved bone micro-architecture. Taking the significantly lower averaged body weight of ES animals at week 6 into consideration, the results of μCT would likely be influenced by other physiological or psychological factors. Furthermore, the results suggested that the trabecular compartment was more sensitive to the changes in mechanical loading and electrical stimulation treatment.

Based on the results of the current study, direct electrical stimulation at DRG by an implantable device preserves bone mineral density and bone micro-architecture in unloaded tibia by enhancing expression of CGRP+ neurons in DRG and proximal metaphysis. The enhancement in CGRP+ neurons, in turn, suppresses activity of osteoclasts but enhances activity of osteoblasts.

ACKNOWLEDGEMENTS

I would like to express my deepest gratitude to my chief supervisor, Dr Guo Xia, Associate Professor of the Department of Rehabilitation Sciences, The Hong Kong Polytechnic University, for her continuous and patient guidance, supervision, invaluable comments, encouragement and support which are indispensable to the success of my PhD study. I must also thank my co-supervisor, Prof Lu-ming Li, Professor of School of Aerospace, Tsinghua University, for his constructive advice and technical support for my research project.

I would like to give my wholehearted thank to my research team members Mr Kevin Po, Mr Omega Chan, Ms Kelly Gao and Dr Alex Cheung for their technical assistance, support and encouragement throughout the study period.

I must also thank my colleagues in the School of Aerospace, Tsinghua University, in particular, Ms Qian Xing and Dr Jiang Changqing, for their technical support especially on the development and design of the implantable micro-electrical stimulator used in this study.

Special acknowledgement must also be given to all the staff of the Centralized Animal Facilities, The Hong Kong Polytechnic University for providing space for conducting animal experiments and taking care of the animals used in this study.

Special thanks also go to my colleagues in the Department of Orthopaedics and Traumatology, The Chinese University of Hong Kong at the Prince of Wales Hospital for their technical support and professional advice on mechanical testing and micro-computed tomography.

I cordially thank the animals involved in the current study. Their sacrifice contributed to our understanding of the treatment potential of electrical stimulation at dorsal root ganglion on preventing disuse osteoporosis which will undoubtedly contribute to medical science advancement.

Last but not least, I would like to give my warm and deepest appreciation thanks to my family, friends and, in particular, my beloved fiancé Vanilla for all their love, endless encouragement, support and patience to me.

Lau Yuen Chi Roy

TABLE OF CONTENTS

LIST OF FIGURES

LIST OF TABLES

LIST OF ABBREVIATIONS

Calcitonin gene-related peptide (CGRP)

Cyclic adenosine monophosphate (cAMP)

Implantable micro-electrical stimulator (IMES)

Dorsal root ganglia (DRG)

Fibroblast growth factors (FGFs)

Insulin-like growth factors (IGFs)

Transforming growth factor-beta (TGF-β)

Bone morphogenetic proteins (BMPs)

Tertrate-resistant acid phosphatase (TRAP)

Bone mineral density (BMD)

Spinal cord injury (SCI)

Receptor activator of nuclear factor kappaB ligand (RANKL)

Tumor necrosis factor (TNF)

Osteoprotegerin (OPG)

Parathyroid hormone (PTH)

Low-intensity pulsed laser (LIPL)

Low intensity pulsed ultrasound (LIPUS)

Cage control (CC)

Hindlimb unloaded (HU)

Electrical stimulation treatment (ES)

Poly-para-xylylen (parylene C)

Deep brain stimulation (DBS)

Ethylene tetrafluoroethylene (ETFT)

Implantable pulse generator (IPG)

Sprague-Dawley rat (SD rat)

Phosphate-buffered saline (PBS)

Region of interest (ROI)

Ethylenediaminetetraacetic acid (EDTA)

Optimal Cutting Temperature (OCT)

Haematoxylin and Eosin (H&E)

4', 6-diamidino-2-phenylindole (DAPI)

Alkaline Phosphatase (ALP)

Peripheral Quantitative Computed Tomography (pQCT)

Bone mineral content (BMC)

Micro-computed Tomography (μCT)

Volume of interest (VOI)

Bone volume fraction (BV/TV)

Connectivity density (Conn.D)

Structural model index (SMI)

Trabecular number (Tb.N)

Trabecular thickness (Tb.Th)

Trabecular separation (Tb.Sp)

Total volume (TV)

Bone volume (BV)

Analysis of variance (ANOVA)

Statistical Package for the Social Sciences (SPSS)

Fisher's Least Significant Difference (LSD)

Standard deviation (SD)

Three-dimensional (3D)

Real-time polymerase chain reaction (real-time PCR)

Vasoactive intestinal peptide (VIP)

CHAPTER 1. INTRODUCTION

It has been generally accepted that mechanical force is one of the main regulators in bone modeling, remodeling, and repair. However, the actual mechanism by which mechanical stimulation is converted to intracellular signal(s) remains unexplained. Most biomechanical researches have concentrated on the effect of mechanical stimulation on bone architecture and strength since the concept reported by Roux (1). In recent years, mechanobiology has become an important research area in which various research include topics such as: how external force and muscle contraction are transferred to the skeletal tissues; how the bone cells sense the mechanical stimulation; and, how the signals are translated into the cascade of biochemical reactions to induce cell differentiation and/or proliferation, and consequent bone anabolic effect (2). On the other hand, there have been numerous investigations on how sensory neurons' activities contribute to the mechanobiological process. For instance, it has been suggested that the sensory nerves in bone can perceive mechanical strain or stress and transfer them afferently to the central neuron where calcitonin gene-related peptide (CGRP) is produced. In turn, CGRP cells readjust their secretions of CGRP and thus participate in osteogenesis and bone remodeling (3-7).

CGRP is a sensory neuropeptide which shares the same gene complex encoding with calcitonin. Calcitonin is produced when the gene expressed in C cells in the thyroid while the CGRP is produced when the same gene expressed in sensory neurons located in the dorsal root ganglion, and is transported peripherally and stored in large electron-dense storage vesicles,

accumulation of which constitutes varicosal enlargements of the sensory axon (8). Calcitonin is a circulating hormone involved in skeletal maintenance and has also been commonly used for treatment of osteoporosis and osteoporotic fractures in orthopaedic clinics (9). However, the physiological function of CGRP in bone metabolism remains for further investigation. The release of CGRP from the nerve terminal was firstly demonstrated by Zaidi et al. (8), since then much interest have been devoted to efferent effects of the CGRP-containing fibers. One very attractive research area is the modulatory effect of CGRP-containing fiber on bone metabolism. Numerous *in vitro* studies have suggested that CGRP modulate activities of bone cells (10, 11), including both osteoblasts and osteoclasts. CGRP has been shown to cause a 30 to 500 fold increase of osteoblastic cyclic adenosine monophosphate (cAMP) via acting on their specific CGRP receptors and thus stimulate osteogenesis (10). CGRP also acts directly on osteoclasts and inhibits bone resorption (11). These findings implicate modulatory roles of osseous CGRP-containing fibers and their specific function, i.e. osseoperception in bone metabolism.

Innervation of bone was first reported in 1945, but has only been studied in detail since the 1980s when immunohistochemical techniques became available. CGRP is a sensory neuropeptide found in two unmyelinated (C type) and small myelinated (A-delta type) primary sensory neurons which perceive pain and mechanical strain or stress (12, 13).

Evidences of involvement of CGRP containing fibers in bone formation are from fracture healing studies. Innervation of fracture callus was observed in rat tibia at 3 days post-fracture, and number of nerve fibers increased from day 14 to 21 (14). Madsen et al. observed the

effects of femoral and sciatic nerve resection on fracture healing and innervation of the fracture callus. At week 5 post-fracture, in the nerve resection group CGRP containing nerve fibers in the fracture callus were less and the stiffness of the callus was significantly lower (15). In animal model, fibular fractures failed to unite after removal of mechanorecptors by periosteal stripping (16). In human samples with delayed union or non-union, of diaphyseal fractures, the most remarkable finding was the insufficiency or lack of peripheral innervations (17). Taken together, these findings imply that the sensory innervation is an important regulator in normal bone turnover and fracture healing.

The premise of mechanobiology is that both modeling and remodeling are regulated by signals to cells generated by mechanical loading. The relevant research questions include how external and muscle loads are transferred to the tissues, how the cells sense these forces, and how the signals are translated into the cascade of biochemical reactions to produce cell expression or induce differentiation. CGRP containing neurons can be a pathway converting mechanical stimuli generated from external loading to a chemical stimuli to target cells based on their anatomy and physiology with following processes: (1) CGRP fibers sense the mechanical stimuli and transfer the signal afferently to the cell bodies; (2) Cell bodies produce CGRP and then deliver them efferently to the target cells those possessing CGRP receptors; (3) CGRP affect cellular function and thus regulate bone modeling or remodeling through the CGRP receptors. A recent study using hindlimb unloading rat model by Guo and co-workers

demonstrated that decreased expression of CGRP and bone loss in rat tibia after 4 weeks unloading (7).

It has been demonstrated by previous studies that there is increased release of CGRP from dorsal horn after electrical stimulation of dorsal root (18, 19). In addition, applications of implantable micro-electrical stimulator (IMES) successfully help patients to increase their activities of daily living and participate in social life again (20, 21). The latest developments in rehabilitation sciences, biomedical engineering, nanotechnologies, and materials sciences have paved the way to new scenarios towards highly complex systems to interface the human nervous system. Different sciences start to interact and discuss the synergies when methods and paradigms from biology, computer sciences and engineering, neurosciences, psychology will be combined (20-22).

The most common bone metabolic disorder is osteoporosis and disuse bone loss is one of the most common causes of osteoporosis. While regular loading or mechanical stimulation is essential to maintain bone mass, significant bone loss can occur when there is disuse, including unloading, of bone. Likewise, an unloading of skeleton during space flight also results in severe bone loss in astronauts.

Although mechanical loading to bone through exercise is the best intervention to increase or maintain bone mass, there is lack of effective intervention for prevention of disuse bone loss in people who are wheelchair-bound, in long-term bed rest, or living in a microgravity

environment. Thus, an effective and easily applicable treatment for prevention of disuse osteoporosis is needed for these people. Thus, the overall objective of this project is to test the hypothesis that electrical stimulation directly to the cell bodies of sensory neurons at dorsal root ganglia (DRG) may prevent disuse bone loss by a mechanism of increased secretion of CGRP similar to that induced by external impact loading. The ultimate goal of this study is to provide insight on development of treatment for reducing or preferably preventing osteoporotic symptoms for people exposed to disuse conditions.

CHAPTER 2. LITERATURE REVIEW

2.1 The composition and organization of bone

Bone is a composite material consisting of both organic and inorganic phases. Inorganic matter constitutes about 60% of the total weight of the tissue, 8–10% is water, and the remaining is organic matter (23). The inorganic phase is mainly made up of crystalline salts, mainly calcium and phosphate, in the form of calcium hydroxyapatite ($Ca_{10}(PO_4)_6[OH]_2$). The organic phase is composed predominately, more than 95% by weight, of type I collagen fibers, the remainder consisting of non-collagen proteins of bone (such as osteocalcin, osteonectin, and osteopontin), plasma proteins, lipids, and glycosaminoglycans. Bone cells constitute about 2% of organic phase (24).

2.1.1 The organic phase of bone

The organic phase of bone plays a wide spectrum of physiological roles influencing the bone structure as well as the mechanical and biochemical properties of the tissue. Growth factors, cytokines, and extracellular matrix proteins contribute only a small proportion of the total volume of bone but have important contributions to its biological function.

2.1.1.1 Type I collagen

Type I collagen is the major structural component of the bone matrix and its solubility is extremely low. The molecule of type I collagen consists of three polypeptide chains, each of them is composed of approximately 1000 amino acid residues (25). The polypeptide chains

form a triple helix cross-linked by hydrogen bonding between hydroxyproline and other charged residues. This structure produces a rigid linear molecule with length about 300 nm (figure 2.1). Each collagen molecule is aligned with the next in a parallel fashion and in a quarter-staggered array to produce a collagen fibril. The collagen fibrils, in turn, are grouped to form collagen fiber. Between the ends of the molecules, gaps known as hole zones and pores exist between the sides of parallel molecules. Non-collagenous proteins or mineral deposits are found in these spaces and mineralization of the matrix is thought to be initiated in the hole zones (25).

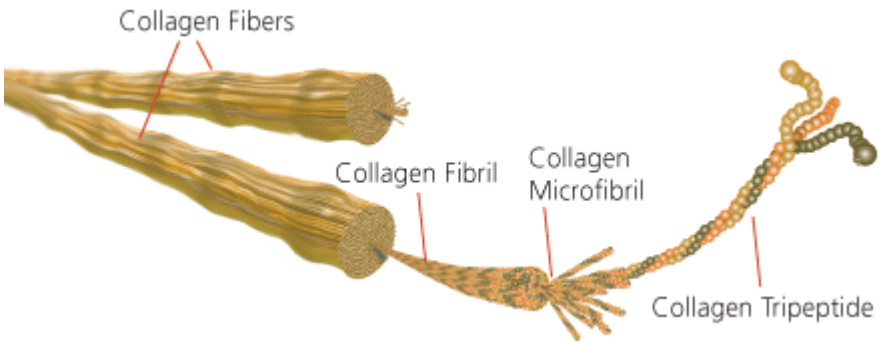

Figure 2.1 Collagen fibers and fibril structure (Adopted from Sigma-Aldrich, 2013)

2.1.1.2 Osteocalcin

Osteocalcin is a small glutamic acid-containing protein in which three glutamic acid residues are carboxylated as a result of a vitamin K-dependent post-translational modification. The carboxylation of these residues confers the calcium and mineral binding properties of this protein (25). Immunohistochemical studies demonstrated that osteocalcin was a mineralized

tissue-enriched bone-matrix protein (26). Because of its affinity for calcium, osteocalcin is believed to serve as a mediator of matrix mineralization. Evidence suggests that osteocalcin may regulate the activities of osteoblasts and osteoclast precursors (27-29). However, there is still no definitive function for this protein. On the other hand, a fraction of osteocalcin exists in circulation and serum osteocalcin has a short half-life and is rapidly cleared by the kidney (30). Serum osteocalcin has been demonstrated to be a valid marker of bone formation (31).

2.1.1.3 Osteonectin

Osteonectin is a glycoprotein isolated from bone matrix. The amino terminus of osteonectin is highly acidic and can take on an alpha helix conformation that results in up to 12 low-affinity calcium binding sites. The calcium binding sites and those present in the amino terminus convey the ability of osteocalcin to bind to hydroxyapatite (32-34). In skeletal tissue, osteonectin is found in osteoblasts, odontoblasts, and a small portion of chondrocytes (35). In general, osteonectin is accumulated in all mineralized tissues. However, the function of osteonectin in the various tissues is not well understood. *In vitro* studies have suggested that osteonectin played a role in regulating proliferation (36) and cell-matrix interactions (37). Previous opinions have stated that osteonectin is involved in a variety of critical functions throughout development and maturity (38) including bone matrix mineralization (25).

2.1.1.4 Osteopontin

Osteopontin is a bone matrix constituent which constitutes about 2% of bone matrix in rat bone (39), with protein backbone bearing various posttranslational modifications such as glycosylation with sialic acid and sulfation. Osteopontin is able to bind tightly to hydroxyapatite (40) and mediate cell attachment for many cell types *in vitro*, including osteoblastic and osteoclastic cells (41, 42). Osteopontin has been identified in many different cell types such as odontoblasts and chondrocytes (43). In the skeleton, osteopontin is found enriched at cement lines (44). Evaluation of the types of cells producing osteopontin suggests that, besides the role in cell-matrix interactions, it may play a role in ion transport.

2.1.1.5 Bone cells: Osteocytes

Osteocytes are the cells embedded in the mineralized matrix of bone. The number of osteocytes in normal adult human bone is about 10 times more than that of osteoblasts (45). The ultrastructure of osteocytes resembles osteoblasts in that osteocytes have prominent nucleoli and nuclei. In addition, abundant rough endoplasmic recticulum and well defined areas of Golgi apparatus, mitochondria, microtubules, and microfilaments are seen in osteocytes. However, with increasing mineralization engulfing the cell the organelles are less identifiable so that osteocytes are identified by the nucleus under a light microscope (figure 2.2).

Osteocytes are in contact with osteoblasts on the bone surface by means of cell processes consisting mostly of microfilaments. Osteoblasts and young osteocytes possess histochemically

demonstrable alkaline and neutral phosphatase activity on their cell membranes. However, mature osteocytes do not have membrane alkaline phosphatase. Osteocytes are predominantly associated with mechanosensory function in bone and potentially in calcium homeostasis (25).

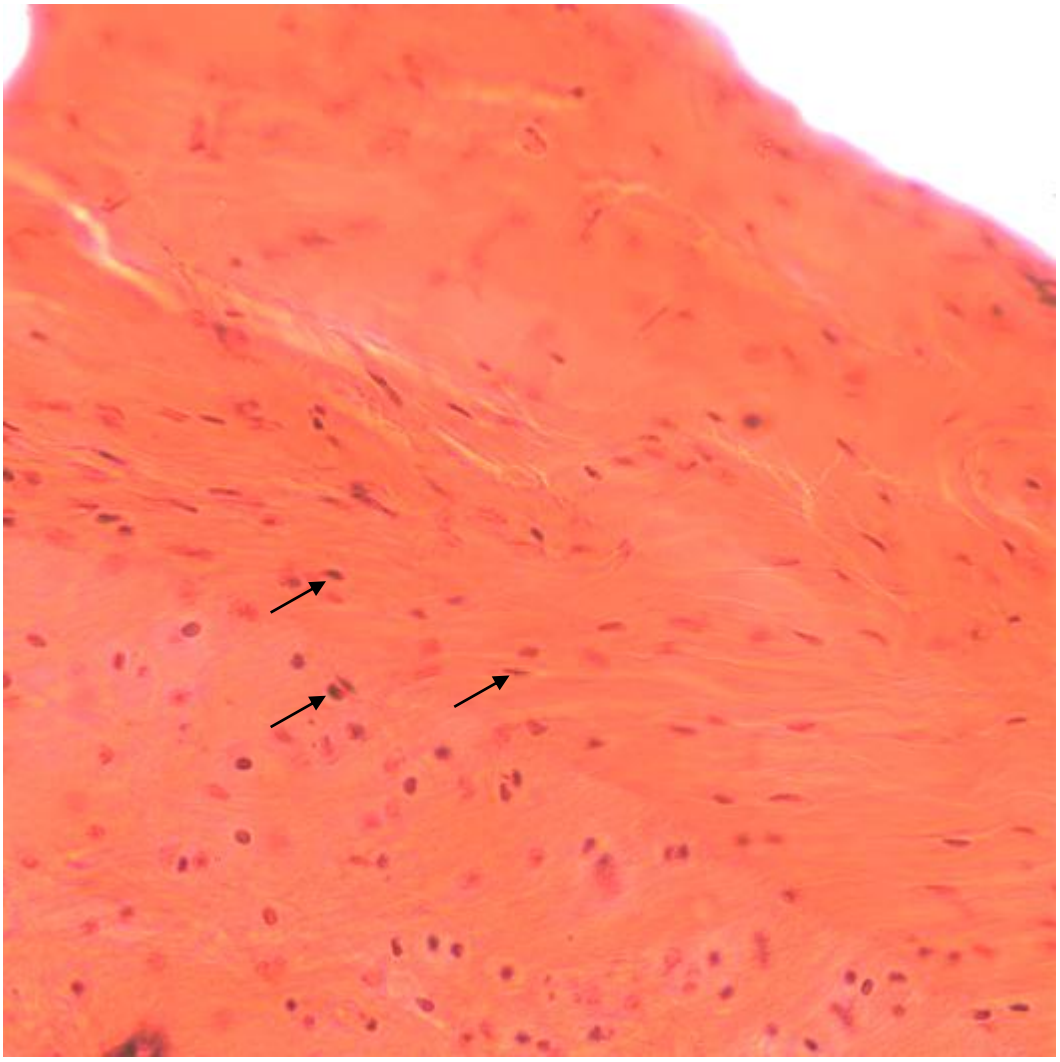

Figure 2.2 Osteocytes in mature cortical bone
Osteocytes (arrow) lie in lacunae and have densely stained nuclei and indistinct cytoplasm.

An osteocyte is the mature version of a osteoblast. However, instead of apoptosis, osteocytes reduce their production of matrix molecules and end up encapsulated in bone matrix. Under the microscope, osteoctyes are characterized by their long processes extending through the lacunocanalicular system of the bone. In lamellar bone, osteocytes lie in oval or flattened lacunae which are generally oriented in the direction of collagen fibers whereas osteocytes in immature bones are found in large round lacunae (figure 2.3). They are the most abundant cellular component of mammalian bone. Importantly, osteocytes form an interconnected network in bone allowing for intercellular communications between osteocytes as well as with surface-lining osteoblasts. Such interconnection between osteocytes allows for the transmission of mechanical and chemical signals across the network through direct transmission of mechanical forces either through the triggering of integrin force receptors, change in membrane conformation, chemical signals via gap junctions, or secreted factors that travel through the extracellular fluid of the lacunocanalicular system (46). This interconnected signaling facilitates adaptation of bone to external mechanical and chemical inputs regulating bone homeostasis.

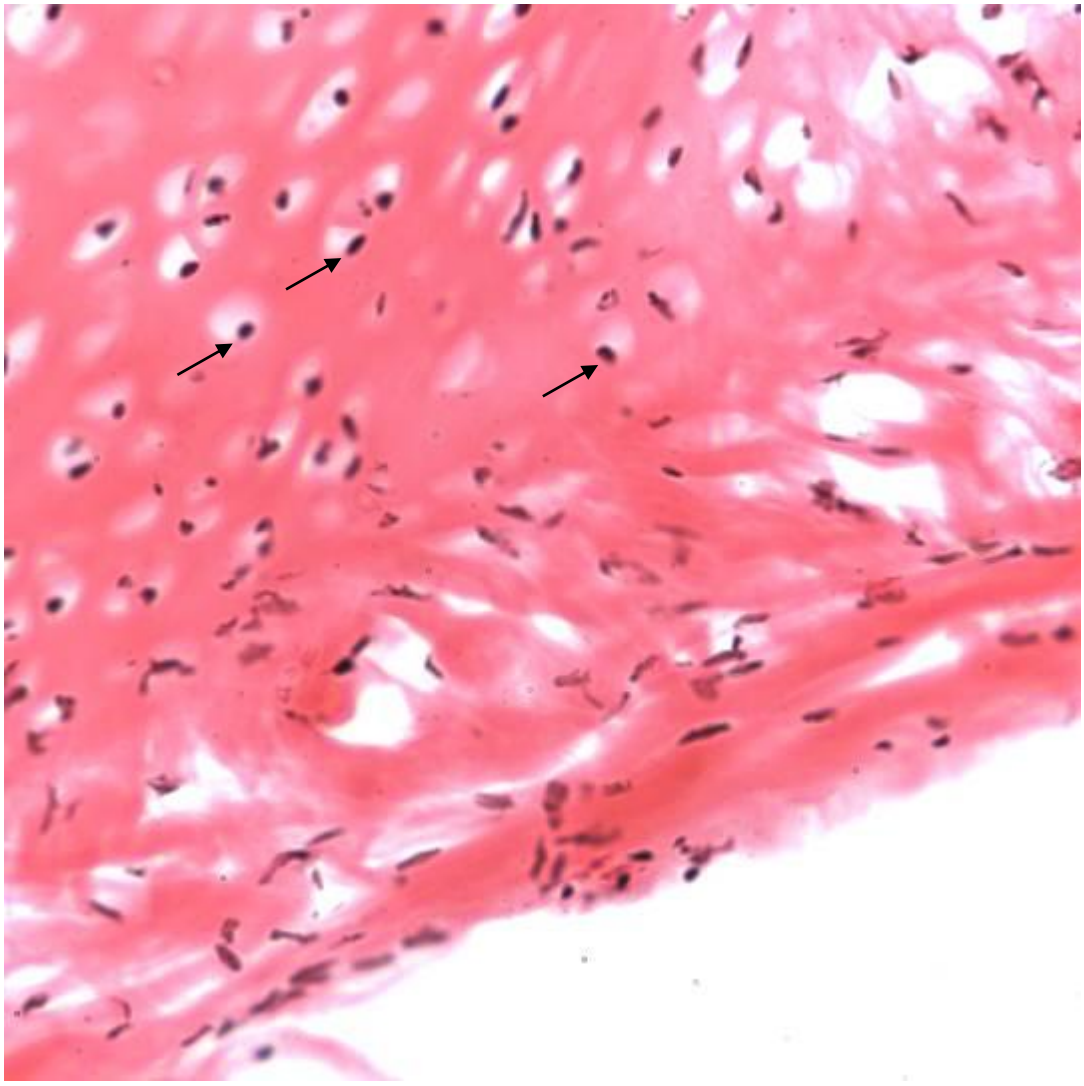

Figure 2.3 Osteocytes in immature bone lie in large round lacunae (arrow)

2.1.1.6 Bone cells: Osteoblasts

Bone formation is carried out by the mesenchymal lineage osteoblast. Osteoblasts synthesize protein matrix of bone made up of type I collagen and several non-collagenous proteins. The protein matrix, known as osteoid, forms a template for mineralization and production of mature bone. In addition to bone formation, osteoblasts are also involved in the initiation of

bone resorption by secreting factors that recruit and promote differentiation of monocytic lineage cells into mature osteoclasts as well as producing neutral proteases that degrade the osteoid and facilitate osteoclast-mediated remodeling (25).

Osteoblasts arise from multipotential bone marrow stromal cells of the colony-forming unit of fibroblast lineage. The specific lineage selection of individual mesenchymal stem cells involves a number of coordinated lineage selection steps and the actions of a number of transcription factors whose activities are modulated in response to the local micro-environment (25). Runx2 and Osterix are two transcription factors that have been demonstrated to be required for osteoblast formation and differentiation (47). Runx2 regulates the expression of various mature osteoblast-related genes such as osteocalcin, osteopontin, and type I collagen. Osterix is an important transcriptional factor for bone formation. A recent study by Chen et al. (48) demonstrated that deletion of osterix led to severe spine deformities including wedged vertebrae, spinal stenosis, and congenital scoliosis. The expression and activity of Runx2 and Osterix are regulated by the local micro-environment and the locally secreted morphogens to which the cells are exposed. Fibroblast growth factors (FGFs), insulin-like growth factors (IGFs), transforming growth factor-beta (TGF-β), bone morphogenetic proteins (BMPs), and Wnts have been demonstrated to play important roles in regulating embryonic osteoblast differentiation (25).

The most characteristic feature of osteoblasts under the light microscope is its ability to stain with basic stain (figure 2.4). Ostoblasts vary in size and shape depending on the degree of cell activity. For instance, inactive osteoblasts stain less intensively than active plump osteoblasts.

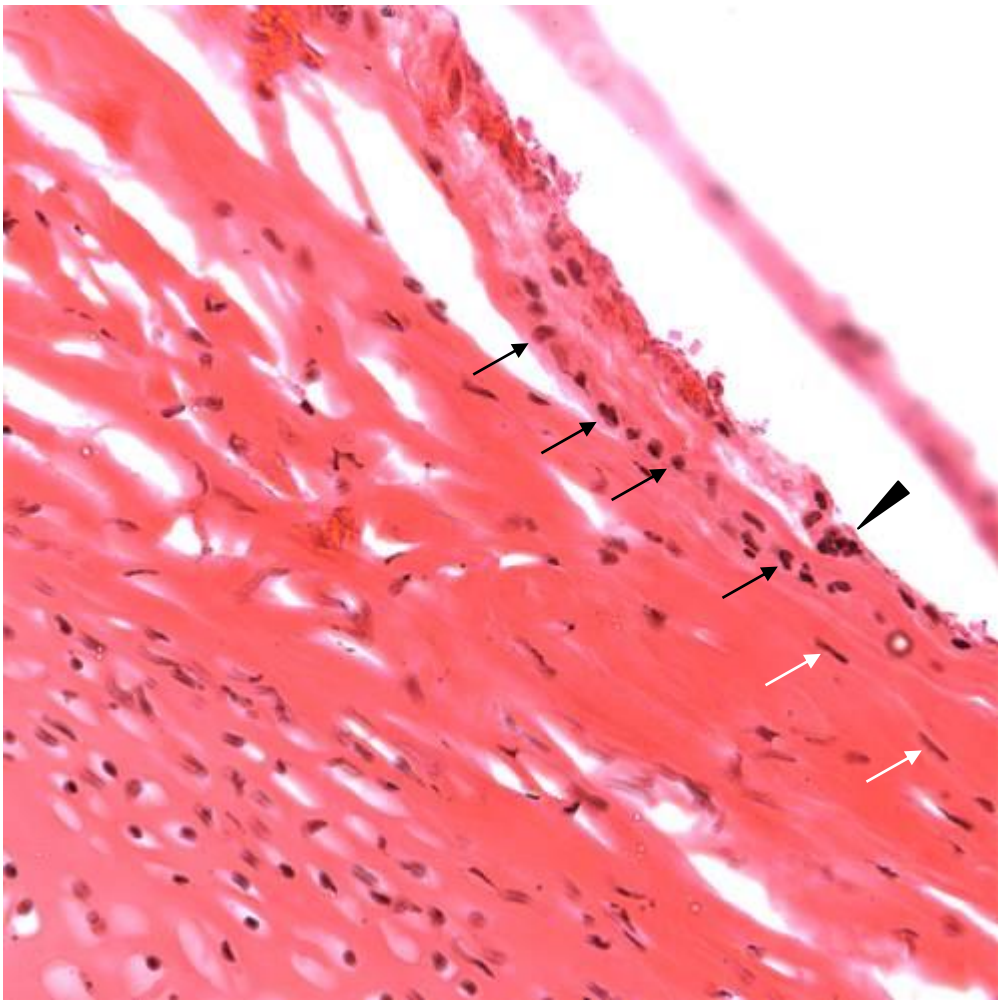

Figure 2.4 Osteoclasts, osteoblasts and bone lining cells
Bone lining cells (white arrow) and Osteoblasts (black arrow) laying down bone matrix along bone surface. Osteoclast (arrowhead) is characterized by its multinucleated structure and abundant cytoplasm.

Osteoblasts have a basophilic or amphophilic cytoplasm and a large hyperchromatic ovoid nucleus which is often polarized away from the bone surface. Osteoblasts contain a large amount of alkaline phosphatase and in normal bone do not show mitotic activity. Osteoblasts can exist as a layer of flattened and elongated cells with little cytoplasm and a thin central basophilic nucleus covering mature or resting bone, known as bone lining cells (figure 2.4) (49).

2.1.1.7 Bone cells: Osteoclasts

Osteoclasts are motile cells that can move randomly along the bone surface, then attach and resorb bone (50). Previous research has suggested that osteoclasts were derived from hematopoietic stem cell-derived granulocyte-macrophage colony forming unit and their differentiation and function were dependent on interactions between hematopoietic cells and bone marrow stromal cells including osteoblasts (51). Osteoprogenitor cells are recruited from the bone marrow and spleen and migrate to bone via the blood stream.

Anatomically, bone resorption is characterized by a clear zone at the site of attachment to bone, and a ruffled border. At the bone interface is the ruffled border allowing abundant cytoplasmic interface with bone (figure 2.4), which is a critical anatomical feature for bone resorption since it is the site of acidic milieu (52).

Resorption of bone mineral by osteoclasts requires the action of carbonic anhydrase II and vacuolar H^+-ATPase pump. Degradation of type I collagen matrix is likely to be dependent on cysteine proteinases and optimal at acidic pH. Thus, the acidic conditions would be needed to

dissolve mineral and facilitate collagen dissolution (53). At the ruffled border, vacuolar H^+-ATPase pump localizes on the basolateral membrane. The pumps provide energy for intracellular organelles. In addition, carbonic anhydrase drives the reaction which raises hydrogen ion concentration at the ruffled border. Carbonic acid is generated from carbon dioxide produced by mitochrondrial metabolism providing the source of hydrogen ions. In turn, the hydrogen ions are pumped through the ruffled border creating the proton-rich acidic milieu, which demineralizes the bone. Upon exposure to acidity, the hydroxyapatite crystals of bone dissolve and uncover the bone collagen for subsequent enzyme degradation.

Under the microscope, osteoclasts are large multinucleated cells commonly found in areas of active bone remodeling and/or cavities on the bone surface termed Howship's lacunae. Osteoclasts have round vesicular nuclei containing prominent nucleoli and the cytoplasm of osteoclasts is strongly acidophilic and contains tertrate-resistant acid phosphatase (TRAP).

2.1.2 The inorganic phase of bone

The inorganic phase of the skeleton is mainly composed of hydroxyapatite. However, other inorganic compounds exist among bone minerals. For instance, carbonate has existed in place of the phosphate groups in bone, which contributes to 4–6% of inorganic bone mineral and makes bone mineral similar to a carbonate apatite known as dahllite. Other documented substitutions are potassium, magnesium, strontium, and sodium in place of calcium ions, and chloride and fluoride in place of the hydroxyl groups (54). The minerals that exist have been proposed to reduce the crystallinity of the apatite (55) and, in turn, to alter certain properties

such as solubility, whereas solubility of bone mineral is critical for mineral homeostasis and bone adaptation (25).

2.1.3 The organization of bone

Long bones, such as femur and tibia, are the standard examples used in discussions of the macro-scale structure of bones. Long bones are divided into three parts: epiphysis, metaphysis, and diaphysis (figure 2.5). The epiphysis is found at either end of the bone and have developed from a center of ossification that is distinct from the rest of the long bone shaft. It is separated from the rest of the bone by a layer of growth cartilage known as physis. The metaphysis is the region between physis and diaphysis, which is the central portion of long bones. Structurally, the metaphysis is the region of transition from epiphysis to diaphysis (25).

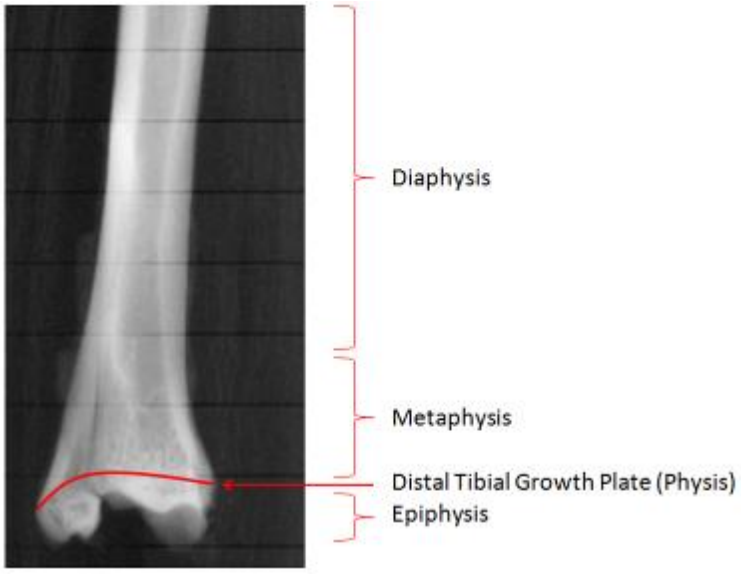

Figure 2.5 Micro-computed tomographic image of distal tibia

The membranes on both inner and outer surfaces of bone play important roles in bone modeling and remodeling as well as in fracture healing. The periosteum, which lines the outer surface of nearly the entire long bone, is composed of an outer fibrous layer and the cambium layer. Progenitors of osteoblasts and chondrocytes are concentrated in the cambium layer. Thus, periosteum contributes to appositional bone growth during bone development as well as expansion of bone diameters with aging. On the inner surfaces of long bones, the endosteum contains the bone surface cells including osteoblasts and bone lining cells.

Mineralized collagen fibrils are the building block of bone tissue. The fibrils can be arranged as a collection of randomly oriented fibrils known as woven bone (figure 2.6) or aligned in thin sheets called lamellar bone (figure 2.7). Woven bone is the first type of bone formed in the developing bone. It is also formed in a variety of pathological conditions where bone formation is rapid such as Paget's disease. The physical strength of woven bone is less strong compared to lamellar bone. The osteocytes in woven bone lie within large osteocytic lacunae (figure 2.3). Under the microscope, woven bone is characterized by the presence of bundles of randomly arranged short thick collagen fibers (49). On the other hand, lamellar bone is a mature form of bone tissue which results from remodeling of woven bone or pre-existing lamellar tissue. The structural organization of lamellar bone provides the highest density of collagen per unit volume of tissue. Thus, the majority of mature bone, including both cortical and trabecular bone, is composed of lamellar bone.

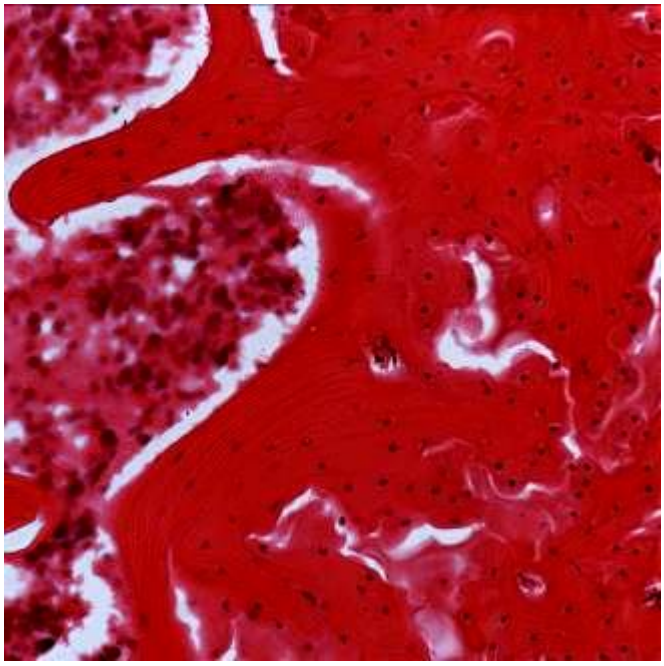

Figure 2.6 Woven bone

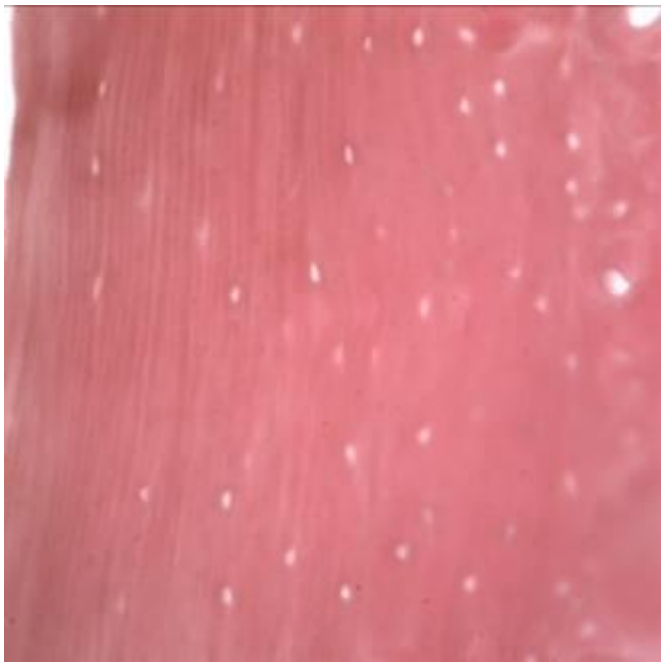

Figure 2.7 Lamellar bone

Macroscopically, there are two types of bone: trabecular (cancellous) bone and cortical (compact) bone. Trabecular bone is found mainly in the axial skeleton such as the skull and in the metaphyses as well as epiphyses of long bones. Trabecular bone is a highly porous structure with a network of rod- and plate-shaped trabeculae surrounding an interconnected space filled with bone marrow (figure 2.8).

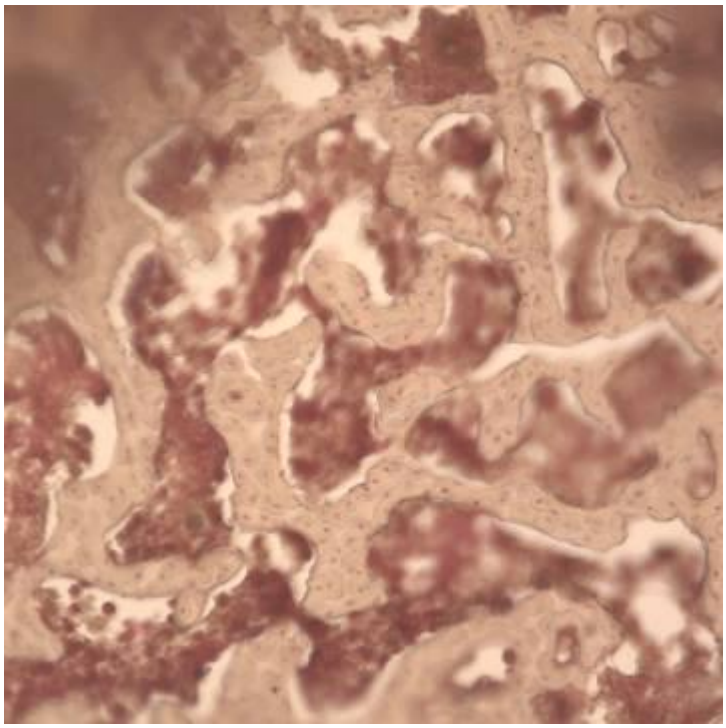

Figure 2.8 Trabecular bone

Trabecular bone is found in the medulla of the bone. In mature bones, trabecular bones are composed of lamellar bone with mineralized collagen fibers oriented in parallel along the long axis of the bone trabecula. Trabeculae are usually thin (thickness ranges between 50 to 300 μm), and do not contain Haversian systems, but are nourished by vessels within hematopoietic

or fatty marrow. Bone trabeculae are lined by a continuous layer of bone lining cells or osteoblasts and are separated by hematopoietic or fatty marrow. The cellular lining of bone comprises the endosteum covering the surface of bone trabeculae, the inner surface of the cortex, and Haversian canals (49).

Both the metaphyses and epiphyses of long bones have a thin shell of cortical bone surrounding the trabecular compartment whereas diaphyses are entirely cortical (figure 2.9). The distinction between cortical and trabecular bone is based mainly on porosity. The porosity of cortical bone ranges between 5 to 20% and is mainly due to the occurrence of Haversian and Volkmann's canals. However, the porosity of trabecular bone can range from 40% in the primary compressive group of the femoral neck to more than 95% in the elderly spine. On the other hand, porosity is the main determinant of stiffness and strength of trabecular bone (56, 57). Due to the presence of marrow space in Trabecular bone, trabecular spacing is a scale established to reflect the porosity of trabecular bone and typical spacing between trabeculae ranges from 100 to 500 μm (25). Further, 80 to 90% of cortical bone volume is mineralized but that of trabecular bone is only about 20%, with the resulting volume occupied by the marrow. Virtually all of the cortical bone interface with soft tissue and marrow is at the endosteal bone surface whereas the trabecular bone is literally bathed in a highly vascularized fatty and hematopoietic tissue. This structural organization suggests that cortical bone function is mainly mechanical and trabecular bone has significant metabolic functions (53).

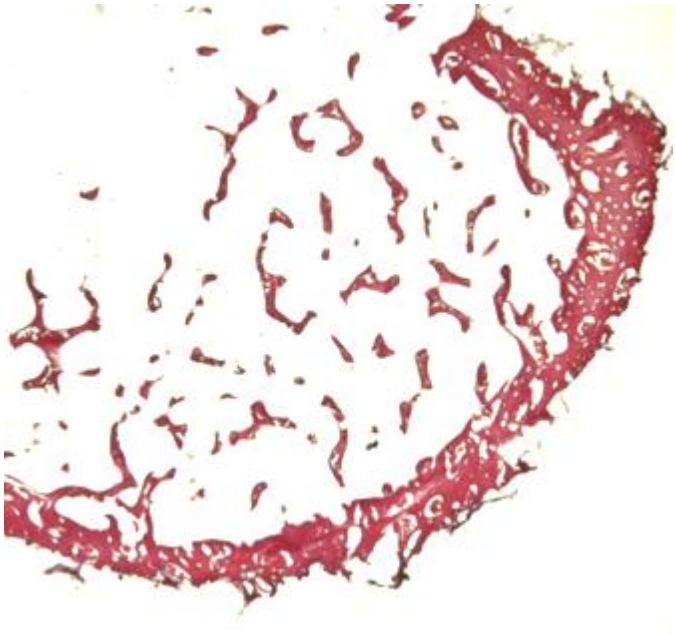

Figure 2.9 Cross-section of tibial metaphysis

The normal bone cortex is composed mainly of lamellar compact bone (figure 2.10). Most of the lamellar bones are arranged concentrically around the Harversian canal which is lined by osteoblastic cells and contains blood vessels. The concentric lamellae are oriented in the axis of the bone forming long cylindrical columns known as Harversian system or osteons. Small segments of lamellar bone, also known as interstitial lamellae, fill the spaces between Harversian systems. Circumferential lamellae are oriented around the long axis of bone on the periosteal and endosteal surfaces (49).

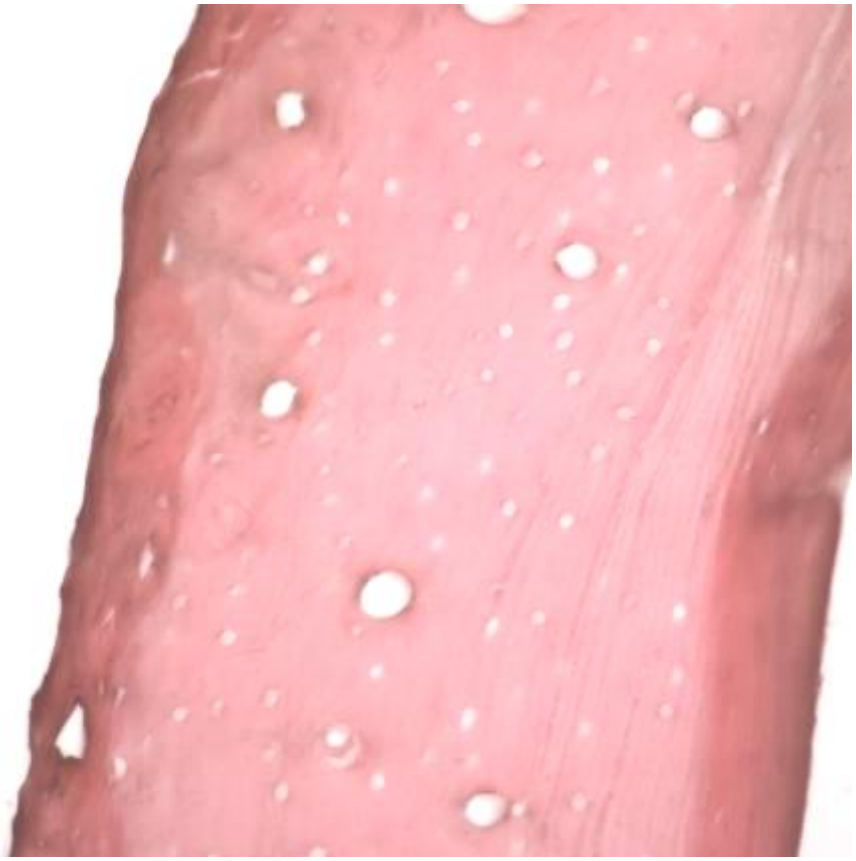

Figure 2.10 Cortical bone

2.2 Current concepts on osteoporosis

Osteoporosis is the condition in which a low bone mass and altered micro-architecture of the bone leads to increased risk of fracture. Traditionally, osteoporosis has been classified into primary and secondary osteoporosis. Primary osteoporosis refers to osteoporotic conditions which are not related to other chronic illnesses and is usually associated with aging and decreased gonadal function, such as decreased levels of estrogen; whereas secondary osteoporosis is the type of osteoporosis caused by other health problems. Disuse is one of the

many reasons inducing bone loss and resulting in secondary osteoporosis (58). Disuse osteoporosis has been shown to be a regional phenomenon in areas with tremendous decreases in weight bearing, like the lower limbs. Bones of the lower limbs are subjected to mechanical stimulations during daily life provided by static gravity-related weight-bearing, ground reaction forces, and dynamic loading generated by muscle contractions during locomotion. Physical exercise is essential for increasing or maintaining bone mass and strength (59). Milliken et al. have investigated the effect of 1-year supervised weight training exercise on bone mineral density (BMD) in postmenopausal women. The result showed higher BMDs of trochanter and femoral neck in women with weight training exercise than in those lacking exercise (60). Chan et al. have studied the effect of Tai-Chi exercise on bone quality in postmenopausal women. Postmenopausal women were randomly assigned to an exercise group or a control group. Subjects in the exercise group performed five sessions of 45 minutes Tai-Chi per week. After one year of Tai-Chi exercise, a greater percentage loss in bone density was observed in the control group when compared to the exercise group, suggesting that performing Tai-Chi exercise could decline bone loss in postmenopausal women (61). In addition, Feskanich et al. have studied prospectively a cohort on the relationship between walking, leisure time activity, and the risk of hip fracture showing that physical activity was inversely associated with the risk of hip fracture, and that the effect was dose-dependent (62).

Although there are many effective treatments available for primary osteoporosis, there is lack of effective treatments for disuse osteoporosis. This is because that the aetiology,

pathophysiology and resultant pathology of disuse osteoporosis differ from those of primary osteoporosis.

2.2.1 The pathology of disuse osteoporosis

Disuse bone loss in general is a reduction of bone mass in relation to bone volume, while the ratio of bone mineral to collagen remains unchanged. The loss of trabecular bone is more rapid and dramatic, while the cortical loss continues for a longer period (63). However, bones of the lower limbs are subjected to three categories of mechanical loadings during daily life: static gravity-related weight bearing; ground reaction forces; and, dynamic loading generated by muscle contractions during locomotion. Different health problems are associated with the absence or decrease in one or more of these mechanical stimulations and will result in bone loss differently in anatomical location, quantity, velocity, and through different mechanisms.

Long-term bed rest results in the absence of ground force reaction and reduction of muscle contractions. Rittweger et al. have carried out a 35 days bed rest trial and assessed bone density 2 weeks after the bed rest. They reported a reduction of bone mass in the cancellous bone-rich areas, 1% at distal femur, 3% at patella, and 2% at distal tibia while no changes were observed in distal radius (64). The same group observed that bone mass in distal radius remained unchanged after 56 days and 90 days bed rest, while bone mass in distal tibia declined 3.6% and 6% correspondingly (65, 66). The decreases of cortical bone thickness and density were below 2% after as long as 90 days bed rest. These results suggest that long-term bed rest does not affect balance of bone metabolism very much.

Disuse osteoporosis includes the reduction of bone mass after spinal cord injury (SCI) and other brain neurologic conditions as well. SCI leads to substantial reduction in ground force reaction and muscle contraction in the lower limbs resulting in dramatic reduction in bone mass. Results of a cross-sectional study carried out by Garland et al. demonstrated more than 20% bone loss at distal femur 3 months after injury in posttraumatic paraplegic and quadriplegic SCI patients. The researchers reported also that the rate of bone loss below pelvis was rapid and linear in the acute stages (67). In another cross-sectional study with a larger sample size, Kiratli et al. found a reduction of bone mineral density by 27%, 25%, and 43% in femoral neck, mid-shaft, and distal femur, respectively, compared with the controls (68). Besides SCI, lower limb amputation, acquired brain injury, and other neurologic conditions can also lead to disabilities which, in turn, result in disuse osteoporosis. A recent cross-sectional study by Smith et al. showed that 42.4% and 23.5% of disabled patients after neurologic traumas, such as SCI or other conditions for at least 3 months, had developed osteopenia and osteoporosis, respectively (69). The researchers suggested further that ambulatory status and duration of disability were independent predictors of bone mineral densities at femoral neck and total proximal femur.

Exposure to microgravity would lead to reduced weight-bearing and ground reaction forces that result in a reduction in bone mass. Several studies on effects of microgravity on the skeleton focused on the impacts on skeletons of astronauts after spaceflights. Collet et al. analyzed the BMD and biochemical parameters of two astronauts who stayed 1 and 6 months,

respectively, in space. A slight decrease in trabecular bone mass in distal tibia metaphysis was observed at the end of the first month of spaceflight, whereas remarkable bone losses in both trabecular and cortical bones was observed after 6 months of spaceflight. After 6 months of recovery, the trabecular bone mass was still significantly lower than normal, whereas no difference could be seen in cortical bone (70). However, the impacts of microgravity on human skeletons are highly varied. Another study on 11 astronauts by Vico et al. showed greater bone losses occurred in cancellous bone compared to cortical bone. The mean decrease in cancellous BMD of the 11 astronauts was 5.4% after 6 months of spaceflight but the range of reduction varied from 0.4% to 23.4%. The astronaut who spent the longest time in space did not have the greatest bone loss (71).

All three causes of disuse osteoporosis — long-term bed rest, paralysis, and microgravity — involve the reduction of ground reaction forces and weight-bearing activities. However, patients with long-term bed rest or paralysis are further subjected to reduced or even the absence of muscular contraction. This situation is different in the case of astronauts whose muscular contractions are not restricted, and this may be a possible reason for the great variations of bone loss in previous findings. Furthermore, muscular contraction can be the most important force out of the three categories of mechanical loading for keeping bone mass.

2.2.2 The pathophysiology of disuse osteoporosis

Disuse osteoporosis can result from failure of the bone to achieve the optimal peak bone mass and strength, if disuse occurred during the period of bone mass accumulation. On the other

hand, disuse osteoporosis can be the result of an accelerated rate of bone resorption and slower bone formation in adults (72).

Ralston indicated that peak bone mass and strength could be determined by genetic factors which affect the level of BMD, biochemical markers of bone turnover, and mechanical properties of bone. Results of association studies have suggested that polymorphisms of components in the gene-signaling pathway of genes such as COL1A1, ESR1, and LRP5 were associated with bone mass level and fracture risk. The influence of genetic factors on skeletal development is most pronounced in young people. The impact of genetic factors diminishes with age because of the increasing impact of environmental and nutritional factors (73).

Skeletal growth and repair occur through bone-remodeling which is a tightly regulated process. The normal bone mass is maintained during remodeling, based on the balance between bone formation and bone resorption. The bone-remodeling cycle begins with the resorption phase during which osteoclasts are recruited to the remodeling site on the bone surface, and these osteoclasts will then excavate the bone surface in the subsequent 2 to 4 weeks. After the resorption phase, the osteoclasts move away from the site, and osteoblast precursors move to the site and differentiate to become osteoblasts. During the subsequent 2 to 4 months of the formation phase, mature osteoblasts deposit an organ matrix, which will then be mineralized (74). However, because of certain events such as hormonal changes in menopause, the balance between bone formation and resorption is disturbed, and resorption occurs at a higher rate than that of formation leading to osteoporosis.

Osteoclasts are multinucleated cells derived from monocyte/macrophage lineage (75) and are the only type of cells capable of resorbing bone (76). The rate of bone resorption is determined by the number and activity of osteoclasts. During bone resorption, osteoclasts adhere to the bone matrix forming a deeply folded membrane and secrete protons and hydrolytic enzymes to the lacuna. The lacuna is then demineralized by the acidic environment due to proton secretion, leading to the exposure of organic components of the bone, such as collagen, to the hydrolytic enzymes, resulting in degradation of the organic components (77). Bone resorption is an important physiological process for bone modeling and remodeling. However, an increased rate of bone resorption may result in the depletion of bone mass and to the disruption of skeletal microarchitecture leading to skeletal fragility. Receptor activator of nuclear factor kappaB ligand (RANKL) is a cytokine that belongs to the TNF family; it is essential for osteoclast formation and function. RANKL is found on the surface of osteoblasts and the interaction between RANKL and its receptors RANK on osteoclast precursors triggers the maturation of osteoclasts, thus inducing bone resorption. The RANKL-RANK interaction is prevented by the natural RANKL inhibitor, osteoprotegerin (OPG). OPG is also a Tumor necrosis factor (TNF) family member that binds to RANKL and, hence, inhibits the binding of RANKL to RANK. Therefore, the activity of osteoclasts is partially dependent on the balance between RANKL and OPG (figure 2.11) (78). In addition to RANKL and OPG, there are many other cytokines such as IL-1, TNF-α, and prostaglandin E_2 that have been identified as regulators for osteoclastic activity (79, 80). Furthermore, Hughes et al. showed that estrogen was able to negatively regulate the formation and function of osteoclast by reducing the

lifespan of the cells by promoting apoptosis (81). This finding provides an insight on the cause of postmenopausal osteoporosis. Osteoclastic bone resorption is a highly regulated process. However, excessive osteoclastic activity without the complementary actions by osteoblasts will result in skeletal fragility. Based on previous studies, it is likely that bone resorption is influenced by complex interactions between different factors with osteoclasts.

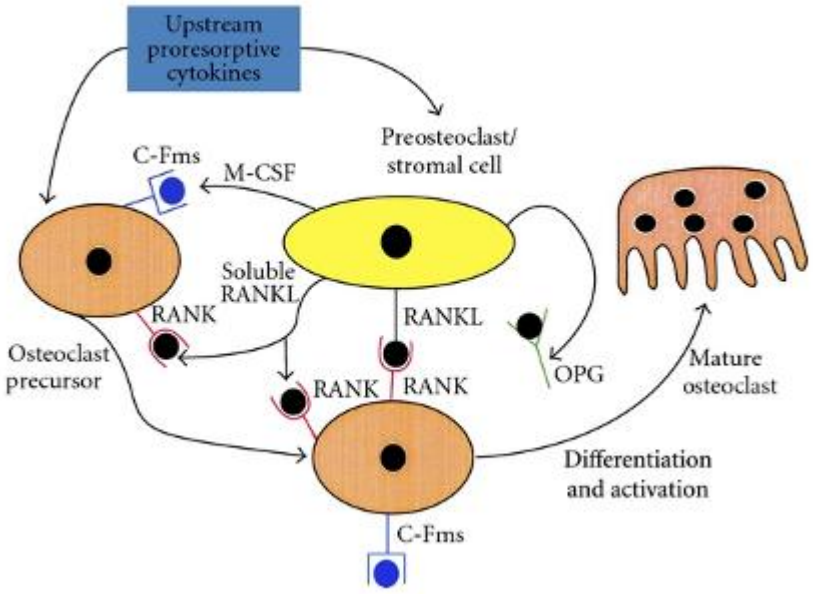

Figure 2.11 Regulatory mechanisms of osteoclastogenesis
(Adopted from Khosla, 2001 (78))

Skeletal remodeling is the result of both bone resorption and bone formation. In cases in which the rate of bone resorption is increased, there could be no apparent bone loss if the rate of bone formation is matched, since the bone removed will be replaced by new bone formation. Osteoporosis is, thus, an imbalance condition where the rate of bone resorption is higher than the rate of bone formation, resulting in continuous loss of bone and deterioration

of skeletal micro-architecture. Hence, it is important to determine what factors will affect the rate of bone formation as well as the coupling process between bone resorption and formation.

Osteoblasts are mononucleate cells which are responsible for bone formation. During ossification, or bone forming, osteoblasts produce an unmineralized, organic portion of the bone matrix known as osteoid. The osteoids produced will then mineralize, with minerals such as calcium and zinc, to form new bone tissue. Osteoblasts arise from mesenchymal progenitor cells, which possess the master gene of osteoblast differentiation, Runx2 (previously known as Cbfa1, Aml3, or Pebp2a1). In 1997, Komori and coworkers demonstrated that intramembranous and endochondral ossification were completely blocked in mice with Cbfa1 gene mutated, where Cbfa1 was a transcription factor belonging to the Runt-domain gene family (82). The same year, Otto et al. showed that homozygous Cbfa1-deficient mice died of respiratory failure shortly after birth. In that study, they found that there was neither osteoblast nor bone in the skeletons of the homozygous Cbfa1-deficient mice. Also, heterozygous mutants exhibited specific skeletal abnormalities that were characteristic of a human heritable skeletal disorder, cleidocranial dysplasia (83). These findings suggested that the Cbfa1 (Runx2) gene is essential for osteoblast differentiation and bone formation.

The differentiation of osteoblasts from mesenchymal progenitor cells is influenced by growth factors such as fibroblasts growth factor (FGF), transforming growth factor beta (TGF-β), and bone morphogenetic proteins (BMPs) (figure 2.12). D'Ippolito et al. (84) pointed out that the

number of osteoblasts tended to decrease as people reach old age. This leads to the decreased rate of bone formation and results in osteoporosis. According to a review by Rosen, the insulin-like growth factor (IGF) system is linked to the process of skeletal acquisition, and IGF-1 is essential for normal bone formation (85). A study by Sakata et al. showed that skeletal unloading led to resistance to the anabolic actions of IGF-I on bone, and this was associated with the reduction in integrin expression. This result suggests that IGF-I may be involved in the reaction mechanism of disuse osteoporosis (86). Besides IGF-I, the levels of various factors and hormones such as BMPs and PTH have been demonstrated to be changed in response to skeletal unloading (87). However, the exact mechanisms of how these factors respond to changes in mechanical loading are still unclear.

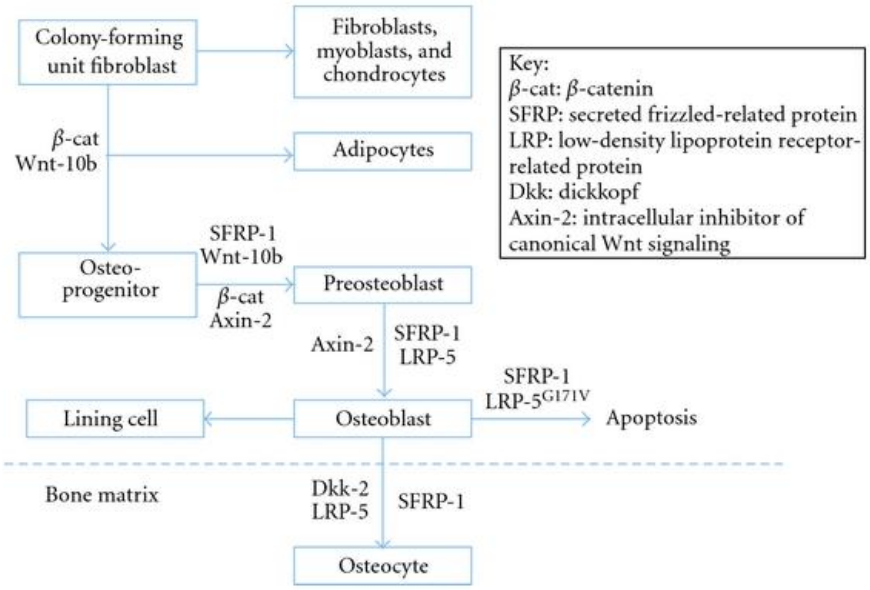

Figure 2.12 The role of canonical Wnt signaling in the control of osteoblastogenesis
(Adopted from Lau and Guo, 2011 (88))

2.3 Current concepts in the treatment of osteoporosis

Osteoporosis is a multi-factorial progressive disorder characterized by decreased bone mass and deteriorated bone micro-architecture, leading to increased risk of fracture. With the increasing proportion of the population aging, the health burden of osteoporosis exerts great pressure not only on the patients and their families, but on the entire healthcare system and the economy of the state. As mentioned in previous sections, experts of different professions have been working on various aspects related to osteoporosis in order to provide a better understanding of the pathology of osteoporosis, and its medical and economic impacts. Epidemiological research provides insight on the risk factors of osteoporosis and corresponding preventive measures. On the other hand, animal experiments serve as a platform for preclinical trials for potential therapeutics of osteoporosis. The ultimate goal of these trials is to provide treatments for osteoporosis which are effective, safe, and easily applicable with no or minimal adverse effects.

Research on osteoporosis treatment can be classified into two main approaches: pharmacological and non-pharmacological (or biophysical). The pharmacological approach focuses on the development of therapeutics, which are administered and act through various metabolic pathways. The biophysical approach aims at treating osteoporosis with physical agents.

2.3.1 The pharmacological approach

Pharmaceuticals for treating osteoporosis can be classified into antiresorptive agents that suppress the bone resorption, and anabolic agents that promote bone formation.

2.3.1.1 Bisphosphonates

Bisphosphonates are a class of drugs developed for treating diseases related to calcium metabolism. Clinically, bisphosphonates are still the first-line medication prescribed for osteoporosis in women. Application of bisphosphonates for treating bone diseases was originally derived from the research on inorganic pyrophosphate. Inorganic pyrophosphate was believed to be a physiological regulator of calcification and decalcification due to its ability to prevent ectopic calcification *in vivo* (89). However, inorganic pyrophosphate can be hydrolyzed readily and it has only little therapeutic benefit. Hence, analogues with similar pharmacological functions, but possessing higher resistance towards hydrolysis are preferred. Bisphosphonates were developed based on these criteria. It was believed that bisphosphonates preserve bone mineral content by binding to both bone minerals (90) and hydroxyapatite in bone (91). However, evidence suggests that bisphosphonates act by inhibiting osteoclastic bone resorption (92).

2.3.1.2 Estrogen analogues

At the time of menopause, the drastic reduction in estrogen production disturbs the balance between bone formation and bone resorption leading to postmenopausal osteoporosis (93).

Estrogen replacement therapy, which is the use of estrogen analogues for treating postmenopausal osteoporosis, was thus believed to be useful in the prevention of osteoporosis. However, the exact mechanism of estrogen on bone remodeling is still poorly understood. Also, it has been confirmed that estrogen replacement therapy is associated with an important increased risk of breast cancer (94). Therefore, the use of estrogen analogues is being seriously reconsidered.

2.3.1.3 Parathyroid hormone (PTH)

Parathyroid hormone is secreted by the parathyroid glands *in vivo*. Its primary function is to regulate serum-ionized calcium levels through its actions on the kidneys and bones (95). Originally, PTH was considered as a bone resorbing hormone since it stimulates the release of calcium from bone (96). However, further studies showed that indirect stimulation of bone resorption was only part of the functions of PTH in bone remodeling because PTH binds to osteoblasts but not osteoclasts, and there is no receptor for PTH on osteoclasts (97). PTH binds to osteoblasts leading to increased expression of RANKL. Binding of RANKL to RANK then stimulates the formation of osteoclasts enhancing bone resorption. Nonetheless, the action of PTH is mediated through osteoblasts and PTH stimulates overall bone turnover but not solely resorption. Reeve (1976) showed that the injection of low doses of PTH to postmenopausal women with osteoporosis could accelerate bone turnover and have anabolic effects on the human skeleton after 6-months of treatment (98). Since then, various clinical trials have been conducted to examine the therapeutic effects of PTH on osteoporosis, and consistent

beneficial anabolic effects were demonstrated in these trials. A systematic review by Cranney confirmed that PTH significantly increased BMD at all skeletal sites, except the radius, and reduced the risk of fractures in postmenopausal women with prior fractures (99).

2.3.1.4 Denosumab

RANKL inhibition has been a treatment strategy for treating osteoporosis that agents, which mimic the action of OPG, inhibit the RANKL-RANK binding leading to reduced rates of osteoclast maturation (100). Denosumab is one of the RANKL inhibitors approved by the FDA for use in postmenopausal women who were at high risk of fracture and for those who had been nonresponsive to other osteoporosis treatments (101). Denosumab prevents the interaction of RANKL with RANK on the osteoclast precursor cells leading to inhibition of differentiation and function of these cells and is associated with fracture prevention at multiple sites (100).

2.3.1.5 Calcitonin

Calcitonin is a natural occurring peptide hormone synthesized and secreted by the thyroidal C-cells. Mature osteoclasts express calcitonin receptors and calcitonin acts on osteoclasts to inhibit resorption *in vitro* (102, 103). However, calcitonin is less effective for increasing BMD in postmenopausal women when compared to alendronate, a type of bisphosphonates (104), and there is evidence suggesting that calcitonin use is associated with increased risk of cancer (105).

2.3.1.6 The new generation of pharmaceuticals for the treatment of osteoporosis

Besides the pharmaceuticals listed above, there are many innovative medications developed for the treatment of osteoporosis. For instance, the treatment potential of sclerostin antibodies for preventing bone loss has been investigated. Sclerostin is expressed by osteocytes and is a negative regulator of bone formation by antagonizing the interaction between Wnt ligand and LRP5/6 co-receptor on osteoblast (105). Sclerostin expression is upregulated during mechanical unloading and unloading-induced bone loss in mice was prevented by sclerostin antibodies (106, 107).

On the other hand, Cathepsin K inhibitors were a potential therapeutic target for osteoporosis as well (108). Cathepsin K is a lysosomal cysteine protease released by osteoclasts during bone resorption and catalyzes the degradation of type I collagen (105). Osteopetrotic phenotype was observed in Ctsk -/- mice and nonsense mutations in cathepsin K were identified in patients with pycnodysostosis (108, 109). Odanacatib is a selective, reversible nonpeptidic biaryl inhibitor of cathepsin K and has been proven to be effective in increasing BMD in postmenopausal women (110, 111).

2.3.2 Biophysical approaches

Non-pharmacological treatments for osteoporosis are usually physical exercises or agents that could preserve BMD. There is strong evidence showing that physical exercises are beneficial for osteoporosis patients in preserving bone density. However, the elderly or patients with physical disabilities who are not able to carry out physical exercises may not be able to enjoy

the benefits. So far, experiments have been conducted on the therapeutic effects of electromagnetic fields, lasers, mechanical stimulation, as well as electrical stimulation on osteoporosis.

2.3.2.1 Electromagnetic fields

The effects of electromagnetic fields on osteoporosis have been investigated for more than two decades. Mishima (112) treated osteoporotic mature ovariectomized female rats with a pulsing electromagnetic field for over 6 months. In that study, no effect was produced in the physiologically aged bones or in the lost cortical bone in the hindlimbs. However, increased bone volume and bone formation activity were observed in cancellous bone of the osteoporotic hindlimbs suggesting the potential preventive effect against bone loss in the hindlimbs.

In another study by Tabrah (113), a pulsing electromagnetic field was applied at the radii of 20 osteoporotic women, and showed that BMDs of radii exposed to the pulsing electromagnetic field were significantly increased after 12 weeks of treatment; the duration of exposure was 10 hours per day. However, after the treatment, BMDs were decreased in the following 36 weeks suggesting that the electromagnetic field may have clinical implications in preventing and treating osteoporosis.

Zati and co-workers attempted to study the effects of different intensities of a pulsed electromagnetic field on osteoporotic rats. They found that a 4-month treatment with

electromagnetic field with parameters of 30 Gauss, 50Hz and 1hr/day were able to slow down bone loss in the ovariectomized rats, with less than 10% bone loss observed, whereas no significant bone loss was observed if the intensity was 70 Gauss (114). Thus, the effect of a pulsed electromagnetic field may be dose-dependent, and optimization of parameters is required.

Besides the technical aspects, the action mechanism of a pulsed electromagnetic field is yet to be understood. Thus, research is ongoing in order to uncover the mechanism of action. In a recent study by Shen and Zhao, a pulsed electromagnetic field was used for treating the immobilized hindlimbs of rats. After 8 weeks, a significant increase in BMD and serum TGF-β1, but a lower IL-6, was observed in the pulsed electromagnetic field-treated group compared with the control group (115). These results suggest that the pulsed electromagnetic field may manipulate bone remodeling through promoting TGF-β1 and inhibiting IL-6 expression. However, more research on the action mechanism of pulsed electromagnetic fields in treating osteoporosis is needed.

2.3.2.2 Therapeutic lasers

The application of therapeutic lasers on osteoporosis is relatively new. Although a therapeutic laser is a punctual beam that limits its application on the whole body, and tests its efficacy in the prevention of osteoporosis, research has been ongoing to investigate the feasibility of using therapeutic lasers as a treatment for osteoporosis. Renno studied the healing effects of therapeutic lasers of different dosages, 60 and 120 J/cm^2, on osteopenic rats (116). The results

demonstrated that the higher dosage of therapeutic laser had stimulatory effects on femora, and that the mechanical strength of therapeutic laser-treated femora was similar to the sham samples, but significantly stronger than those without treatment. A recent study by Xu on the effects of low-intensity pulsed laser (LIPL) on rat calvarial cells showed that LIPL stimulated OPG mRNA expression but lowered RANKL mRNA expression (117). Thus, this suggests that LIPL may promote osteoblast proliferation and differentiation, and inhibit osteoclast maturation. Hence, LIPL can be a valuable therapeutic candidate for osteoporosis. There is increasing evidence showing the efficacy of therapeutic lasers on osteoporosis. However, further studies for optimization of technical parameters, such as wave length, duration, dosage and frequency of treatment are required.

2.3.2.3 Mechanical stimulation

Previous studies have demonstrated that mechanical stimulation in the form of low intensity vibration was effective in preventing early post-ovariectomy bone loss in animal models. Flieger and co-workers treated 3-month-old ovariectomized rats with low intensity vibrations (50 Hz, 2 g, 30 min./day) for 3 months and found that the treatment could prevent early reduction in bone mineral density (118). On the other hand, Oxlund et al. studied the effects of whole-body, low-magnitude, and high-frequency vibrations on tibias of adult ovariectomized female rats. In this study, vibrations of different frequencies and magnitudes (17 Hz – 0.5 g; 30 Hz – 1.5 g; and, 45 Hz – 3.0 g) were tested. They showed that all the vibration regimens could prevent the decrease in strength of tibias after ovariectomy, and that vibration at 45 Hz, 3 g,

30 min./day for 90 days could increase the periosteal bone formation rate, inhibit the endocortical bone resorption, and inhibit the weakening of bone induced by ovariectomy (119). Besides vertical vibration, mechanical stimulation can be applied as low intensity pulsed ultrasound (LIPUS). Wu examined the effects of LIPUS on cell differentiation, bone mineralized nodule formation and core-binding factor A1 (Cbfa1) expression in human osteoblast cultures, and the ovariectomized rat model. Results showed that LIPUS stimulated bone nodule formation and enhanced alkaline phosphatase activity (120). Moreover, decreased expression of Cbfa1 and earlier calcification were found in LIPUS treated groups. Hence, based on their results, LIPUS treatment is expected to accelerate osteogenesis and prevent bone loss.

2.3.2.4 Electrical stimulation

The concept of treating osteoporosis with electrical stimulation can be traced back to the 1960s. McElhaney et al. carried out an experiment to investigate the effects of electrical fields on osteoporosis of disuse (121). Martin and Gutman repeated McElhaney's experiment and showed that transcutaneous electrical fields of 30 Hz and 100 V/cm for either two, or eight hours a day was able to reduce disuse bone loss in immobilized femurs of rats, and efficacy increased with longer treatment duration per day (122). In a review by Stein, electrical stimulation could increase muscle strength and endurance, and reverse a certain level of osteoporosis in bones stressed by the stimulation in patients who had suffered from spinal cord injury. However, the patients involved in the studies were not bed- or wheelchair-bound and conserved a certain walking ability; the outcomes were thus combined effects of

stimulation and additional walking exercises (123). Another recent review by Creasey et al. (124) mentioned that electrical stimulation of motor neurons could improve muscle strength and endurance, as well as cardiovascular fitness; it may also have an effect on reducing osteoporosis. They also suggested an implantable design of stimulation system for long term use. However, the application of electrical stimulation for the prevention of osteoporosis is still controversial. Clark et al. carried out a controlled trial on the physiological effects of electrical stimulation on bone loss prevention in acute spinal cord injured patients. The stimulation was applied at the lower limbs of the patients twice a day, and the duration of each session was 15 minutes. After 5 months of treatment, no significant difference in BMD was observed between the treatment group and the control one (125).

Therefore, based on previous studies, the target tissue of electrical stimulation seems to be a determining factor for the treatment outcome.

2.4 Calcitonin gene-related peptides (CGRPs)

The calcitonin/CGPR gene complex encodes a family of peptides such as calcitonin, katcalcin and CGRP. CGRP is a neuropeptide with 37 amino acid residues and is concentrated in sensory nerve endings innervating bone metaphysis and periosteum (126).There are 2 subtypes of CGRP, namely CGRP-α and CGRP-β, which share structural and functional homology with the calcitonin molecules and play a local role in bone metabolism. CGRP has profound effects on calcium metabolism that are species specific (127). In addition, CGRP inhibits IL-1α-mediated bone resorption because of its direct regulation of osteoclast activity (128). In rats, CGRP

stimulates cAMP formation in rat calvarium, inhibits reabsorption of intact bone and inhibits spreading motility and reabsorption of bone by isolated osteoclasts (129). In man, the infusion of CGRP does not affect plasma calcium, but the peptide causes a rise in cAMP levels in normal human osteoblasts (126). On the other hand, CGRP plays an important role in the regulation of motor function at developing and regenerating neuromuscular junctions by promoting myotube differentiation (130) and upregulation of nicotinic acetylcholine receptors (131). However, Zaidi reported that high dosages of CGRP significantly inhibited bone resorption in rats, and CGRP might serve as a local regulator of bone cell function (10). Ballica demonstrated that transgenic mice with osteoblasts expressing CGRP had their trabecular bone density and bone volume higher than that of those transgene negative. Also, the increase in bone volume was shown to be associated with increased bone formation rate (132). Moreover, CGRP was shown to decrease receptor activator of nuclear factor kappa B (NF-κB) ligand (RANKL) and increase osteoprotegerin (OPG) mRNA and protein levels in pre-osteoblastic cells *in vitro* suggesting that CGRP had an important role in suppressing bone resorptive activities through RANKL/OPG pathway (133). However, CGRP was found to inhibit bone reabsorption in ovariectomized rats but effect was less pronounce compared to calcitonin that CGRP-treated rats had a loss of 46% of cancellous bone whereas calcitonin-treated rats had s loss of 21% suggesting that CGRP is either less potent than calcitonin in inhibiting bone reabsorption or is very rapidly degraded (134). Moreover, Imai mentioned that the CGRP distributed abundantly in bone via sensory nerves, especially in the epiphyseal trabecular bones, and was endogenously expressed in osteoblasts. These findings suggest that CGRP probably affects

bone metabolism via the nervous route as well as via an autocrine loop (11). Importantly, it has been demonstrated by Brooks that CGRP secretion from the dorsal horn could be stimulated by electrical stimulation of a dorsal root (19). Moreover, release of CGRP could be evoked by electrical stimulation (8 minutes, 20V, 0.5msec and 10 Hz) across dorsal roots from isolated spinal cord of monoarthritic rats at 7 days after induction of hind paw monoarthritis (135). Additionally, Schaible et al (1994) demonstrated that electrical stimulation to unmyelinated afferent fibres of tibial nerve in cat was able to increase the release of CGRP in the gray matter and up to the surface of the spinal cord (136). The expression of CGRP in dorsal root ganglion (DRG) neurons plays an important role in regulating neurogenic inflammation and pain (137) and expression of CGRP in DRG has been demonstrated extensively in previous studies (138, 139). Hence, it would be possible that electrical stimulation at DRG would enhance expression of CGRP and the increased CGRP expression would, in turn, possibly prevent or even reverse bone loss.

2.5 Summary of literature review

The literature review has summarized that bone is a highly complicated organ playing a wide spectrum of physiological functions. The physical and biochemical properties of bone are affected by behaviors of various types of cells and biochemical factors. For instance, osteocalcin mediates bone matrix mineralization whereas osteopontin facilitates osteoblastic and osteoclastic cells attachment. Also, the modeling and remodeling of bone is regulated by

the actions of osteoblasts and osteoclasts, which differentiation, proliferation, as well as maturation in turn are influenced by complicated biochemical cascades.

Bone modeling and remodeling are dynamic processes in which bones are formed and resorpted continuously in response to internal and/or external stimulations. Normally, the rate of bone formation by osteoblasts equals bone resoprtion rate by osteoclast and the bone mass is thus maintained. However, pathological conditions would be caused when the balance between rates of bone formation and bone resorption is disturbed. In the cases when bone resorption rate exceeds that of bone formation, osteoporosis occurs. Osteoporosis is characterized by the substantial decline in bone mass and deteriorated bone micro-architecture leading to increased risk of fracture. Osteoporosis can either be primary, which is usually associated with aging and decreased gonadal function, or secondary, which is caused by other health problems. Disuse is one of the major causes of the osteoporotic condition. Long-term bed rest, paralysis, and exposure to microgravity are commonly associated with disuse osteoporosis by reducing or removing skeletal mechanical loading in different anatomical locations at different rates and through different mechanisms.

In tackling osteoporotic symptoms, various treatments have been developed and numerous research works on potential treatments for osteoporosis are ongoing. Currently, different classes of pharmaceuticals have been developed such as antiresorptive agents which suppress bone resorption and anabolic agents which promote bone formation. However, the efficacies of the therapeutics vary in different pathological conditions and some might be associated

with adverse side effects such as the increased risk of breast cancer of using estrogen analogue. Therefore, further work on therapeutic development for osteoporosis is needed.

In parallel with the pharmacological approach, trials on biophysical treatments for osteoporosis have been carried out. Physical agents such as electromagnetic fields, therapeutic lasers, and mechanical stimulation have been applied in various human and/or animal models and their impact on osteoporosis was evaluated. Electrical stimulation is one of the physical agents used in previous investigations. Former works using electrical stimulation tended to stimulate skeletal muscles inducing muscular contractions which, in turn, conveyed mechanical signals to bone. However, there is no consensus on the treatment outcome.

Previous reports demonstrated the roles played by CGRP in bone modeling and remodeling. For instance, inhibition in bone resorption was observed in rats treated with high dosages of CGRP. In addition, transgenic mice with CGRP expression had their trabecular bone density and bone volume higher than those transgene negative. Importantly, the expression of CGRP at dorsal horn could be stimulated by electrical stimulation at dorsal root and this presents the potential of preventing osteoporotic symptoms mediated by enhanced secretion of CGRP by electrical stimulation at dorsal root.

2.6 Hypothesis

It is hypothesized that direct electrical stimulation to the cell bodies of sensory neurons at DRG may prevent disuse bone loss by a mechanism of increased secretion of CGRP.

2.7 Aims of study

The aim of this study is to investigate the impact of electrical stimulation at DRG on preventing disuse osteoporosis and the underlying mechanism. The ultimate goal of the current study is to provide information on the impact of electrical stimulation at DRG on disuse bone loss and the subsequent therapeutic development for osteoporotic pathology, i.e. decline in bone density and deterioration in bone micro-architecture. Based on this aim, the following research questions are addressed:

1. Is electrical stimulation at DRG effective in enhancing expression of CGRP at DRG *in vivo*?
2. How does histomorphology of tibia change under unloading with or without electrical stimulation at DRG?
3. Is electrical stimulation at DRG effective in reducing bone loss of unloaded tibia, in terms of bone mineral density and micro-architecture, assessed by densitometry and histomorphometry?
4. What is the prolonged impact of electrical stimulation at DRG on quality of bones under unloading in terms of histomorphology, bone mineral density, bone micro-architecture and biomechanical properties?

With regards to the research questions addressed above, the below objectives are defined:

I. To investigate whether *in vivo* electrical stimulation at DRG can enhance CGRP expression in DRG.

II. To investigate the histomorphological change in tibias under unloading with or without electrical stimulation at DRG.

III. To compare the difference in change in bone mineral density, bone micro-architectural parameters and biomechanical properties of unloaded tibias between electrical stimulated and non-stimulated animals.

IV. To investigate the prolonged effects of electrical stimulation at DRG on tibia quality in terms of histomorphology, bone mineral density, bone micro-architecture, and biomechanical properties.

In the coming chapters of this thesis, the details of the current study are presented. In the methodology chapter (Chapter 3), the detailed study design and animal treatment are presented. In addition, the details of the implantable micro-electrical stimulator (IMES) for generating electrical stimuli at DRG and the protocol for *in vivo* validation of electrical signals generated by IMES are described. Furthermore, the protocols for histological assessment for DRG and tibias as well as the procedures for assessing bone mineral density, bone micro-architecture, and biomechanical properties are described as well. The findings in the current study are demonstrated in the results chapter (Chapter 4). The effects of electrical stimulation at DRG on CGRP expression in DRG and bone quality of unloaded tibia are illustrated in the

discussion chapter (Chapter 5). A detailed summary of the current findings and the conclusion of the current study are presented in the conclusion chapter (Chapter 6). In addition to the effects in DRG and unloaded tibia, the current animal samples demonstrated that prolonged electrical stimulation at the spinal region would promote spinal fusion and the corresponding results are presented in the extra chapter (Chapter 7).

CHAPTER 3. METHODOLOGY

3.1 Study design

The current study was an experimental study investigating the effectiveness and efficacy of electrical stimulation to sensory nerves in increasing CGRP secretion and prevention of disuse osteoporosis in animal models. Animals were randomly assigned into the three treatment groups — cage control (CC); hindlimb unloaded (HU); and, hindlimb unloaded with electrical stimulation treatment (ES) — and treated for with 2 or 6 weeks. The results in bone mineral density of the animals were measured both before and after the treatment period whereas data on bone micro-architecture, histomorphology and biomechanical properties as well as CGRP expression in DRG were collected after harvesting the tissues. The differences in CGRP levels and bone quality among the treatment groups were evaluated based on the results obtained (figure 3.1).

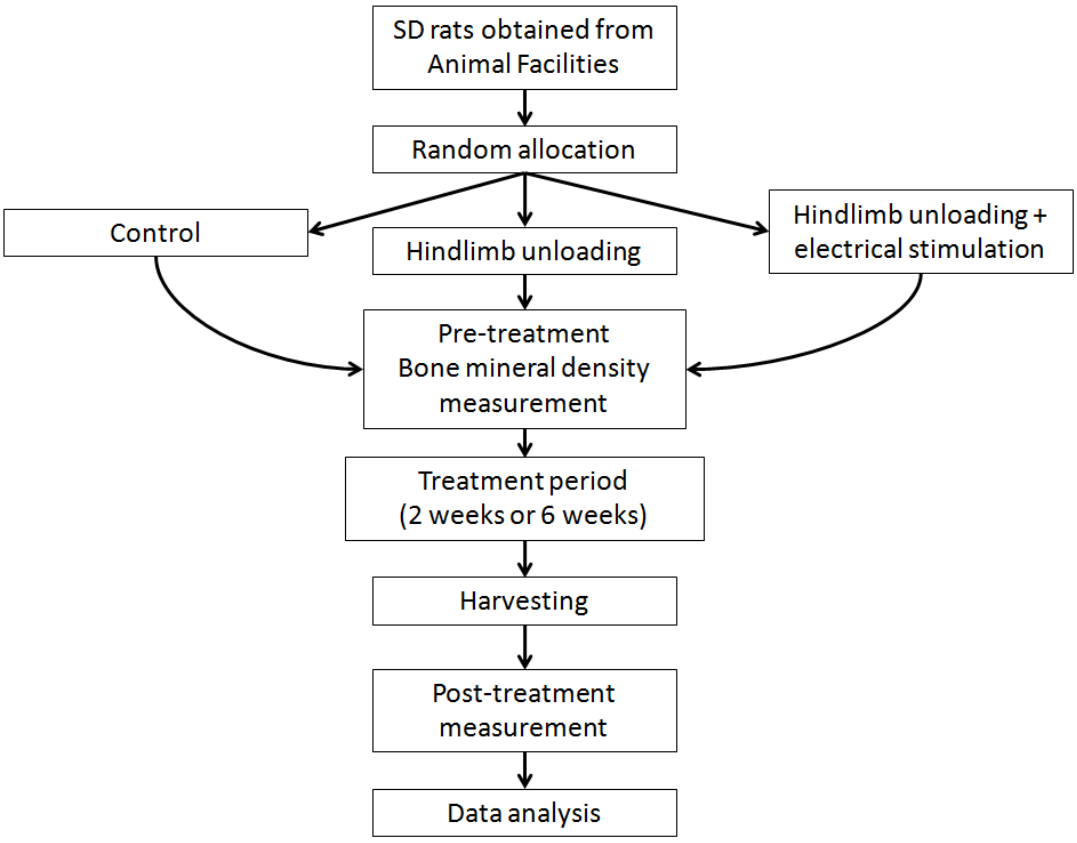

Figure 3.1 Flowchart of study design

3.2 Animal treatment

Sixty male Sprague Dawley rats aged three months were used in this study. Male rats were used since females tend to start losing bone earlier than males and the bone loss would proceed more rapidly in women than in male (140). Besides, 3-month-old was considered as youth age for rats (141) and former work demonstrated that bones of adult animals were likely to exhibit delayed and diminished response loading (142). Thus, rats of 3-month-old were used in the current study. The animals were randomly allocated into six groups of 10 rats each. The

animals were subjected to different treatments according to the treatment groups: (1) cage control (CC), in which animals were kept in cages without further intervention throughout the treatment period; (2) hindlimb unloaded (HU), in which animals had their hindlimbs unloaded throughout the entire treatment period using tail suspension protocol described in previous studies (143-145); and, (3) hindlimb unloaded with electrical stimulation (ES), in which animals were implanted with the implantable micro-electrical stimulators (IMES) before the treatment period, then they were kept in the same fashion as the HU group in that they had their hindlimbs unloaded throughout the treatment period. The implantation protocol and the treatment parameters will be described in next section. In this study, the effects of treatments were evaluated at two different time points respectively at 2 weeks or 6 weeks. After the treatment period, the animals were euthanized by CO_2 inhalation. The right hindlimbs were harvested and kept frozen at –80℃ until further experimental procedures. The spinal cords together with the dorsal root ganglia at spinal level L4 to L6 were harvested and fixed in 4% paraformaldehyde at room temperature. The group allocation is summarized in table 3.1 below.

Table 3.1 Group allocation of animals

	Control (CC)	Hindlimb unloaded (HU)	Hindlimb unloaded + IMES (ES)
2 weeks	n = 10	n = 10	n = 10
6 weeks	n = 10	n = 10	n = 10

The treatment protocol in the current study was approved by the animal ethics sub-committee of the Hong Kong Polytechnic University and complied with the regulations under Animal (Control of Experiments) Ordinance Cap. 304 of Hong Kong law (Ref no. of animal experiment

license: (10-57) in DH/HA&P/8/2/4 Pt.3). All animals were exposed to standardized 12hr day-night cycles and were provided with unlimited sources of water and food. Also, all animals, including those hindlimb unloaded, were allowed to move freely within the cages. The conditions of the animals were monitored by research personnel on a daily basis.

3.3 Hindlimb unloading protocol

Rats were suspended with a tail harness that raised their hindlimbs and kept them in a head-down position (Figure 3.2). The angle formed between the body of the rat and the floor of the cage was 30^{o} (144, 145). This prevented the animals from contacting the ground and bearing any weight with their hindlimbs. The animals were free to move with their forelimbs.

Figure 3.2 Hindlimb unloaded rat

3.4 Implantable micro-electrical stimulator (IMES)

In the current study, electrical stimulation was applied directly at DRG by an implantable device. Briefly, the IMES was implanted into the animal subcutaneously and controlled by a remote control unit. A detailed description of the IMES, implantation, and stimulation protocol is presented in this section.

3.4.1 The components of IMES

Electrical stimulation was generated by an IMES developed by the Department of Aeronautics & Astronautics Engineering, Tsinghua University, China (20, 146). The implanted stimulator unit consists of three parts: a body consisting of a circuit board and a button-type battery; three electrodes; and, wires connecting the body to the electrodes (figure 3.3). The dimension of the body is 25 mm x 20 mm x 8 mm and the weight of it is 5.86 g. In order to resist corrosion of components in the tissue environment, the body is coated with poly-para-xylylen (parylene C) and silicone rubber. The body connects to three coaxial electrodes. The outer layer of an electrode is a stainless steel tube serving as a reference pole. The core is fitted on a stainless steel wire coated with a layer of parylene. The uncoated tip of the core serves as the stimulating pole of negativity polarity (figure 3.4). The implanted stimulator unit is controlled externally with a remote control unit. Treatment parameters, including stimulation frequency, pulse duration, stimulation voltage as well as on- and off-time, can be adjusted with the remote control unit for various purposes.

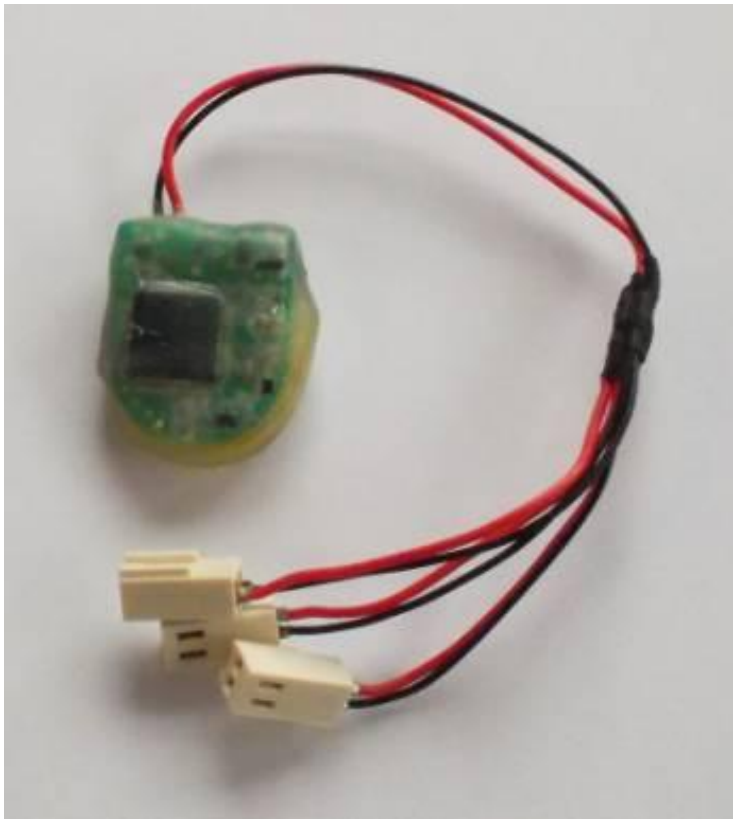

Figure 3.3 Implantable micro-electrical stimulator (IMES)

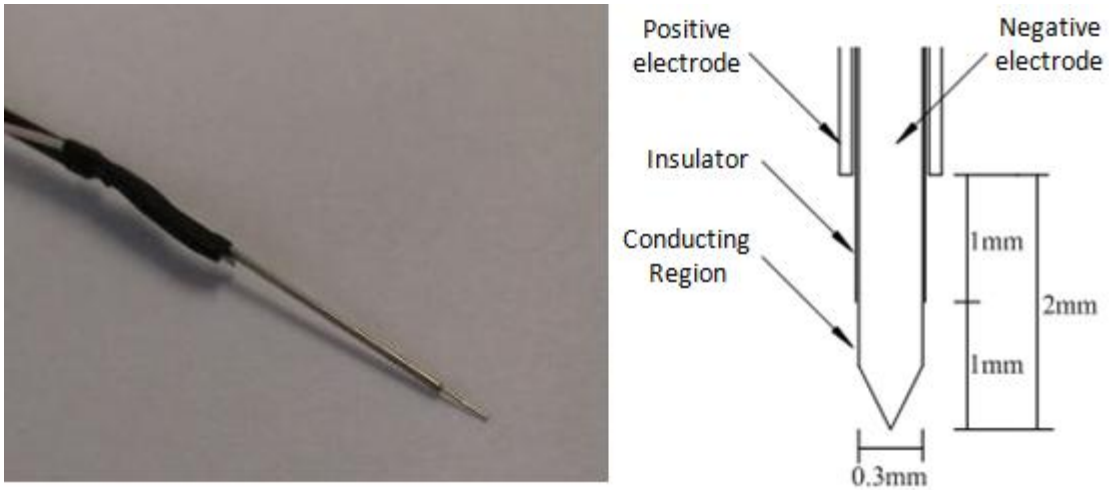

Figure 3.4 Uncoated tip region of coaxial electrode

3.4.2 Implantation protocol

In this study, electrical stimulation was applied at DRG of L4–L6 regions, which innervated tibial and common peroneal regions in rats (figure 3.5) (147). Thus, the stimulation electrodes were implanted at these levels. The anatomical information of the lumbar spine region of rats was referenced from the previous work by Zhang (148). Before implantation surgery, the rats were anesthetized with a cocktail of ketamine and xylazine (vol. ratio = 2:1, dosage = 0.1 ml per 100 g body mass). Then, vertebras L4 to L6 were exposed and holes of 1mm diameter were made at the location of DRG on transverse process of L4 to L6 vertebras. After drilling holes on transverse processes, electrodes were inserted into the holes (figure 3.6).

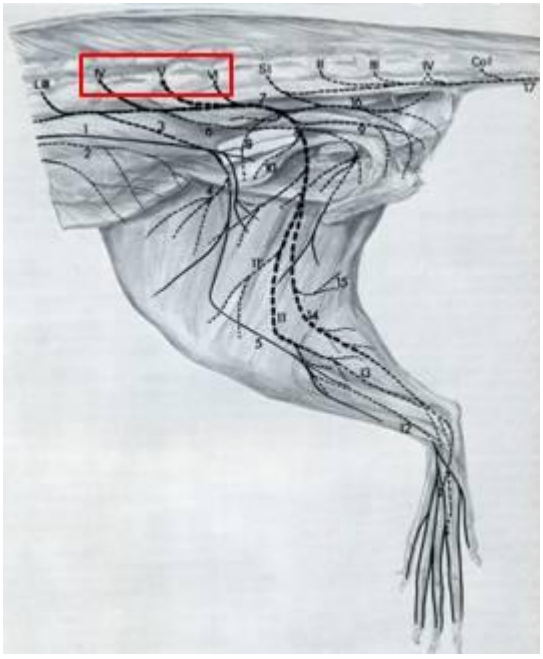

Figure 3.5 Innervation of tibial and common peroneal regions in rats (adopted from Greene (147))

After inserting the electrodes into the appropriate positions, the muscle wound was sutured and the positions of the electrodes were thus fixed. The electrical stimulator was then inserted into the space created under the skin. The electrodes were then connected to the stimulator after the position of the stimulator was fixed. The schematic illustration of IMES implantation is shown in figure 3.7. In order to confirm whether the electrodes remained in the original positions, the positions of electrodes were monitored by X-ray imaging after the treatment period (figure 3.8).

Figure 3.6 Vertebras of L4 to L6 with micro-electrodes inserted at the transverse processes

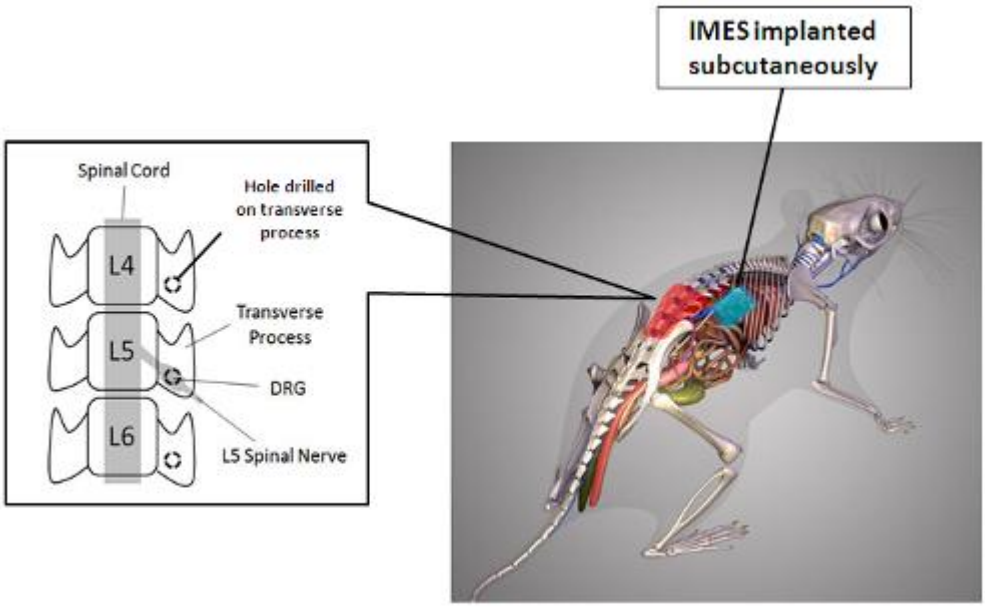

Figure 3.7 Schematic illustration of IMES Implantation
(Electrodes and connecting wires not shown)

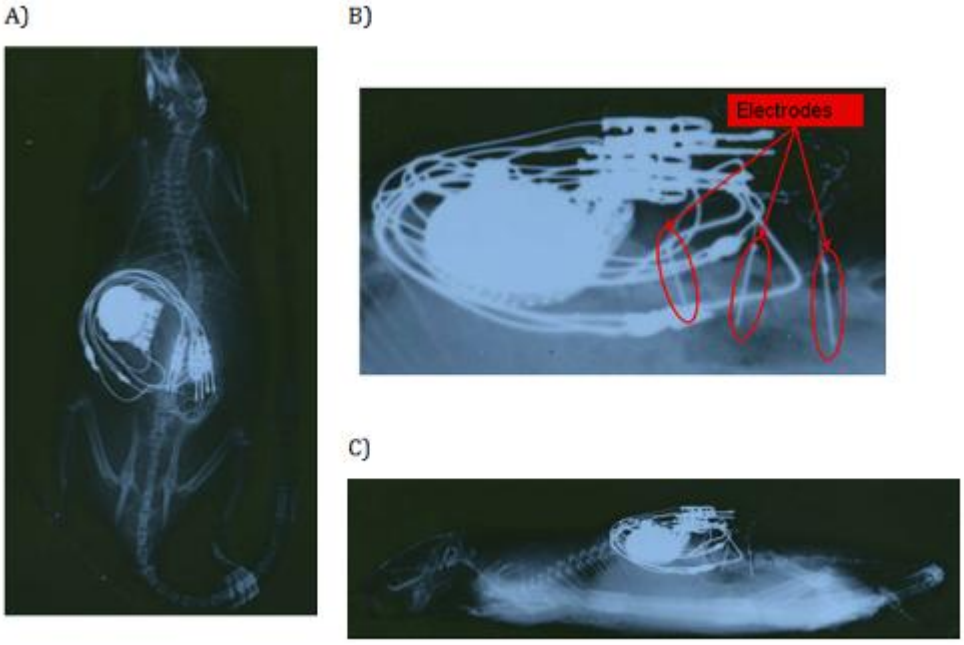

Figure 3.8 X-ray images of implanted electrodes and IMES after 2-weeks of treatment
(A) Dorso-ventral view, (B) Magnified lateral image showing positions of electrodes implanted, and (C) Lateral view.

For the *in vivo* validation of electrical stimulation signal generated by the IMES, similar surgical procedures were performed. However, instead of stimulating at L4 to L6 DRGs, only DRG at L5 was stimulated. In addition, 2 orifices were made on the right transverse process that one of them was for stimulation electrode whereas the other was for insertion of recording electrode.

In the in vivo validation experiment, stimulation and recording electrodes were implanted at the transverse process of L5 vertebra of seven female Sprague-Dawley rats (3-month-old; 250–300 g; Biomechanics Institute, School of Aerospace, Tsinghua University, China). Stimulation electrodes were implanted at the position of L5 DRG whereas the recording electrode was implanted 2 mm in front of the site of stimulation. The rats were anesthetized by intraperitoneal injection of sodium pentobarbital (dosage: 60 mg/kg). Based on the course of the spinal nerve, it was determined that the DRG was located approximately 2 mm off the inferior edge of the transverse process as shown in figure 3.9.

The overall experimental setup is illustrated in figure 3.10. All the surgical and treatment protocols were approved by the Animal Subjects Ethics Sub-Committee of The Hong Kong Polytechnic University and complied with the Animal (Control of Experiments) Ordinance Cap. 304 of Hong Kong law.

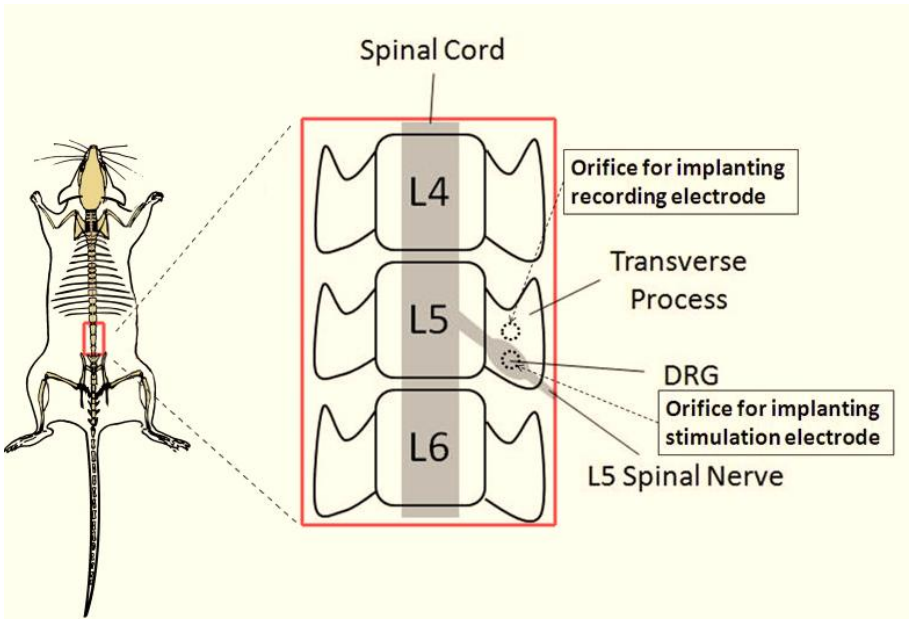

Figure 3.9 Anatomy of L5 spinal region showing the location of DRG
Broken lines indicate the positions of orifices drilled on the transverse process for the implantation of stimulation and recording electrodes respectively.

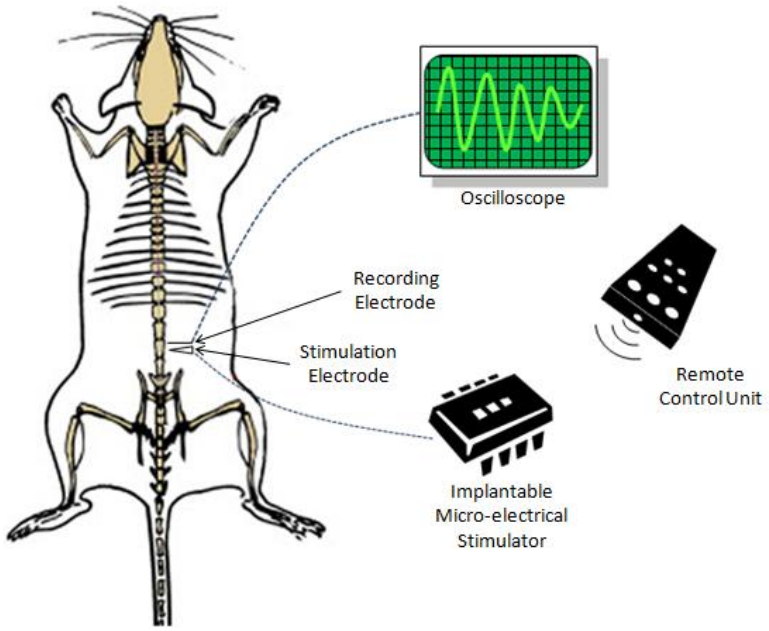

Figure 3.10 Experimental setup for *in vivo* measurement of electrical signal

Voltages generated by the stimulation electrode were measured and stored for subsequent analysis with an oscilloscope (Tektronic, model: MSO 4104) via recording electrode. The average peak cathodic voltage was calculated by averaging peak voltages of 1500 waveforms (10 seconds x 150 Hz) recorded for each voltage tested. The average voltage change between stimulation and recording electrodes at different input voltages was thus measured.

3.4.3 Stimulation protocol

The electrical stimulation signal was in a rectangular pulse waveform and constant amplitude (146). The pulse width, frequency, current, and voltage of the electrical stimulation applied were 90 μs, 150 Hz, 61.3 μA, and 0.25 V. The stimulation voltage used in this study was defined as the maximum stimulation voltage applied without triggering visible muscular contraction in the muscles innervated. Based on the observations, no muscle contraction was induced when stimulation voltage was 0.25 V but *in vivo* electrical signals were still detectable under this voltage (detailed information of *in vivo* measurement of electrical signal is described in section 3.5). In the ES group, each animal was stimulated for 20 minutes per day for either 2 weeks or 6 weeks depending on the treatment group.

3.5 *In vivo* validation of stimulation signals

In vivo validation of stimulation signals would justify the treatment parameters used for electrical stimulation and serve as a tool for optimizing current treatment protocol. Previous studies on physiological effects of electrical stimulation at dorsal root used mainly isolated tissues or slices and evaluated the effects *in vitro* (18). Hence, *in vivo* information on electrical

DRG stimulation is needed for evaluation of its physiological impacts. In recent research by Miocinovic et al., they demonstrated *in vivo* measurement of voltage distribution generated by deep brain stimulation (DBS) using a rhesus monkey model (149). However, because of the differences in anatomical structure and electrical properties of the tissue medium, *in vivo* stimulation of DRG and recording of the electrical signals generated by an implantable stimulator was performed in order to measure the electrical signals received by DRG.

The voltages induced by DRG stimulation were recorded with a microelectrode positioned at 2 mm apart from the site of electrical stimulation. By varying the input voltages of stimulation, multiple recordings were obtained and the difference between input and recorded signals was evaluated. Current-controlled stimulation was used throughout the validation experiment.

The overall diameter of the stimulating electrode was 0.5 mm whereas the diameter of the stimulating electrode was 0.3 mm and the length of the tip region of the stimulating electrode was 2 mm that 1 mm of which was wrapped by insulating layer and the remaining 1 mm was uncoated serving as the conducting end. The recording electrode was a metallic wire which was made of an alloy of platinum and iridium with diameter of 0.1 mm. The recording electrode was electrically isolated by coating it with ethylene tetrafluoroethylene copolymer (ETFT). Its conducting tip was 0.2 mm in length for receiving electrical signals.

The output electrical stimuli generated by the device were validated according to established protocol with an oscilloscope (Tektronic, model: MSO 4104). Table 3.2 shows the

characteristics of the rectangular stimulation pulse waveform. Typical implantable pulse generator (IPG) parameters settings used in our experiments were 90 µs and 150 Hz with input voltage varying from 0.25 V to 2.5 V. The IPG generated a traditional rectangular stimulation pulse waveform with constant amplitude as shown in figure 3.11. The parameters settings used in this study were defined based on practical cases of DBS treatments reported (20, 146, 150).

Table 3.2 Characteristics of rectangular stimulation pulse waveform

Parameters	Range
Pulse amplitude	0–2.5V (in 0.1 V or 0.05 V steps)
Pulse frequency	2–250 Hz
Pulse width	60–450 µs (in 30 µs steps)
On-time	0.1 sec. – 24 hr: 0.1–1 sec. (in 0.1 sec. steps), 1–60 sec. (in 1 sec. steps), 1–30 min. (in 1 min. steps), 0.5–24 hr (in 0.5 hr steps)
Off-time	0.1 sec – 24hr: 0.1–1 sec. (in 0.1 sec. steps), 1–60 sec. (in 1 sec. steps), 1–30 min. (in 1 min. steps), 0.5–24 hr (in 0.5 hr steps)
Waveform	No envelope; sine, triangular or exponential envelope

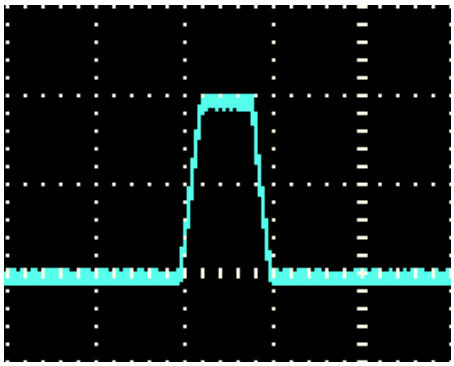

Figure 3.11 Current-controlled stimulus waveform

3.5.1 Validation of in vivo measurement of electrical stimuli

Voltages generated by DRG stimulation were recorded. The waveforms of the recorded signals closely resembled those of the stimulation signals. However, compared with the stimulation signal, the waveform of the *in vivo* recorded signal rose slightly and reached the peak voltage at the end of the pulse (figure 3.12). This phenomenon was observed in a previous study as well (149) and it was suggested to be caused by capacitance of the tissue medium (151).

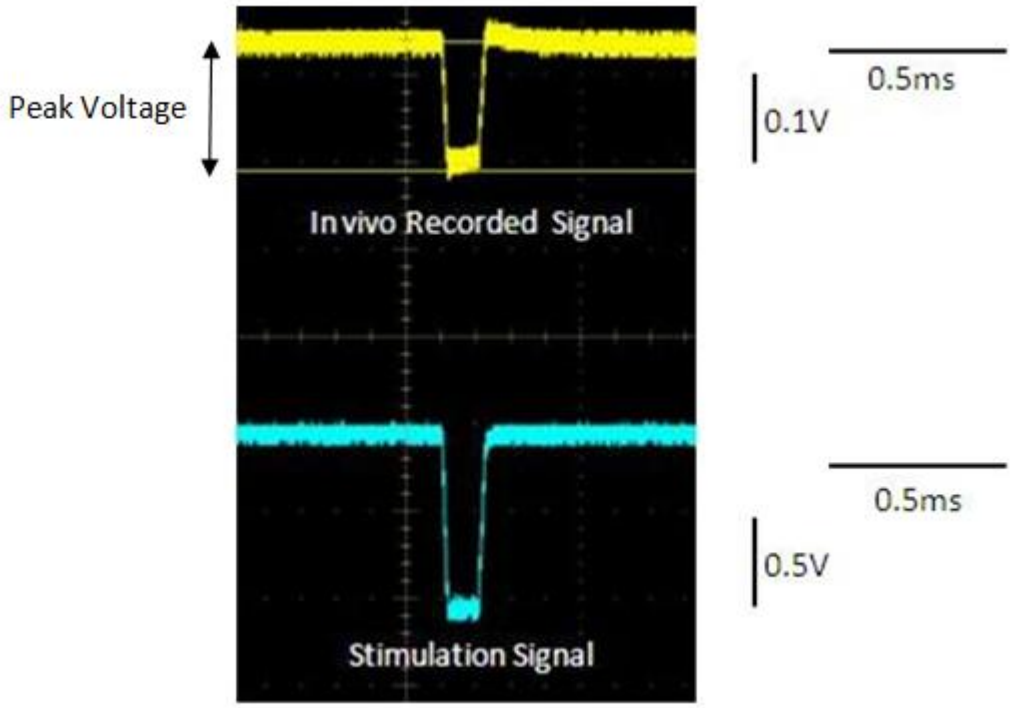

Figure 3.12 Waveforms of *in vivo* recorded and stimulation signals
(Stimulation parameters: 1 V, 90 µs, and 150 Hz)

The average peak voltage recorded had a linear relationship with the stimulation voltage and this observation was consistent throughout the range of voltage tested, i.e. 0.25 V to 2.5 V

(figure 3.13). However, for all voltages tested, a dramatic reduction of voltage was observed in the *in vivo* recorded signal (table 3.3). This implied that most of the electrical stimulation was lost along the distance between stimulation and recording electrodes (2 mm) similar observation was reported in a previous study of DBS in monkeys (149).

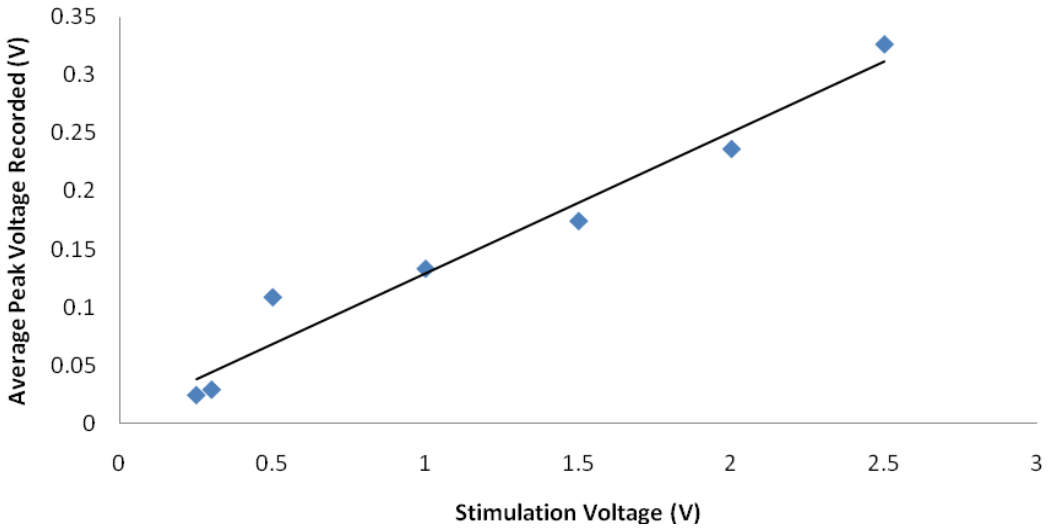

Figure 3.13 Peak voltage recorded vs. applied stimulation voltage

Table 3.3 Average voltage reduction for different stimulation voltages

Stimulation voltage (V)	**0.25**	**0.3**	**0.5**	**1**	**1.5**	**2**	**2.5**
Average peak voltage recorded (V)	0.0243	0.029	0.1085	0.133	0.174	0.236	0.326
Average voltage reduction	90.28%	90.33%	78.30%	86.70%	88.40%	88.20%	86.96%

3.5.2 Suitable voltage for DRG stimulation

In this study, the suitable voltage for DRG stimulation was defined as the maximum stimulation voltage applied without triggering any visible muscular contraction in the muscles innervated, i.e. muscles in the tibial region, since muscular contraction was possible to introduce extra effects additional to electrical stimulation at DRG. The voltage defined in this

study can be considered as the benchmark value for subsequent investigations on DRG stimulation. By varying the input voltages for DRG stimulation, muscle contraction in the hindlimbs of the rats were observed in some cases. The muscle contraction was localized in the hindlimb, mainly in the tibial region which was innervated by the L5 spinal nerve, on the right hand side. The muscles contracted corresponded with the site of stimulation as expected suggesting that the current treatment produced a localized effect at the specified region. The muscular behavior triggered upon electrical stimulation is summarized in table 3.4. Based on the observations, no muscle contraction was induced when stimulation voltage was 0.25 V but *in vivo* electrical signals were still detectable under this voltage. Therefore, 0.25 V would be a suitable voltage for DRG stimulation. Also, the results of *in vivo* measurement of electrical signals demonstrated a linear relationship between stimulation signals and the recording signals that the information would be useful for subsequent electrical stimulation protocol.

Table 3.4 Summary of muscular behavior triggered upon electrical stimulation

Voltage	Observation
< 0.3 V	No visible muscle contraction
0.3 V to 0.5 V	Slight to mild muscle contraction occurred
> 0.5 V	Vigorous muscle contraction occurred

3.6 Histological assessment

3.6.1 CGRP expression at DRG

The harvested specimen of spinal cord and DRGs were rehydrated in 0.01 M phosphate-buffered saline (PBS) containing 20% sucrose for 5 hours at room temperature. Then, the DRG samples were sectioned at a thickness of 7 μm on a cryostat. The immunohistochemical

staining was done according to an established protocol (152). Briefly, the DRG sections were treated in 0.5% horse serum (Gibco, USA) for 30 minutes at room temperature. The sections were then incubated with rabbit antibody to CGRP (1:50; Abcam, USA) for 24 hours at 4℃ followed by incubation with goat anti-rabbit Alexa Fluor 555 fluorescent antibody conjugate for visualization (1:1000; Invitrogen, USA). Finally, the sections were mounted with aqueous-based mounting agent with 4', 6-diamidino-2-phenylindole (DAPI; Vector Labs, USA). The sections were examined using a fluorescence microscope (Nikon eclipse 80i; Nikon, Japan) (figure 3.14) immediately after immunostaining. The fluorescence microscope was equipped with a mercury lamp and filters of various excitation ranges that red fluorescent signals of CGRP could be detected within the excitation range of 550 to 590 nm (153) whereas the DAPI produced blue fluorescent signals with excitation at about 360 nm (154).

The captured images of labeled DRG sections were further analyzed using ImageJ version 1.46r (NIH, USA). For size distributions of the CGRP+ neuronal profile, the areas of over 2000 DRG neurons were measured on the stimulated (ipsilateral) side. To calculate the amount of CGRP+ neurons, 100 fluorecent images of ipsilateral DRGs were extracted per animal at random, and the area of CGRP neurons was counted. Only CGRP+ neurons with visible nuclei were selected for measurement. The total area of CGRP fibers was quantitatively evaluated. The intensity of the signals and the number of pixels within the region of interest (ROI) were generated using the built-in histogram function of the software. The actual area of the ROI was estimated from the proportion of number of pixels within the ROI and the total number of pixels captured.

Significant enhanced signals were defined as signals with intensity higher than the mean intensity within the ROI for 1 time of the standard deviation. In addition, intense signals were defined as signals with intensity higher than the mean intensity within the ROI for 2 times of the standard deviation. The proportion of enhanced signals and the density of intense signals were thus estimated.

Figure 3.14 Fluorescence microscope for immunohistochemical examination

3.6.2 Histomorphology of tibia

Harvested tibia samples from four rats of each treatment group were decalcified with 10% ethylenediaminetetraacetic acid (EDTA) (Sigma, St Louis MO, USA) and ultrasonic decalcifier for 2 days (155). After dehydration with 10% sucrose (Sigma, St Louis MO, USA), the fibula was removed and the diaphyseal and metaphyseal portions of tibia samples were extracted that the diaphyseal portion included the region between the mid-point of the entire tibia and 2 mm proximal to the mid-point whereas the metaphyseal portion was defined as the region 2–4 mm apart from the proximal end of the tibia (figure 3.15). The extracted portions were then embedded in Optimal Cutting Temperature (OCT) compound (Thermo Electron Corporation, USA) and serial cross-sections of thickness 7 µm were created using a cryostat microtome (Model no.: CM1900, Leica Instruments). Prepared sections were kept at –20°C until further procedures.

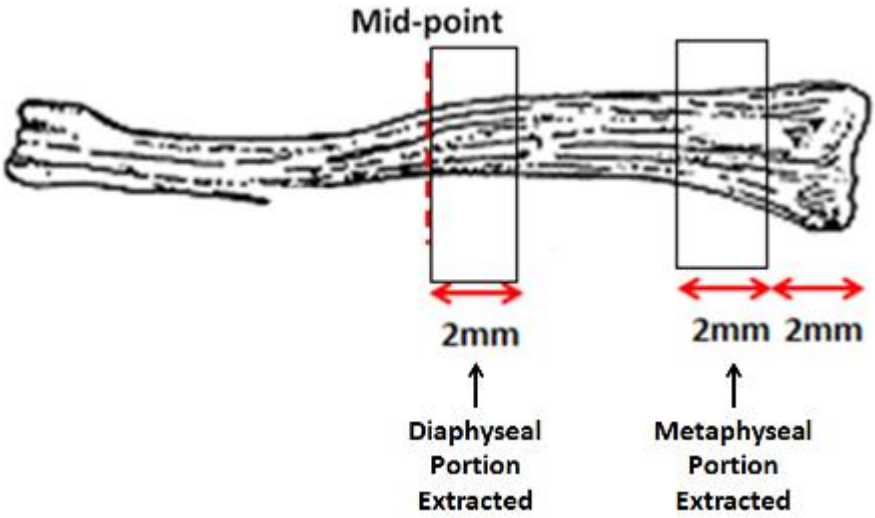

Figure 3.15 Diaphyseal and metaphyseal portions extracted for histomorphological analysis
Boxes indicate regions extracted for histomorphological analysis.

3.6.2.1 Haematoxylin and eosin (H&E) staining

In order to show the general histology of the bone samples, three sections were randomly selected from each bone sample and were stained with haematoxylin and eosin according to established protocol as listed in table 3.5 below. Histological examination was performed under a light microscope which was connected to a personal computer.

Table 3.5 H&E staining protocol

Rehydration	Absolute ethanol 1	5 mins
	Absolute ethanol 2	5 mins
	90% ethanol	5 mins
	70% ethanol	5 mins
Haematoxylin staining	Harris' Haematoxylin	45 mins
	Wash in distilled water	1 min
	Acid alcohol	10 secs
	Wash in distilled water	1 min
	Scotts tap water	1 min
	Wash in distilled water	1 min
Eosin staining	Eosin Y	10 mins
Dehydration	70% ethanol	1 min
	90% ethanol	1 min
	Absolute ethanol 1	5 mins
	Absolute ethanol 2	5 mins
	Xylene 1	10 mins
	Xylene 2	10 mins
Mount the slides with xylene-based mounting agent		

3.6.2.2 CGRP Expression at bony tissue

Similar to the quantification protocol of CGRP expression in DRG, images of tissue sections (magnification: 100x) were captured by the camera attached to the microscope system (Nikon, Japan) and saved in the connected personal computer. The captured images of labeled tibia sections were further analyzed using ImageJ version 1.46r (NIH, USA). The actual area of the ROI was estimated from the proportion of the number of pixels within the ROI and the total number of pixels captured. Significant enhanced signals were defined as signals with intensity higher than the mean intensity within the ROI at 2 times of the standard deviation. The results

were expressed as the nerve fiber immunofluorescent area in relation to the total tissue area. The mean values of the eight sections were determined for each bone sample.

3.6.2.3 Tartrate-resistant acid phosphatase (TRAP) staining for osteoclasts

Multinucleated osteoclasts are characterized by the presence of TRAP activity and pit-forming activity on bone (156). In order to assess the number of TRAP-positive osteoclasts, tibia sections were stained for TRAP using an acid phosphatase, leukocyte commercial kit (Sigma, St Louis MO, USA). Briefly, the two sets of slides of each bone sample were fixed by immersing them in a fixative solution for 30 seconds and then rinsing them thoroughly in deionized water. A total of 0.5 ml of Fast Gamet GBC Base Solution (Catalog No: 387-2, Sigma) and 0.5 ml of sodium nitrite solution (Catalog No.: 91-4, Sigma) were added to each of the two test tubes and mixed by gentle inversion for 30 seconds. Then, 45 ml of preheated deionized water at 37℃, 1 ml of diazotized Fast Gamet GBC Base Solution prepared, 0.5 ml of Naphthol AS-BI Phosphate Solution (Catalog No: 387-1, Sigma) and 2 ml of Acetate Solution (Catalog No: 386-3, Sigma) were added to each of the two labeled beakers, A and B. In beaker B, 1 ml of Tartrate Solution (Catalog No: 387-3, Sigma) was added. The solutions were then heated to 37℃. The two sets of slides were then incubated in each of the solutions in 37℃ water bath protected from light for 1 hour. Then the slides were rinsed thoroughly in deionized water followed by counterstaining for 15 seconds in Gill No.3 Hematoxylin (Catalog No.: GHS-3, Sigma). The slides were then rinsed in alkaline tap water for 2 minutes until blue nuclei appeared.

The occurrence of TRAP-positive osteoclastic cells was assessed using a microscope system (Nikon eclipse 80i; Nikon, Japan), and images of tissue sections (magnification: 100x) were captured by the camera attached. The captured images of labeled tibia sections were further analyzed using ImageJ version 1.46r (NIH, USA). The actual area of the ROI was estimated from the proportion of the number of pixels within the ROI and the total number of pixels captured. The density of TRAP-positive osteoclasts per mm^2 of tissue was estimated.

3.6.2.4 Alkaline phosphatase (ALP) staining for osteoblasts

In order to evaluate the activity of alkaline phosphatase presented by osteoblasts, ALP staining of the tibia sections was performed using an alkaline phosphatase commercial kit (Sigma, St Louis MO, USA). Preweighed capsules of Fast Blue RR Salt (Catalog No.: FBS-25, Sigma) was dissolved and mixed in 48 ml of distilled water at 25℃. A total of 2 ml of Naphthol AS-MX Phosphate Alkaline Solution (Catalog No.: 85-5, Sigma) was added and mixed with the Fast Blue RR Salt solution. Then, the tibia slides were fixed by immersing them in the fixative solution for 30 seconds followed by rinsing in deionized water for 45 seconds. After fixation, the slides were added to the alkaline-dye mixture and incubated for 1 hour at 25℃ protected from direct light. After incubation, the slides were rinsed thoroughly in deionized water for 2 minutes followed by counterstaining with Meyer's hematoxylin for 10 minutes.

The areas of ALP activity-positive sites were assessed using a microscope system (Nikon eclipse 80i; Nikon, Japan), and images of tissue sections (magnification: 100x) were captured by the camera attached. The captured images of labeled tibia sections were further analyzed using

ImageJ version 1.46r (NIH, USA). The actual area of the ROI was estimated from the proportion of the number of pixels within the ROI and the total number of pixels captured. The total areas of ALP activity-positive sites were measured and the proportion of ALP activity-positive area to total bone area was estimated.

3.7 Peripheral quantitative computed tomography (pQCT)

Tomographic scans of tibias were performed before treatment *in vivo* and after harvesting the bone samples *ex vivo* using a pQCT scanner with software version 5.2 (Stratec XCT2000, Norland) (figure 3.15). Each tibia was cross-sectionally scanned at 2, 3, and 4 mm from the proximal end of the bone where it is rich in cancellous bone. Another three slides were scanned at diaphysis at the midpoint of the total length of the tibia (figure 3.16). A standardized analysis for either the epiphyseal region (contour mode 3, peel mode 2, outer attenuation threshold 0.214 g/cm^3, inner attenuation threshold 0.605 g/cm^3) or diaphyseal region (separation 1, attenuation threshold 0.605 g/cm^3) was applied to each slide obtained (157). The total bone mineral content (BMC), total, cortical and cancellous bone mineral density (BMD) were measured in the epiphyseal region whereas cortical BMC and BMD were measured in the diaphyseal region. Parameters in the slide with the highest total BMD value at each site were used for further analyses.

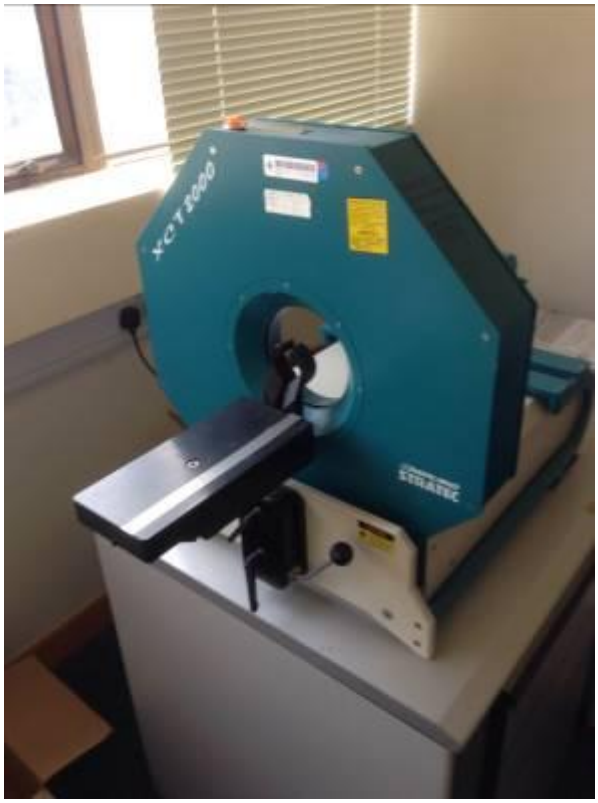

Figure 3.16 pQCT equipment

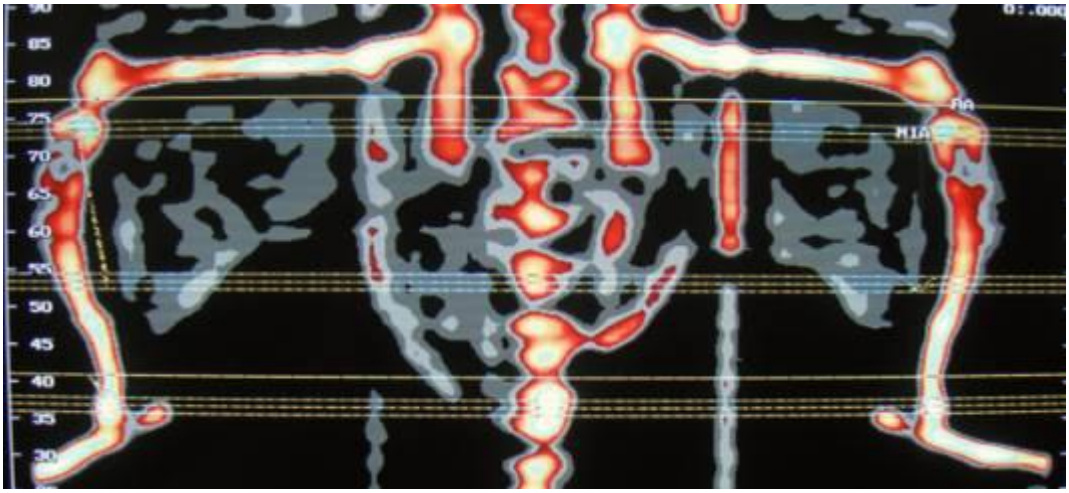

Figure 3.17 *In vivo* pQCT scan of tibia. Broken lines indicate the sites of scanning.

3.8 Micro-computed tomography (μCT)

The harvested tibiae were examined with a high resolution μCT scanner (μCT-40, SCANCO Medical AG, Bassersdorf, Switzerland) (figure 3.17). The basic parameters were set as following: voltage 70 kV, current 114 μA, and integration time 170 ms. The proximal metaphysis and diaphysis of the tibias were scanned at a resolution with an isotropic voxel size of 19 μm and 38 μm respectively. In order to suppress the noise in the results, all images were evaluated with a constrained 3D Gaussian filter (filter width: $\sigma = 1.2$; filter support: $S = 2$). The volume of interest (VOI) at proximal metaphysis was defined as the 200 μm region beginning at 100 μm below the growth plate whereas the VOI for diaphysis was defined as the 200 μm region at the mid-length of the tibia (figure 3.18). The threshold values for proximal metaphysis and diaphysis were respectively 250 and 220 mg/cm^3. All scans were reconstructed with the same parameters for different portions. The trabecular bone microarchitecture could be visualized and quantitatively analyzed with the software μCT Evaluation Program V6.0 (Scanco Medical, Zurich, Switzerland). The quantitative analysis of trabecular bone microarchitecture included the following indices at the proximal metaphysis: bone volume fraction (BV/TV), connectivity density (Conn.D), structural model index (SMI), trabecular number (Tb.N), thickness (Tb.Th), and separation (Tb.Sp). At the diaphysis, the indices included BV/TV, total volume (TV), bone volume (BV), and mean density of TV and BV.

Figure 3.18 High resolution µCT scanner and computer system for image analysis

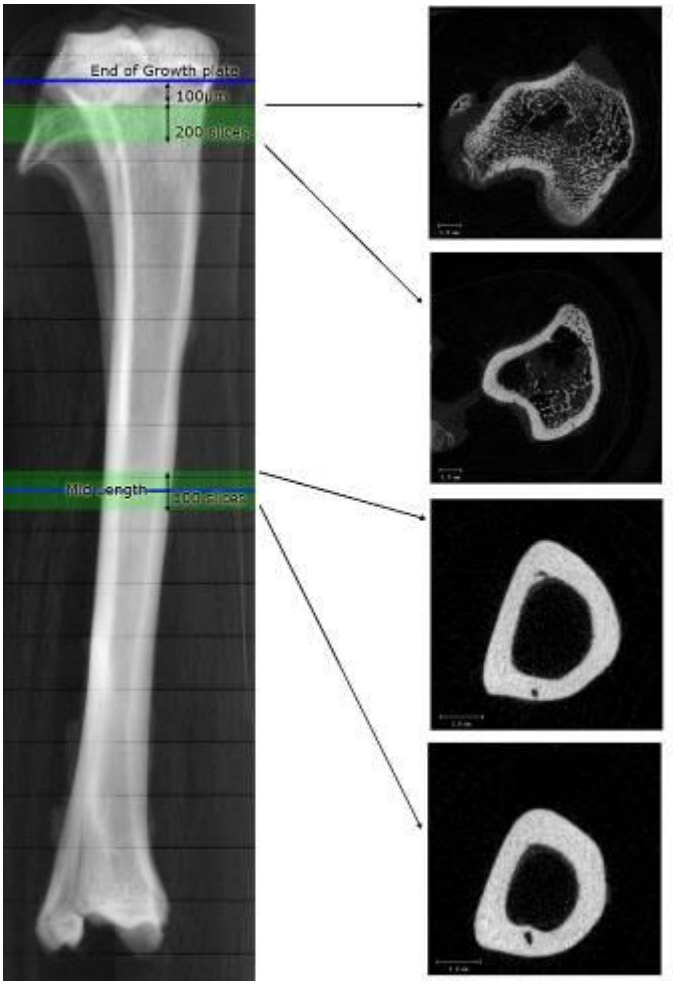

Figure 3.19 Designated VOIs at proximal metaphysis and diaphysis, and cross-section images of the borders of each VOI

3.9 Mechanical testing of tibia

Right tibias of four randomly selected rats were collected to test for the biomechanical properties. Before the mechanical testing, the bone samples were allowed to thaw in normal saline-soaked gauze at room temperature for 2 hours. Then, the fibula was removed from each of the tibia sample. The 3-point bending test was performed using a material testing machine

(Model: H25KS, Hounsfield, Surrey, UK) (figure 3.19). The tibias were loaded to failure using a 2.5 kg static load cell at a displacement rate of 10 mm/min. Load-displacement data (50 data records per second) were collected by a personal computer connected to the material testing machine equipped with material testing software.

During the test, the tibia sample was mounted on a stainless steel platform and the tibia was positioned horizontally with the right side downward and centered on the lower supports. A constant span length of 20 mm was set between the two lower supports for each sample whereas the upper indenter was positioned at the mid-point of the sample (figure 3.20). Hence, the pressing force was directed vertically to the midshaft of the tibia.

Figure 3.20 Material testing machine and adjustable platform

Figure 3.21 Setup and position of tibia for 3-point bending

The load-displacement curve generated by the computer system was used for analysis. The biomechanical properties of the bone samples were evaluated based on the ultimate load and stiffness. The ultimate load was defined as the bending load at failure (158) whereas stiffness was calculated as the slope of the linear portion between 20 to 70% of the maximum load from the load-displacement curve (159) (figure 3.21).

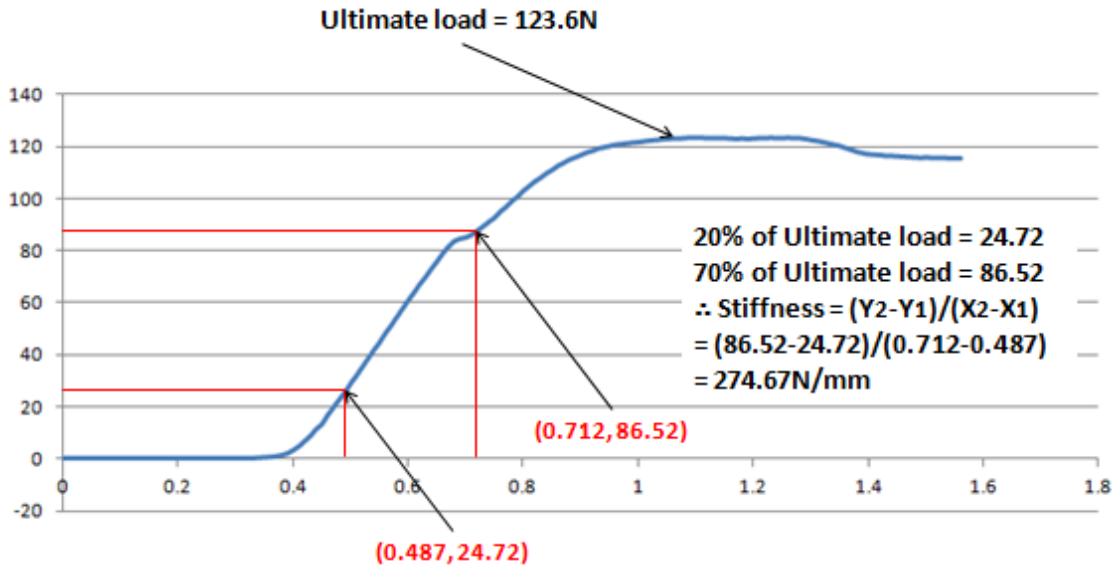

Figure 3.22 Load-displacement curve of a tibia sample

3.10 Statistical analysis

Statistical analysis was performed using SPSS ver.20 (IBM, New York, The United States). The results were given in mean and standard deviation. For pQCT data, percentage changes in bone quality parameters between pre- and post-treatment measurements of each group were calculated using the equation 1. To answer the question whether stimulation to DRG has an effect on bone turn over, intergroup differences in BMC and BMD changes measured from right tibiae were evaluated using one-way ANOVA and post-hoc LSD tests.

For micro-computed tomography, the differences in micro-structural parameters among groups were evaluated using one-way ANOVA and post-hoc LSD tests.

For immunohistochemistry, TRAP and ALP staining of tibia, the differences in proportion of nerve fiber immunofluorescent area as well as differences in densities of osteoclastic signal and proportions of ALP activity-positive area among groups were evaluated using one-way ANOVA and post-hoc LSD tests.

For mechanical testing of tibia, differences in ultimate load and stiffness among groups were evaluated by non-parametric Kruskal-Wallis tests. In the case that a significant difference was detected, post-hoc Mann-Whitney U test would be applied for pair-wise comparison.

For all quantitative statistical analyses in the current study, statistical significance was considered if $p \leq 0.05$.

Change in bone quality parameter (%)

= 100% x (bone quality parameter after treatment period – bone quality parameter at day 0)

/ bone quality parameter at baseline (1)

CHAPTER 4. RESULTS

4.1 Expression of CGRP at DRG

4.1.1 2-week treatment

After 14 days of treatment, all animals were in good condition. CGRP+ neurons in DRG were visualized by immunohistochemistry (figure 4.1). By comparing the CGRP signals in the right DRG among the three groups, enhanced CGRP signals were observed in the ES group (figure 4.1H) that, according to the results of one-way ANOVA and post-hoc LSD test, the average proportion of CGRP+ neuron in DRG of ES animals was significantly higher and that of the HU animals ($p = 0.006$). In addition, the proportion of CGRP+ neuron in DRG of HU group was significantly lower than that of cage control animals ($p = 0.034$). However, no significant difference in proportion of CGRP+ neuron in DRG was observed between the CC and ES groups ($p = 0.424$) (table 4.1). On the other hand, intense enhancement of CGRP signals was observed in the ES group but not in the CC and HU groups. The averaged density of intense signal was $155.03 \pm 56.26/mm^2$. The enhanced CGRP signal complied with the occurrence of DAPI signals (figure 4.1G–4.1I), where DAPI bound DNA and produced fluorescent signals upon excitation.

Based on the results of immunohistochemistry of the 2-week treated samples, the expression of CGRP in DRG could be enhanced by direct electrical stimulation at the tissue.

Table 4.1 Average proportion of CGRP+ neuron in right DRG

	CC	HU	ES
Averaged proportion of CGRP+ neuron at week 2 [%]	17.8±1.2	14.8±0.6*	18.8±1.7^
Averaged proportion of CGRP+ neuron at week 6 [%]	16.6±0.1	15.7±0.1*	17.0±0.3^

Values were means±SD.
*: Significant difference ($p < 0.05$) against cage control
^: Significant difference ($p < 0.05$) against hindlimb unloaded

4.1.2 6-week treatment

After 6 weeks, no infection was observed in the animals. Occurrence of CGRP+ neurons in stimulated DRG were visualized by immunohistochemistry (figure 4.2). Similarly to the results of the 2-week treatment, enhancement in CGRP signals was observed in the ES group. By comparing the average proportion of CGRP+ neuron among the three treatment groups with one-way ANOVA and post-hoc LSD tests, the proportion of CGRP+ neuron in the HU group was significantly lower than the CC and ES groups ($p = 0.008$ and $p < 0.001$ respectively). No significant difference in proportion of CGRP+ neuron existed between the CC and ES groups ($p = 0.058$). Moreover, intense CGRP signals were observed in the ES group but not in the non-stimulated ones. The average density of intense signal was 21.78/mm^2 (S.D. = 4.40). In addition, the enhanced CGRP signal complied with the occurrence of DAPI signals.

Based on the results of immunohistochemistry of the 6-week treated samples, the expression of CGRP in DRG could be enhanced by direct electrical stimulation at the tissue and the effect of treatment could be sustained for prolonged periods.

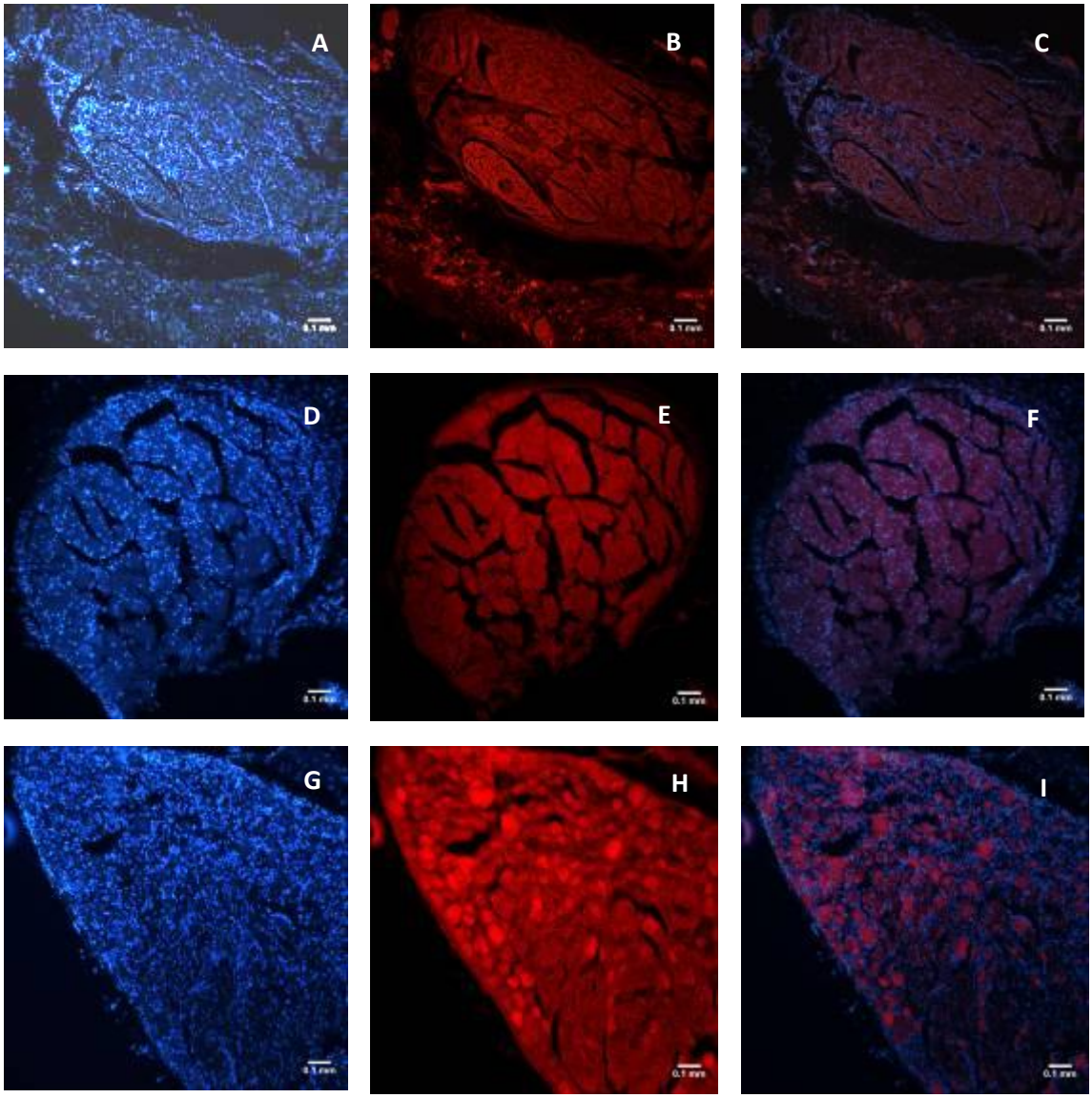

Figure 4.1 Immunofluorescent images of right DRG (2-week). A, B, and C show fluorescent signals in control (CC) DRG whereas D, E, and F show signals in DRG of hindlimb unloaded (HU) group. G, H, and I show fluorescent signals in electrical stimulated (ES) DRG. DAPI-labeled nuclei signals (A, D, and G). CGRP-immunoreactive signals (B, E, and H). Combined images of DAPI and CGRP signals (C, F, and I). (Scale bar = 0.1 mm)

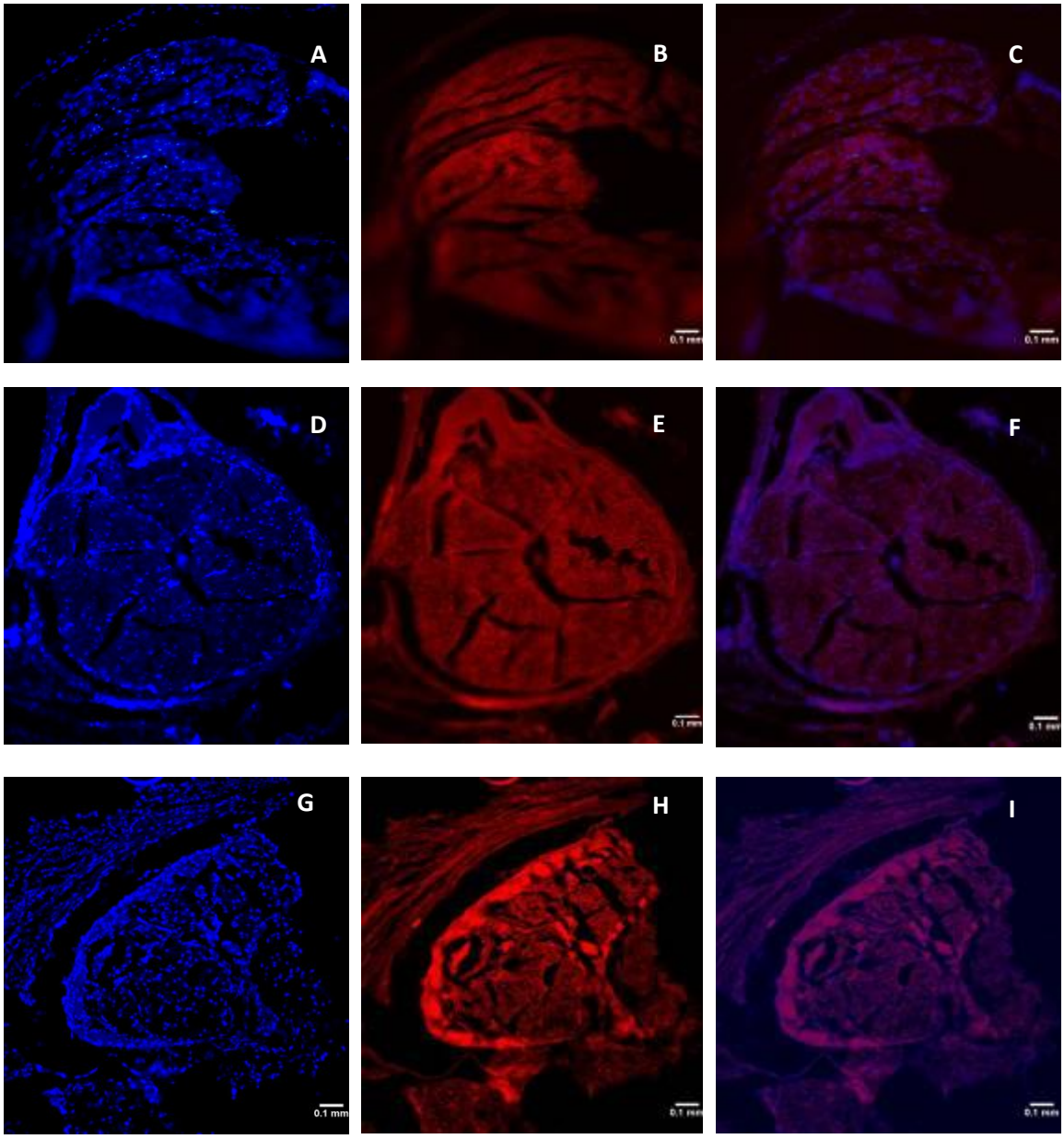

Figure 4.2 Immunofluorescent images of right DRG (6-week). A, B, and C show fluorescent signals in control (CC) DRG whereas D, E, and F show signals in DRG of the hindlimb unloaded (HU) group. G, H, and I show fluorescent signals in the electrical stimulated (ES) DRG. DAPI-labeled nuclei signals (A, D, and G). CGRP-immunoreactive signals (B, E, and H). Combined images of DAPI and CGRP signals (C, F, and I). (Scale bar = 0.1 mm)

4.2 Histomorphology of tibia

4.2.1 H&E staining

4.2.1.1 2-week treatment

At week 2, smaller trabecular numbers and thickness was observed in the proximal tibial metaphysis of the HU and ES groups compared to the CC group. In addition, the trabeculae were widely separated in the HU and ES groups (figure 4.3).

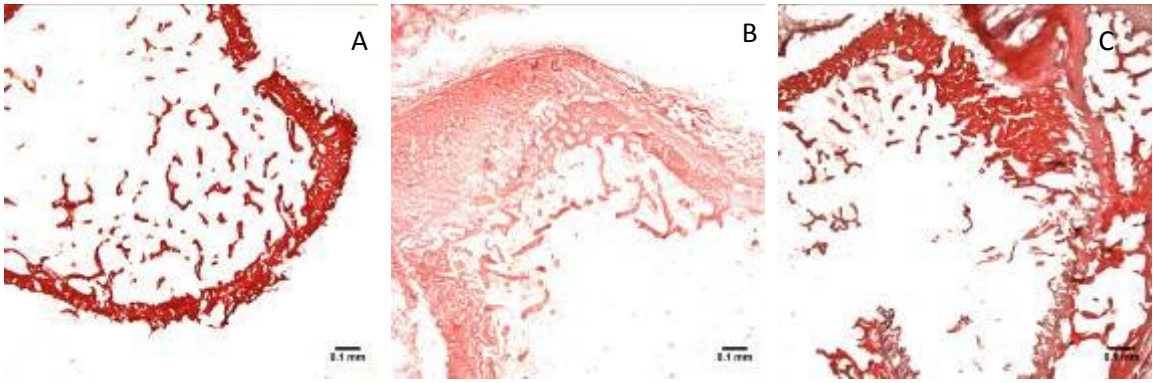

Figure 4.3 Histomorphology of proximal tibial metaphysis of 2-week groups (H&E staining)
A, B, and C show right tibias of the CC, HU, and ES groups respectively (Scale bar = 0.1 mm)

Figure 4.4 shows the histomorphology of tibial diaphysis at week 2. Howship's lacunae which indicated bone resorption by osteoclasts appeared in some HU and ES samples (figure 4.4B and 4.4C). In normal mature bone, osteoclasts were uncommonly seen. However, the occurrence of Howship's lacunae in the samples would imply the possibility of active bone remodeling in the region. In figure 4.4A and 4.4C, by comparing the edges of the cracks, the cracks were likely caused by stretching during tissue processing.

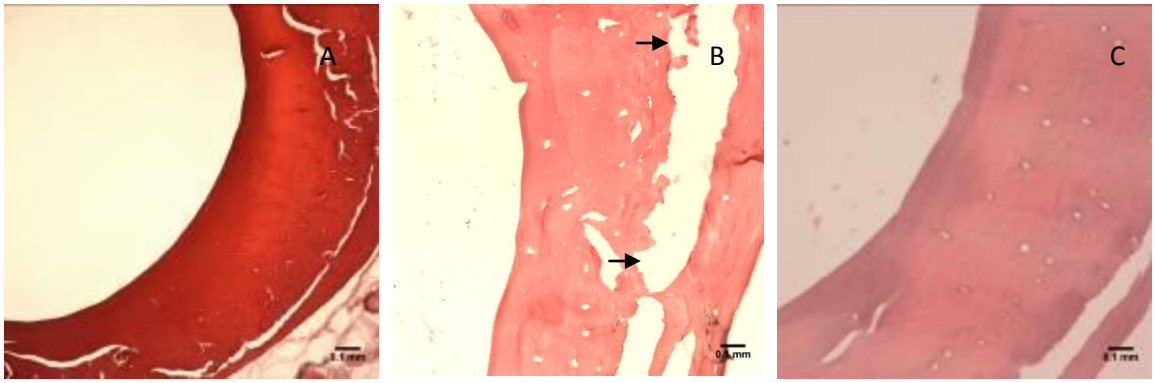

Figure 4.4 Histomorphology of tibial diaphysis of 2-week groups (H&E staining)
A, B, and C show right tibias of the CC, HU, and ES groups (Scale bar = 0.1 mm).
Arrows indicate locations of Howship's lacunae.

4.2.1.2 6-week treatment

At week 6, obvious osteoporotic conditions appeared in hindlimbs of HU animals. For instance, button phenomenon, which small islands of trabecular bones occurred instead of bars, was observed in trabecular compartments of proximal tibial metaphysis as indicated in figure 4.5B. Further, the number of trabecula in the HU and ES groups appeared to be less than that of CC samples (figure 4.5).

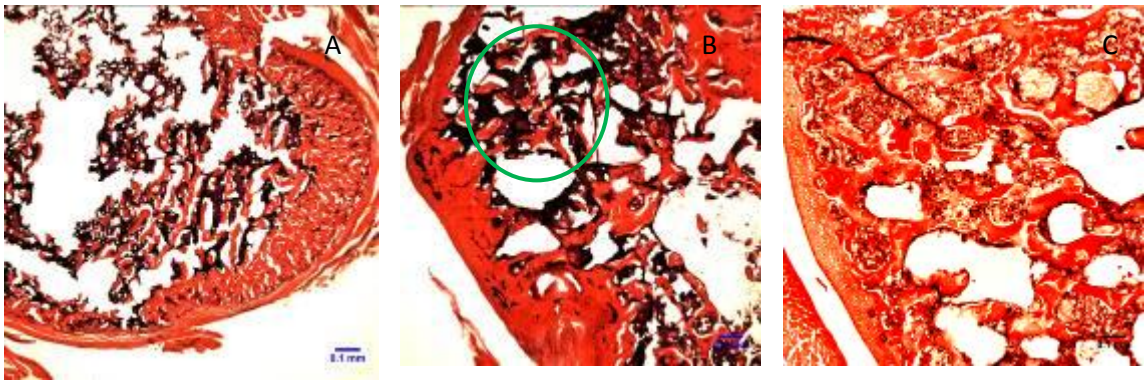

Figure 4.5 Histomorphology of proximal tibial metaphysis of 6-week groups (H&E staining)
A, B, and C show right tibias of the CC, HU, and ES groups respectively (Scale bar = 0.1 mm).
Circle indicates region showing button phenomenon.

After 6 weeks of treatment, no obvious change in morphology was observed in diaphysis of control samples. However, bone resorption as reflected by the occurrence of Howship's lacunae could be seen in both the HU and ES groups (figure 4.6). In addition, multiple cementing lines could be observed in the hindlimbs of the HU and ES animals indicating the occurrence of active bone remodeling at the diaphysis.

According to the results of hematoxylin and eosin staining, osteoporotic features appeared after 2 weeks of hindlimb unloading such that, in the proximal metaphysis, thinning of trabeculae could be observed and the number of trabeculae appeared to be less than the cage control. In the case of cortical bone, osteoclastic activity as reflected by the occurrence of Howship's lacunae was found in diaphysis of some unloaded tibia samples. The degree of osteoporotic deterioration appeared to be more pronounced upon prolonged unloading. After 6 weeks of hindlimb unloading, further deterioration in trabecular architecture appeared such that, in proximal metaphysis of some of the HU and ES samples, trabeculae existed in the form of small islands instead of bars which is known as button phenomenon. In addition, the degree of trabecular separation in hindlimb unloaded groups including both the HU and ES groups was higher while trabecular number and thickness were less compared to cage control. In the diaphyseal region, normal lamellar bone was observed in cage control samples whereas features of osteoclastic activity were found in both HU and ES samples. Similar to 2-week samples, Howship's lacunae were observed in diaphysis of both HU and ES samples but were more abundant after 6 weeks of hindlimb unloading. Further, multiple cementing lines could

be found in some samples implying that intensive bone remodeling activities occurred in the diaphyseal region of the unloaded tibias. Quantitative results from bone mineral density and bone micro-architecture measurement by pQCT and μCT would provide further information on the intergroup comparison on bone density and micro-structure among the three treatment groups.

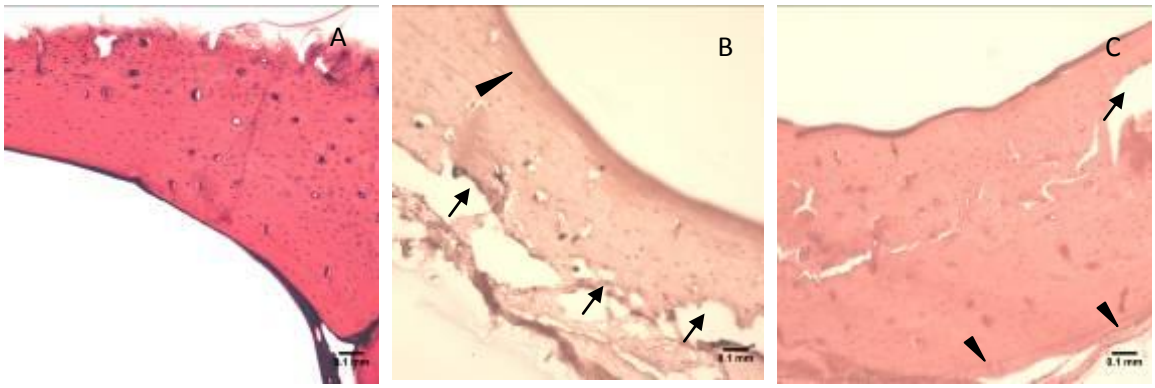

Figure 4.6 Histomorphology of tibial diaphysis of 6-week groups (H&E staining)
A, B, and C show right tibias of the CC, HU, and ES groups respectively (Scale bar = 0.1 mm).
Arrows indicate locations of Howship's lacunae whereas arrowheads indicate cementing lines.

4.2.2 CGRP Expression at bony tissue

4.2.2.1 2-week treatment

The expression of CGRP+ fibers in proximal tibial metaphyses was visualized by immunohistochemistry and fluorescence microscopy. After 2 weeks of treatment, CGRP+ nerve fibers were observed in all of the three groups. Co-staining with DAPI showed that CGRP+ signals co-existed with DAPI signals and were found mainly in the trabecular compartment (figure 4.7). By comparing the expression of CGRP signals among the three groups with one-way ANOVA and post-hoc LSD tests, the averaged density of CGRP+ fibers in

proximal tibial metaphyses of hindlimb unloaded animals was significantly lower than the cage control as well as the electrical stimulated animals ($p = 0.015$ and $p = 0.049$ respectively). However, no significant difference in averaged CGRP+ fiber density was found between the ES and CC group ($p = 0.446$) (table 4.2). Based on the quantified results of immunohistochemistry, hindlimb unloading was associated with reduced expression of CGRP+ fiber in proximal metaphyses of tibias. However, direct electrical stimulation at DRG appeared to reduce the decline in expression of CGRP+ fiber.

Table 4.2 Average CGRP+ fiber density in right proximal tibial metaphysis

	CC	HU	ES
CGRP+ fiber density at week 2 [mm^{-2}]	446.5±59.3	247.1±80.7*	398.2±107.2^
CGRP+ fiber density at week 6 [mm^{-2}]	542.02±285.20	112.7±34.1*	247.4±179.5

Values were means±SD.

*: Significant difference ($p < 0.05$) against cage control

^: Significant difference ($p < 0.05$) against hindlimb unloaded

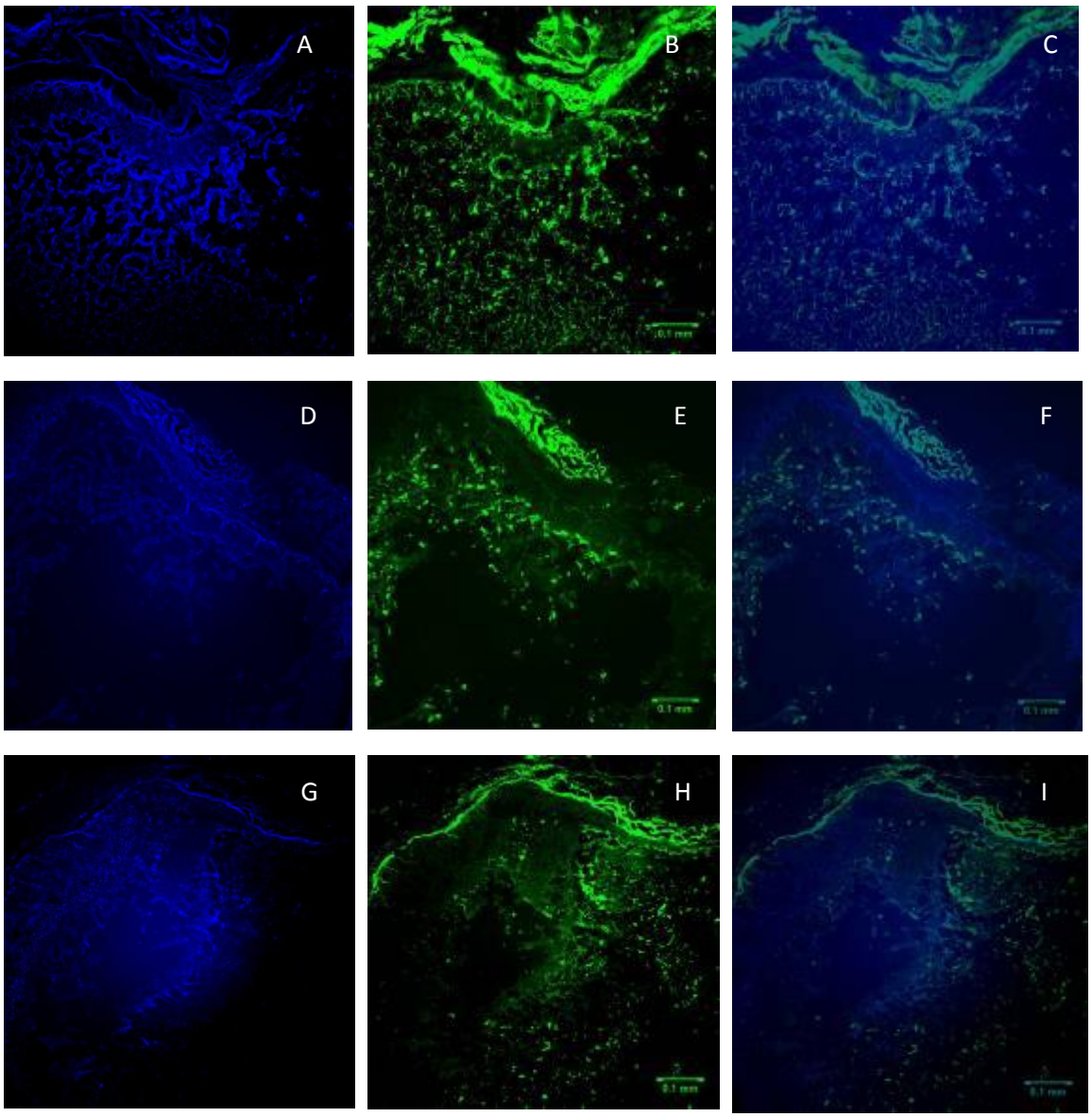

Figure 4.7 CGRP expression at right proximal tibial metaphysis of 2-week groups

A, B, and C show fluorescent signals in the control (CC) group whereas D, E, and F show signals in tibias of the hindlimb unloaded (HU) group. G, H, and I show fluorescent signals in the electrical stimulated (ES) group. DAPI-labeled signals (A, D, and G). CGRP-immunoreactive signals (B, E, and H). Combined images of DAPI and CGRP signals (C, F, and I). (Scale bar = 0.1 mm)

4.2.2.2 6-week treatment

The expression of CGRP+ fiber in proximal tibial metaphysis was visualized by immunohistochemistry (figure 4.8). After 6 weeks of hindlimb unloading, the average CGRP+ fiber density in proximal tibial metaphyses of the HU group was significantly lower than that of the cage control ($p = 0.012$, one-way ANOVA with post-hoc LSD test). However, unlike the results of 2-week treatment, no significant difference in average CGRP+ fiber density was observed between the HU and ES group ($p = 0.437$, one-way ANOVA with post-hoc LSD test). In addition, ANOVA revealed that no significant difference in expression of CGRP+ fiber in proximal tibial metaphyses existed between CC and ES as well ($p = 0.085$) (table 4.2).

The 6-week treatment demonstrated the prolonged effect of hindlimb unloading and electrical stimulation at DRG. According to the results of immunostaining, similar to the results of 2-week treatment, lower expression of CGRP+ fiber in tibial metaphyses was associated with unloading and the decline expression of CGRP+ fiber could probably be reduced by direct electrical stimulation at DRG. The treatment effects were expected to be sustainable for prolonged periods.

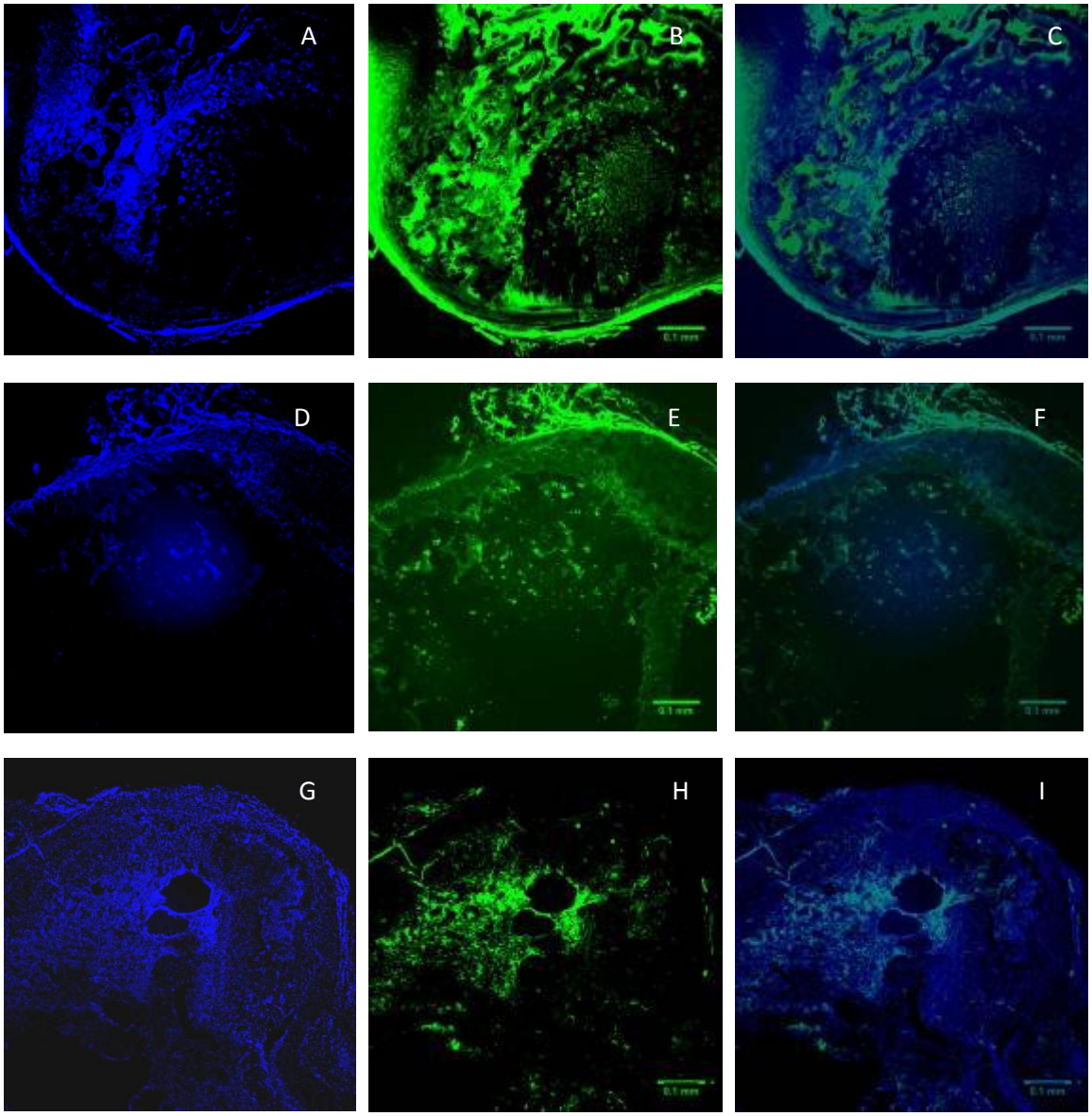

Figure 4.8 CGRP expression at right proximal tibial metaphysis of 6-week groups

A, B, and C show fluorescent signals in the control (CC) group whereas D, E, and F show signals in tibias of the hindlimb unloaded (HU) group. G, H, and I show fluorescent signals in the electrical stimulated (ES) group. DAPI-labeled signals (A, D, and G). CGRP-immunoreactive signals (B, E, and H). Combined images of DAPI and CGRP signals (C, F, and I). (Scale bar = 0.1 mm)

4.2.3 TRAP staining for osteoclasts

4.2.3.1 2-week treatment

In order to assess the activity of osteoclasts under decreased mechanical stimulation and in the presence of electrical stimulation at DRG, TRAP staining was performed on histological sections from proximal tibial metaphyses. Osteoclastic cells with TRAP activity were stained and visualized (figure 4.9). In general, osteoclasts were found mainly in periosteal and endosteal regions of the cortical compartments. Also, osteoclasts could be found randomly in trabecular compartments as well. After 2 weeks of treatment, TRAP+ cells were observed in all of the three treatment groups. However, based on the results of one-way ANOVA and post-hoc LSD test, the average density of TRAP+ cells in the hindlimb unloaded animals was significantly higher than both the cage control ($p = 0.018$) and the electrical stimulated group ($p = 0.013$) whereas no difference was found between the CC and ES groups ($p = 0.802$) (table 4.3). The results indicate that significantly higher osteoclastic activity exists in unloaded tibias. However, the osteoclastic activity was effectively inhibited by direct electrical stimulation at DRG.

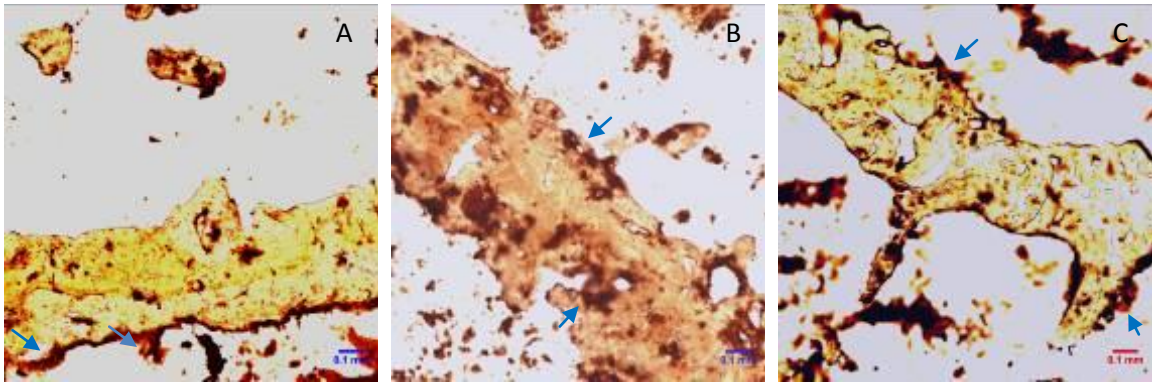

Figure 4.9 Localization of osteoclastic cells at proximal tibial metaphysis of 2-week groups
A, B, and C show right tibias of the CC, HU, and ES groups respectively (Scale bar = 0.1 mm). Arrows indicate osteoclastic cells stained in brown or brick-red color.

Table 4.3 Average osteoclastic cell density in right proximal tibial metaphysis

	CC	HU	ES
Osteoclastic cell density at week 2 [mm^{-2}]	30.4±16.8	69.0±17.8*	27.3±6.9^
Osteoclastic cell density at week 6 [mm^{-2}]	21.8±5.9	69.4±29.6*	10.8±1.2^

Values were means±SD.
*: Significant difference ($p < 0.05$) against cage control
^: Significant difference ($p < 0.05$) against hindlimb unloaded

4.2.3.2 6-week treatment

At week 6, osteoclastic activity was observed in all of the three treatment groups as well. The distribution pattern of TRAP+ signals was similar to the results of 2-week treatment. In addition, the results of one-way ANOVA and post-hoc LSD tests reflected that the average density of TRAP+ cells of the hindlimb unloaded animals was significantly higher than that of the cage control ($p = 0.013$) and electrical stimulated groups ($p = 0.011$). Moreover, no significant difference in osteoclastic cell density was observed between the CC and ES groups

(p = 0.502) (table 4.3). This result implies that the electrical stimulation at DRG could be sustained for prolonged periods.

4.2.4 ALP staining for osteoblasts

4.2.4.1 2-week treatment

The osteogenic activity by osteoblasts can be reflected by the activity of alkaline phosphatase (ALP). After 2 weeks of treatment, the activity of osteoblasts in proximal tibial metaphyses was visualized by ALP staining. The stained ALP regions located mainly at endosteum as well as periosteum (figure 4.10). According to the results of one-way ANOVA and post-hoc LSD tests, the average proportion of ALP active area among total bone area estimated in proximal metaphysis of hindlimb unloaded tibias was significantly lower than that of the cage control tibias (p = 0.012). However, there was no significant difference in proportion of ALP active area between cage control and electrical stimulated animals (p = 0.120). Further, there was no difference found between the HU and ES groups (p = 0.191) (table 4.4). These results imply that lowered osteoblastic activity in tibias was associated with decreased mechanical loading of hindlimb and the impact of unloading could be reduced by direct electrical stimulation at DRG.

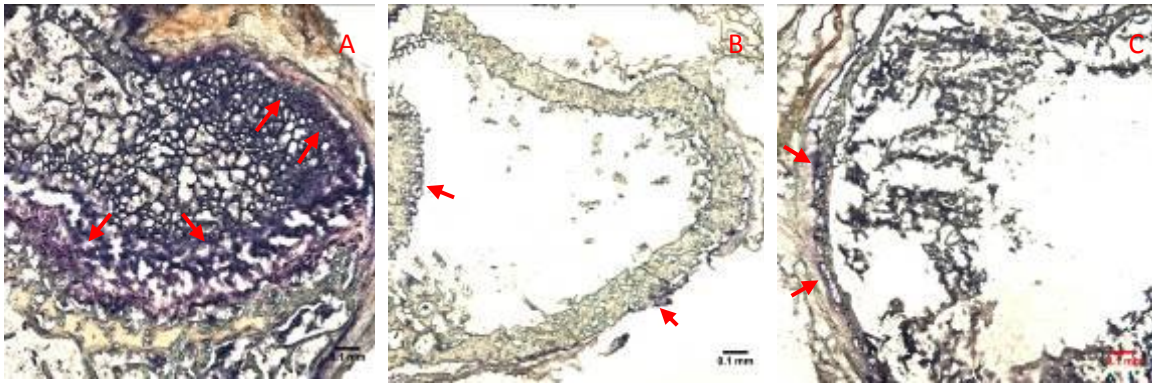

Figure 4.10 Localization of osteogenic activity at proximal tibial metaphysis of 2-week groups
A, B, and C show right tibias of the CC, HU, and ES groups respectively. (Scale bar = 0.1 mm)
Arrows indicate regions with intensive ALP activity.

Table 4.4 Average proportion of ALP active area in right proximal tibial metaphysis

	CC	HU	ES
Proportion of ALP active area at week 2 [% Bone area]	45.55±15.24	12.90±10.69*	27.65±17.47
Proportion of ALP active area at week 6 [% Bone area]	28.33±8.05	0.33±0.32*	23.13±15.64^

Values were means±SD.
*: Significant difference ($p < 0.05$) against cage control
^: Significant difference ($p < 0.05$) against hindlimb unloaded

4.2.4.2 6-week treatment

After 6 weeks of hindlimb unloading, the proportion of ALP active area in proximal metaphyses of unloaded tibias was very low and was significantly lower than that of the cage control ($p = 0.009$) and electrical stimulated groups ($p = 0.024$). However, the difference in proportion of ALP active area between the CC and ES groups was not significant ($p = 0.513$) (table 4.4). This result implied that prolonged hindlimb unloading would lead to dramatic decreased ALP activity and hence osteogenic activity by osteoblasts. However, direct electrical stimulation at DRG would effectively prevent the decline in osteoblastic activity under prolonged unloading.

4.3 Peripheral quantitative computed tomography of tibia

4.3.1 2-week treatment

Total BMC in proximal right tibia increased in the CC and ES groups while it decreased in the HU group. Comparing the percentage change in parameters measured from right tibias among three groups using one-way ANOVA, significant bone loss in terms of reduced total BMC as well as total and trabecular BMD was observed in proximal tibiae in the HU group as compared to the CC and ES groups ($p < 0.05$). There was no significant difference in cortical BMD among the three groups ($p > 0.05$) (Table 4.5).

In diaphysis, cortical BMD increased in all three groups. Cortical BMC decreased in the HU group, but one-way ANOVA showed no significant difference in percentage change of cortical BMD and BMC among the three groups ($p > 0.05$) (Table 4.6).

Table 4.5 Percentage change in bone quality parameters at right proximal metaphysis (time = 2 weeks)

	Cage control	Hindlimb unloaded	Hindlimb unloaded with electrical stimulation
Total BMC	16.91%±15.69%	–25.89%±12.02%*	3.76%±13.53%^
Total BMD	2.9%±5.52%	–22.98%±6.9%*	–6.19%±15.61%
Cortical BMD	–0.2%±5.37%	–7.7%±15.76%	–4.49%±15.19%
Trabecular BMD	5.87%±8.87%	–29.24%±7.13%*	–2.31%±21.22%^

Values were means±SD. BMC: Bone mineral content. BMD: Bone mineral density

*: Significant difference ($p < 0.05$) against cage control

^: Significant difference ($p < 0.05$) against hindlimb unloaded

Table 4.6 Percentage change in bone quality parameters at right diaphysis (time = 2 weeks)

	Cage Control	Hindlimb Unloaded	Hindlimb Unloaded with Electrical Stimulation
Cortical BMD	5.85%±4.62%	4.05%±3.19%	9.46%±3.72%
Cortical BMC	1.02%±3.31%	–0.85%±8.07%	0.10%±8.97%

Values were means±SD. BMC: Bone mineral content. BMD: Bone mineral density
*: Significant difference ($p < 0.05$) against cage control
^: Significant difference ($p < 0.05$) against hindlimb unloaded

4.3.2 6-week treatment

One-way ANOVA and post-hoc LSD tests showed that, upon 6 weeks of hindlimb unloading, significant decreases in bone mineral content and density were observed in proximal metaphyseal region of the HU group as compared to the CC group whereas increments in BMD and BMC were found in the cage control group ($p < 0.01$) (table 4.7). A significant decline in total and cortical BMD were observed in proximal metaphyseal regions of the ES group as compared to the CC group ($p < 0.01$). However, the decline in total and trabecular BMD and total BMC in proximal metaphysis in the ES group was significantly less than the HU group ($p < 0.01$). On the other hand, there was no significant difference in percentage change in metaphyseal cortical BMD observed between the HU and ES groups ($p = 0.059$).

In diaphysis, increased cortical BMD was observed in the right hindlimbs of all three groups. No significant difference in percentage change in diaphyseal cortical BMD existed among the three groups ($p > 0.05$, one-way ANOVA and post-hoc LSD tests). On the other hand, decreased cortical BMC was found in diaphysis of the HU and ES groups, but the cage control group showed a positive change (table 4.8). Further, the percentage change in cortical BMC in the right diaphysis of the HU and ES groups was significantly different from that of the CC

group (p = 0.003 and p = 0.002 respectively, one-way ANOVA and post-hoc LSD tests). However, the difference of diaphyseal cortical BMC and BMD was not significant between the HU and ES groups (p = 0.883, one-way ANOVA and post-hoc LSD tests).

Table 4.7 Percentage change in bone quality parameters at right proximal metaphysis at 6 weeks

	Cage control	Hindlimb unloaded	Hindlimb unloaded with electrical stimulation
Total BMC	21.44±25.20	–63.92±11.72*	2.70±25.06^
Total BMD	9.61±9.17	–46.79±8.13*	–9.15±5.88*^
Cortical BMD	12.35±8.23	–20.43±11.85*	–8.94±8.70
Trabecular BMD	2.66±11.30	–52.85±10.16*	–8.17±14.66^

Values were means±SD.
BMC: Bone mineral content. BMD: Bone mineral density
*: Significant difference (p < 0.05) against cage control
^: Significant difference (p < 0.05) against hindlimb unloaded

Table 4.8 Percentage change in bone quality parameters at right diaphysis at 6 weeks

	Cage control	Hindlimb unloaded	Hindlimb unloaded with electrical stimulation
Cortical BMD	8.42±4.13	4.53±5.99	4.58±2.04
Cortical BMC	11.23±7.80	–1.0±3.65*	–1.52±5.75*

Values were means±SD.
BMC: Bone mineral content. BMD: Bone mineral density
*: Significant difference (p < 0.05) against cage control

4.4 Bone micro-architecture of tibia

4.4.1 2-week treatment

Upon 2 weeks of hindlimb unloading, deteriorated micro-structural parameters were observed in the trabecular compartment of proximal tibial metaphysis of hindlimb unloaded groups including both the HU and ES groups (figure 4.13). By one-way ANOVA and post-hoc LSD tests, significantly reduced bone volume fraction (p = 0.038), lower connectivity density (p = 0.008), lower trabecular number (p = 0.034), but larger trabecular separation (p = 0.044) were

measured in the HU group compared to the CC group. In addition, larger structural model index (SMI) ($p = 0.011$) was estimated in the HU group indicating that a rod-like structure of trabeculae was induced upon unloading (160) (table 4.9). In the case of the electrical stimulated group, reduced deterioration of micro-architecture at the trabecular compartment of proximal tibial metaphysis was observed. Although significantly lower connectivity ($p = 0.032$) but larger SMI ($p = 0.044$) occurred in the ES group compared to the CC group, no significant difference in other micro-structural parameters existed between the ES and CC groups (table 4.9). In diaphysis, no significant difference in any of the micro-structural parameters existed among the treatment groups (table 4.10).

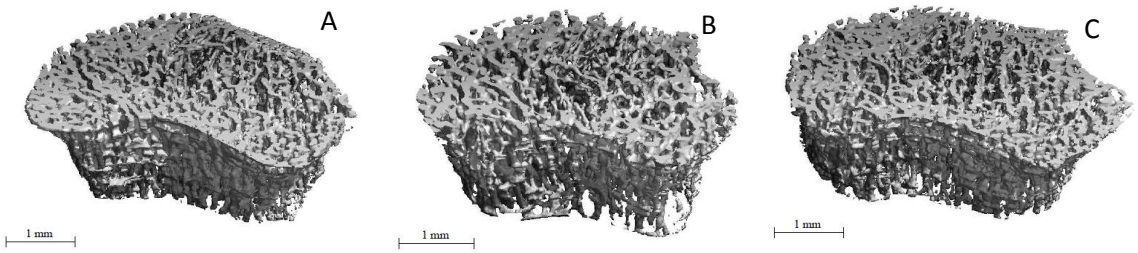

Figure 4.11 3D microstructures of proximal tibial metaphysis at week 2
A, B, and C show right tibias of the CC, HU, and ES groups respectively (Scale bar = 1 mm).

Table 4.9 Micro-structural parameters of proximal metaphysis of right tibia at week 2

	CC	HU	ES
BV/TV (%)	20.51±4.46	11.74±6.53*	13.46±4.03
Conn.D (#/mm^3)	81.84±20.38	33.21±25.38*	45.71±12.67*
SMI(#)	2.17±0.20	2.70±0.32*	2.56±0.15*
Tb.N (#/mm)	3.80±0.83	2.80±0.94*	3.07±0.66
Tb.Th (μm)	0.078±0.002	0.072±0.007	0.073±0.006
Tb.Sp (μm)	0.26±0.067	0.38±0.130*	0.33±0.091

*$p < 0.05$ against cage control

Table 4.10 Micro-structural parameters of diaphysis of right tibia at week 2

	CC	HU	ES
BV/TV (%)	65.12±2.53	63.92±2.75	67.07±2.28
TV mm^3	15.54±1.03	15.92±1.12	13.94±1.59
BV mm^3	10.12±0.75	10.16±0.71	9.33±0.83
Mean Density of TV (mgHA/ccm)	637.66±47.94	603.71±31.75	648.14±34.55
Mean Density of BV (mgHA/ccm)	1021.42±18.65	1010.46±10.15	1016.11±19.65

4.4.2 6-week treatment

At week 6, deteriorated micro-structural parameters were observed in proximal tibial metaphysis of hindlimb unloaded groups including both the HU and ES groups (figure 4.11). Significantly reduced bone volume fraction, lower connectivity density, lower trabecular number, but larger trabecular separation was measured in both the HU and ES groups compared to the CC group ($p < 0.05$). In addition, significantly larger trabecular spacing ($p = 0.029$) was estimated in the ES group compared to the CC group but the difference in trabecular spacing between the HU and CC groups was not significant ($p = 0.114$) (table 4.11). Further, no significant difference in trabecular thickness among treatment groups was observed ($p > 0.05$). No significant difference in all of the micro-structural parameters measured could be observed between the HU and ES groups ($p > 0.05$). In diaphysis, no significant difference in any of the micro-structural parameters existed between the HU and CC groups ($p > 0.05$). However, the total volume (TV) and bone volume (BV) of the ES group were significantly lower than that of the CC group ($p = 0.017$ and $p = 0.002$ respectively, one-way ANOVA and post-hoc LSD tests) (table 4.12).

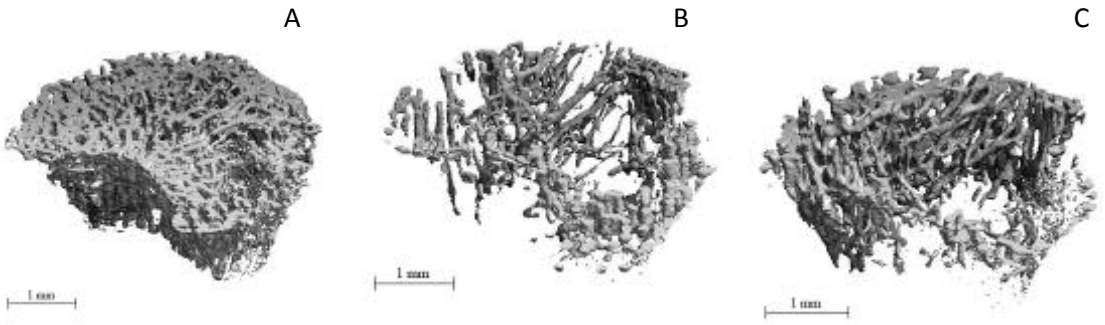

Figure 4.12 3D microstructures of proximal tibial metaphysis at week 6
A, B, and C show right tibias of the CC, HU, and ES groups respectively (Scale bar = 1 mm).

Table 4.11 Micro-structural parameters of proximal metaphysis of right tibia at week 6

	CC	HU	ES
BV/TV (%)	20.03±3.49	6.97±3.80*	3.03±3.21*
Conn.D(#/mm^3)	67.42±14.14	14.76±12.53*	4.88±6.01*
SMI(#)	2.25±0.25	2.86±0.22*	3.16±0.26*
Tb.N(#/mm)	3.04±0.51	1.78±0.74*	1.03±0.38*
Tb.Th(μm)	0.085±0.005	0.078±0.004	0.070±0.012
Tb.Sp(μm)	0.35±0.064	0.65±0.268	1.06±0.320*

*p < 0.05 against cage control

Table 4.12 Micro-structural parameters of diaphysis of right tibia at week 6

	CC	HU	ES
BV/TV (%)	64.27±0.89	63.30±2.28	60.85±2.68
TV mm^3	17.99±1.29	17.40±0.71	15.96±0.85*
BV mm^3	11.56±0.69	11.01±0.47	9.71±0.70*
Mean Density of TV (mgHA/ccm)	633.88±20.28	644.79±14.80	587.37±39.66
Mean Density of BV (mgHA/ccm)	1048.77±2.54	1035.38±6.81	1038.54±9.57

*p < 0.05 against cage control

4.5 Biomechanical properties of tibia

4.5.1 2-week treatment

Four out of ten right tibias were extracted from each group for biomechanical property evaluation. The stiffness and ultimate load of the tibias were evaluated by 3-point bending tests. According to the results of independent samples Kruskal-Wallis test, no significant

difference in stiffness (p = 0.61) and ultimate load (p = 0.288) was observed among the treatment groups after 2 weeks of treatment (table 4.13).

Table 4.13 Average stiffness and ultimate load of right tibial diaphyses (2 weeks)

	CC	HU	ES	p
Stiffness (N/mm)	216.63 (7.36)	248.65 (9.30)	263.10 (31.29)	0.61
Ultimate load (N)	98.97 (1.76)	108.33 (10.37)	110.40 (17.41)	0.288

(): Standard deviation, *p < 0.05 against cage control (CC)

4.5.2 6-week treatment

Independent samples Kruskal-Wallis test showed that there was no significant difference in stiffness and ultimate load among the treatment groups after 6 weeks of treatment (p = 0.061 and p = 0.066 respectively) (table 4.14).

Table 4.14 Average stiffness and ultimate load of right tibial diaphyses (6 weeks)

	CC	HU	ES	p
Stiffness (N/mm)	264.49 (22.64)	253.26 (18.98)	185.57 (19.34)	0.061
Ultimate load (N)	110.97 (1.83)	113.97 (7.93)	93.17 (18.44)	0.066

(): Standard deviation, *p < 0.05 against cage control (CC)

CHAPTER 5. DISCUSSION

5.1 The effects of electrical stimulation at DRG on CGRP expression in DRG

The results of this current study demonstrate that expression of CGRP in DRG could be enhanced by electrical stimulation generated by implantable devices. This finding suggests the electro-excitability and neuroplasticity of CGRP positive sensory neurons. In the study carried out by Brooks et al. electrical stimulation was applied on rat spinal cord slices *in vitro*. The stimulation parameters (20 V, 0.5 ms, and 10 Hz) had been demonstrated to evoke reliable CGRP-like immunoreactivity release (19). The parameters differed from those adopted in the current study (0.25 V, 90 μs, 150 Hz, and 61.3 μA) suggesting that excitation of CGRP-positive neurons could be achieved in a wide range of stimulation parameters. Non-invasive electrical stimulation has a poor spatial resolution (161). By comparing the occurrence of enhanced signals of CGRP, the enhancement of CGRP+ neuron expression was significantly higher in the stimulated DRGs than the non-stimulated DRGs of the hindlimb unloaded only (HU) group. In addition, the occurrence of CGRP+ signals in the HU group was significantly lower than that of the cage control group suggesting that mechanical stimulation would be one of the factors affecting the histomorphology of DRGs. However, no significant difference in CGRP+ neuron expression was observed between cage control and electrical stimulated DRGs. Nonetheless, intense CGRP+ signals, which were defined as signals with fluorescence intensity higher than the specific mean intensity by 2 times of standard deviation, were observed only in electrical stimulated DRGs but not in the CC and HU groups. These results suggest IMES can achieve high

near-cellular spatial resolution of electrical neurostimulation. And the expression of CGRP+ neurons could be enhanced effectively by electrical neurostimulation.

Previous studies demonstrate the compartment-specific differences of skeletal response to unloading and deficits in bone mineral density were likely to develop with longer duration unloading (157, 162-164). Thus, the temporal impact of unloading as well as electrical stimulation at DRG was investigated in the current study. Based on the results of prolonged 6-week treatment, an identical trend with the 2-week treatment could be observed that the average proportion of CGRP+ neuron in hindlimb unloaded animals was significantly lower than that of the cage control as well as the electrical stimulated animals. Although no significant difference in enhanced signals could be observed between cage control and electrical stimulated group, intense signals were observed only in electrical stimulated DRGs. The result suggests that, in addition to enhancing the expression of CGRP+ neuron in DRG, the effect of direct electrical stimulation at DRG could be sustainable after prolonged periods.

5.2 The effects of electrical stimulation at DRG on bone quality of unloaded tibia

5.2.1 Histomorphology

5.2.1.1 H&E staining

It has been well published that disuse conditions would induce osteoporotic symptoms (64-68). For instance, unloading was shown to induce bone loss in both humans (70, 71) and animals (88, 143). In the current study, smaller trabecular number and thickness but larger trabecular

spacing was observed in proximal metaphyses of unloaded tibias including both HU and ES groups compared to cage control after 2 weeks of hindlimb unloading. On the other hand, bone resorption indicated by the occurrence of Howship's lacunae was observed in tibial diaphyses of both HU and ES samples. These observations suggest the possibility of active bone remodeling in the regions and the bone remodeling was likely to be associated with hindlimb unloading.

After a prolonged period of hindlimb unloading, severe osteoporotic conditions were found in hindlimb unloaded tibias that further decline in trabecula number, and button phenomenon of trabecular bones occurred in the trabecular compartment of proximal tibial metaphyses. In addition, bone resorption as reflected by the occurrence of Howship's lacunae could be seen in both HU and ES groups. Furthermore, multiple cementing lines were observed in tibial diaphysis of HU and ES animals indicating the occurrence of active bone remodeling at the region.

These observations complied with the findings in former studies that unloading would lead to deterioration on bone micro-architecture and the deterioration was more pronounced in trabecular compartment (157). Further analysis of quantified results of pQCT and μCT would facilitate intergroup comparison on bone quality among the treatment groups.

5.2.1.2 CGRP expression at bony tissue

A previous study by Ivanusic (2009) demonstrated by retrograde labeling that rat tibial periosteum, medullary cavity, and trabecular bone were all innervated by sensory CGRP immunoreactive neurons (165). More importantly, Offley et al. (2005) demonstrated that capsaicin-sensitive sensory neurons contributed to the maintenance of trabecular bone integrity. Capsaicin-sensitive neurons had efferent functions in the tissues they innervated and the effects were mediated by transmitters released from the peripheral nerve terminals (166-168) where capsaicin treatment would destroy unmyelinated sensory axons, reduce CGRP content in sciatic nerve and proximal tibia and inhibit neurogenic extravasation. In rat tibias, loss of BMD in the metaphyses but increased osteoclast number and surface were observed after 4 weeks of capsaicin treatment. In addition, impaired osteoblast activity and bone formation as well as diminished trabecular bone volume and connectivity occurred after capsaicin treatment as well (166). Based on the evidence of impaired CGRP signaling and its associated adverse impact on bone integrity, expression of CGRP+ neurons in tibias was crucial for maintaining bone integrity. Thus, the expression of CGRP+ neurons in proximal tibia was evaluated in the current study.

In the current study, expression of CGRP+ fibers was observed in proximal tibial metaphyses of all treatment groups. Co-staining with DAPI showed that CGRP+ fibers were found mainly in the trabecular compartment. After 2 weeks of hindlimb unloading, the average density of CGRP+ fibers of hindlimb unloaded animals was significantly lower than that of cage control as

well as electrical stimulated animals but no difference was observed between the cage control and electrical stimulated groups suggesting that unloading was likely to down regulate the expression of CGRP+ fibers in unloaded tibias. However, the impact of unloading would be reduced by direct electrical stimulation at DRG. Further, by comparing the expression of CGRP+ neurons in DRG and proximal tibial metaphysis, the expression of CGRP+ fibers at proximal tibial metaphysis was likely to be associated with CGRP+ neurons expressed in DRG.

Similarly, after 6 weeks of treatment, the average density of CGRP+ fibers in hindlimb unloaded animals was significantly lower than that of cage control but the difference in CGRP+ fiber expression between hindlimb unloaded only and those with electrical stimulation at DRG was not significant. However, there was no significant difference in CGRP+ fiber expression between the cage control and electrical stimulated groups as well. The results suggest that the impact of hindlimb unloading in terms of reducing CGRP immunoreactive neurons at proximal tibial metaphysis could be sustained for prolonged periods and direct electrical stimulation at DRG was likely to reduce the reduction.

5.2.1.3 Osteoclastic activity

Mechanical stimulation is important for maintaining bone mass and integrity (169). Upon unloading condition, impairments in maintenance of bone mass result due to loss of mechanical stress (170). Previous studies have reported that osteopenia induced by skeletal unloading was caused by inhibition in bone formation, decreased trabecular bone, and cortical thickness as well as accumulation of marrow fats (171-173). These changes were associated

with the reduction in osteoblasts on the bone surface (174-177). However, the effect of skeletal unloading on bone resorption was less clear. The findings in previous animal studies were not consistent: reports suggested that unloading would increase the number of osteoclasts on bone surface and bone resorption (178, 179), whereas other works showed that unloading had no effect on osteoclastic activity (174, 175, 180).

In the current study, increased osteoclastic activity was observed after 2 weeks of hindlimb unloading as reflected by the significant higher averaged density of TRAP+ cells in the HU group compared to the cage control group. The osteoclastic activity was concentrated mainly in the periosteal and endosteal regions of the cortical compartment. The average density of TRAP+ cells in electrical stimulated samples was significantly lower than those in hindlimb unloaded only sample and no difference was found between the cage control and electrical stimulated groups suggesting that electrical stimulation at DRG would inhibit osteoclastic activity in unloaded tibias.

According to the TRAP staining results of 6-week treated samples, the average density of osteoclastic cells in unloaded proximal tibial metaphyses was significantly higher than that of cage control implying that higher osteoclastic activity as well as bone resorption occurred in hindlimb unloaded animals. Similar to the findings of 2-week treated samples, osteoclastic cell density in electrical stimulated animals was significantly lower than that on hindlimb unloaded ones while the difference between cage control and electrical stimulated groups was not

significant. These results suggest that the impact of prolonged unloading on osteoclastic activity in unload tibias would be suppressed effectively by direct electrical stimulation at DRG.

5.2.1.4 Osteoblastic activity

Bone remodeling homeostasis depends on the tightly coupled bone formation and resorption. Disturbance in the balance between bone formation and resorption would lead to an abnormal increase in bone mass such as osteopetrosis or, on the contrary, osteoporosis. Previous reports demonstrated that unloading would cause increased and rapid bone resorption by osteoclasts and decreased bone formation by osteoblasts (181-184). The results of the current study complied with the previous findings that osteoclastic activity would be increased by unloading. However, it is important to understand the impact of unloading on bone formation by osteoblasts as well as its response to electrical stimulation at DRG. Thus, ALP staining was performed to evaluate the level of osteoblastic activity.

In proximal tibial metaphyses, osteoblastic activity was found to be concentrated in the endosteal and periosteal regions. After 2 weeks of hindlimb unloading, the averaged proportion of ALP active area among total bone area estimated in unloaded tibias was significantly lower than that of the cage control group but no difference was found between the ES and HU groups. However, the difference in proportion of ALP active area between cage control and electrical stimulated groups was not significant. Thus, the current results suggest that osteoblastic activity would be suppressed by unloading and electrical stimulation at DRG would reduce the suppression on osteoblastic activity.

At week 6, a significantly lower proportion of ALP active area was observed in the hindlimb unloaded only group compared to that cage control and electrical stimulated groups whereas the difference between the cage control and electrical stimulated groups was not significant. The results further confirm that prolonged unloading would lead to a decline in osteoblastic activity but the impact could likely be reduced by direct electrical stimulation at DRG.

5.2.1.5 Summary of histomorphological results

Summarizing the results of histomorphology, features of enhanced bone resorption could be observed in unloaded tibias of the HU and ES groups that the number and thickness of trabeculae in proximal metaphyses were decreased as compared qualitatively to the cage control group. In addition, signs of bone resorption were found in diaphysis as well. The osteoporotic features were more obvious after prolonged treatment. Typically, button phenomenon of trabeculae was found in proximal tibial metaphyses of hindlimb unloaded animals including both HU and ES groups. Further resorption was observed in diaphyses of HU and ES samples and intensive bone remodeling was likely to occur at diaphyseal region as indicated by the occurrence of multiple cementing lines. Based on qualitative observation, unloading would induce osteoporotic conditions in unloaded tibias compared to cage control rats and the impact was more pronounced after prolonged treatment. However, the difference between electrical stimulated and non-stimulated animals could not be distinguished precisely by qualitative observation.

The expression of CGRP-immunoreactive neurons in proximal tibial metaphysis could be altered by unloading as well as electrical stimulation at DRG so that the density of CGRP+ neurons in the hindlimb unloaded group was significantly lower than that of cage control. However, no difference in the density of CGRP+ neurons could be found between the cage control and electrical stimulated groups indicating that the impact of unloading on the expression of CGRP+ neurons would likely to be reduced by direct electrical stimulation at DRG. In addition, the results of prolonged treatment suggested the sustainability of effect of electrical stimulation.

The balance between bone resorption by osteoclasts and bone formation by osteoblasts was crucial for maintainance of bone mass and integrity. The current results of TRAP and ALP staining demonstrated the impact of different treatments on the activities of osteoclasts and osteoblasts respectively. After 2 weeks of hindlimb unloading, the density of osteoclasts in proximal metaphysis of unloaded tibias was significantly higher than that of the cage control and the electrical stimulated samples whereas the average proportion of ALP active areas in the proximal tibial metaphyses of the hindlimb unloaded only group was significantly lower than the CC and ES groups. However, the difference in TRAP and ALP activities between the cage control and electrical stimulated groups were not significant. These results indicate that unloading would increase osteoclastic activity but decrease osteoblastic activity. Direct electrical stimulation at DRG would counteract the impact of unloading by suppressing the increase in osteoclastic activity and reduce the decline in osteoblastic activity. Moreover, the

results of prolonged treatment further confirmed the treatment effects of direct electrical stimulation at DRG on the activities of osteoclasts and osteoblasts in unloaded proximal tibia to be sustainable. Further, the altered activities of osteoclasts and osteoblasts in proximal tibial metaphyses was likely to be affected by the expression of CGRP+ neurons at the region as suggested by a previous study (185).

5.2.2 Bone densitometry

The results demonstrated the impacts of unloading as well as electrical stimulation at DRG on bone mineral density in rats. After 14 days of hindlimb unloading, a dramatic decline in total BMC and trabecular BMD occurred in proximal tibia metaphysis. These results complied with findings reported in previous studies (157, 186) that decrease of bone mineral density could be induced by hindlimb unloading and the effects were mainly in trabecular bone. In evaluating the effects of electrical stimulation at DRG on bone mineral density, the percentage change in bone quality parameters between the HU and ES groups were compared. It was found that the decrease of total BMD and trabecular BMD in the ES group was significantly less than that in the HU group. This finding suggests that the electrical stimulation to DRG can effectively reduce bone loss caused by unloading.

The results of 6-week pQCT complied with previous findings that a decline in bone mineral content and density could be induced upon prolonged unloading (186, 187). Also, the deterioration was more pronounced in the trabecular compartment as compared to the cortical region. Further, it was confirmed that direct electrical stimulation at DRG was effective

in reducing bone loss due to hindlimb unloading as reflected by the significant difference in percentage loss in BMC and BMD between the HU and ES groups. In metaphysis, although a significant decrease in total BMD against cage control was observed in the ES group, percentage loss in total and trabecular BMD as well as total BMC of the ES group was significantly less than the HU group. On the other hand, in diaphysis, increment in cortical BMD was found in all three groups of animals. However, the trend of increment in hindlimb unloaded groups was lower than the CC group though the difference was not significant. This observation agreed with previous results that the impact of unloading was more concentrated in the trabecular compartment (187). Nonetheless, a significant difference in percentage change in cortical BMC was observed between cage control and hindlimb unloaded animals (both HU and ES) and a decrease in cortical BMC was observed in both the HU and ES groups. Summarizing the results in metaphyseal and diaphyseal regions, prolonged electrical stimulation at DRG could effectively reduce the decline in bone mineral in the trabecular compartment. However, its effect in the cortical region was not significant in both metaphysis and diaphysis.

To our knowledge, this is the first study on the effect of electrical stimulation to DRG via IMES on preventing disuse bone loss. It has shown promising results in the high near-cellular-spatial resolution and the effectiveness in reducing disuse bone loss and the effect was obvious in the trabecular compartment.

The pQCT results suggest potential application of IMES in the prevention and treatment of musculoskeletal diseases. Together with the results of bone histomorphology, it was expected that the reduced decline in BMC and BMD in electrical stimulated animals was mediated by the suppressed osteoclastic activity and enhanced osteoblastic activity, which in turn was triggered by enhanced expression of CGRP+ neurons at proximal metaphyseal region of the unloaded tibias.

5.2.3 Bone micro-architecture

According to the results of micro-computed tomography, significant deterioration in bone micro-architecture was observed in the HU group as reflected by the substantial lower proportion of bone content, connectivity density, and the trabecular number in trabecular compartment of proximal tibial metaphysis compared to the control group. Also, the trabecular separation of the proximal metaphyseal region in the HU group was significantly larger than that of the control group which further demonstrated the deterioration in bone micro-architecture in the trabecular compartment upon unloading. These observations complied with the findings of previous studies (188, 189). The SMI of the HU group was significantly larger than that of the control group suggesting the occurrence of conversion from plate elements to rod elements in trabeculae of the HU animals (160). In comparing the micro-structural parameters between the ES and CC groups, the trabeculae of the ES animals was significantly less connected than that of control group and the SMI of the ES group was larger than that of the CC group as well. These indicated that a certain level of micro-

architectural deterioration did occur in the metaphysis of tibias of the ES animals. However, no significant difference in other measured micro-structural parameters existed between the ES and CC groups. Thus, by comparing the differences in micro-structural parameters with CC of HU and that of ES, the deterioration in micro-architecture of tracbeculae at proximal tibial metaphysis in ES was less severe compared to HU. However, no significant difference was observed in diaphysis among the three groups indicating that the impact of unloading exposure as well as electrical stimulation treatment was concentrated in the trabecular compartment but not in the cortical compartment during the 2-week treatment.

In the case of the 6-week treatment, a significant deterioration in bone micro-architecture was observed in both the HU and ES groups in particular that significant lower bone volume fraction, lower trabecular connectivity and number were found as compared to the cage control group. In addition, a substantial increase in SMI in both the HU and ES groups was found indicating the occurrence of conversion from plate elements to rod elements in trabeculae. However, trabecular spacing of the electrical stimulated groups was significantly higher that of the cage control group but that between the CC and HU groups was not significant suggesting that the deterioration in micro-architecture of electrical stimulated animals was more severe than the HU group though no significant difference in any of the micro-structural parameters between the ES and HU groups was observed. In the diaphysis, no significant difference in micro-structural parameters was observed between cage control and hindlimb unloaded only animals. However, the total volume and bone volume of the ES group

were significantly less than those of the cage control group. However, no significant difference in bone volume fraction as well as mean density of total volume and bone volume existed among the treatment groups. Thus, the significant lower total volume and bone volume would be due to the smaller physical size of tibia samples in the ES animals, which could be reflected by the body weight of animals (table 5.1). Further, the Pearson's correlations between final body weight and micro-architectural parameters of 6-week treated animals were evaluated and significant correlations with weight were observed in all micro-architectural parameters except mean density of TV in diaphysis (table 5.2 and 5.3). This suggested the possibility that physiological and/or psychological factors existed and affected both body weight and bone micro-architecture of the animals.

Table 5.1 Average body weight of 6-week treated animals

	CC	HU	ES
Initial body weight [g]	426.4±13.1	440.7±26.7	397.4±39.7^
Final body weight [g]	531.2±22.0	408.0±25.1*	323.1±62.2*^

Values were means±SD.

*: Significant difference ($p < 0.05$) against cage control

^: Significant difference ($p < 0.05$) against hindlimb unloaded

Table 5.2 Pearson's correlation between final body weight and micro-architectural parameters of 6-week treated animals (proximal metaphysis)

	BV/TV	Conn.D	SMI	Tb.N	Tb.Th	Tb.Sp
Weight	0.917**	0.928**	-0.865**	0.896**	0.614*	-0.804**

**: Significant correlation ($p < 0.01$)

*: Significant correlation ($p < 0.05$)

Table 5.3 Pearson's correlation between final body weight and micro-architectural parameters of 6-week treated animals (diaphysis)

	BV/TV	TV	BV	Mean Density of TV	Mean Density of BV
Weight	0.587*	0.669*	0.776**	0.475	0.586*

**: Significant correlation ($p < 0.01$)

*: Significant correlation ($p < 0.05$)

Osteoporosis is characterized by substantial reduction on bone density and deteriorated bone micro-architecture (88). The majority of previous investigations on osteoporosis tended to evaluate bone quality based on bone mineral density (BMD) (66, 115, 190, 191). Micro-computed tomography is an evolving technique which is capable of providing three-dimensional (3D) bone micro-architectural data in an automated, objective, and non-destructive manner (192). Thus, 3D bone micro-structural data were crucial for comprehensive evaluation of bone quality. In the current study, the impact of electrical stimulation at DRG on bone micro-architecture of tibias exposed to unloading was evaluated. The results of 2-week treatment showed that reduced deterioration in bone micro-architecture was observed in the trabecular compartment of proximal tibial metaphysis of electrical stimulated animals. The prolonged treatment results demonstrated that the treatment effect of electrical stimulation was attenuated and no significant difference in bone micro-structural parameters was observed between the HU and ES groups. However, it is important to realize that the metabolism of bone could be affected by various factors. After the prolonged treatment period, body weights of the HU and ES animals were significantly lower than that of the cage control animals and the ES rats were significantly lighter than the HU rats (table 5.1). There were various potential reasons for the weight loss in the hindlimb unloaded animals such as malnutrition and mental stress. However, either malnutrition (193) or mental stress (194, 195) had been reported to be associated with decreased bone density and thus these factors might interfere with the treatment effect to a certain extent. On the other hand, inflammation induced after surgical procedures would be associated with depression in ES rats leading to

weight loss as well (196-198). For instance, during the course of an infection, sickness behaviors could be observed in animals (199). Further, the condition would include sickness symptoms that show considerable overlap with depression such as depressed mood, reduced social interaction and sleep disturbance (200).

5.2.4 Biomechanical properties

After 2 weeks of treatment, no significant difference in stiffness and ultimate load among all groups was observed. This result was consistent with the results of both pQCT and μCT. In this study, 3-point bending was performed to evaluate the biomechanical properties of tibia samples. However, force was applied only at the diaphyseal region of the tibia during bending and thus the results obtained reflected only the stiffness and ultimate load at diaphyseal region. No significant difference in change in bone mineral density and micro-structural parameters in diaphysis were observed among the treatment groups. In addition, the results complied with previous findings that the impact of unloading in diaphysis was less obvious compared to metaphysis (157).

At week 6, although diaphyseal cortical BMC of the ES and HU groups was significantly lower than that of the cage control group and total volume and bone volume of the ES group was significantly lower than that of the control group, no significant difference in stiffness and ultimate load existed among the three groups. However, the trend of biomechanical properties matched the trends of both pQCT and μCT in that lower stiffness and ultimate load were observed in the electrical stimulated group. As discussed, the lower stiffness and

ultimate load could be partially explained by the smaller physical sizes of the tibia samples of the ES group as reflected by the significant lower total volume and bone volume.

5.2.5 Summary

Summarizing the findings of the current study, direct electrical stimulation at dorsal root ganglion via implanted stimulator was able to enhance the expression of CGRP+ neurons and this enhancement was associated with the increased expression of CGRP+ neurons at proximal metaphysis of unloaded tibias. It has been well reported that unloading would induce disuse osteoporosis especially in weight bearing bones such as femurs and tibiae. The results of the current study demonstrate that a decline in bone mineral density and deteriorated bone micro-structural occurred upon unloading and the impact would be more obvious after prolonged periods. Moreover, the osteoporotic symptoms were concentrated in the trabecular compartment whereas the progress of bone loss in the cortical area occurred at a slower pace. Upon unloading, increased osteoclastic activity and lower osteoblastic activity were observed in hindlimb unloaded only animals. The altered activities of osteoclasts and osteoblasts led to a disturbance in the balance between bone resorption and formation and would explain the decline in bone mineral density and deteriorated bone micro-architecture. In the presence of electrical stimulation at dorsal root ganglion, expression of CGRP+ neurons in DRG as well as CGRP+ fibers at proximal tibial metaphysis was enhanced. The enhancement in CGRP+ fibers altered the rates of bone formation and resorption by changing the activities of osteoblasts and osteoclasts respectively. Thus, reduced decline in bone mineral density and bone micro-

structure were observed in unloaded tibias of the ES animals compared to the HU group. After prolonged treatment, suppressed osteoclastic activity, enhanced osteoblastic activity and reduced decline in bone mineral density were observed in electrical stimulated animals as compared to the hindlimb unloaded only group. These results demonstrated the prolonged efficacy of direct electrical stimulation at DRG on preserving bone quality under exposure to micro-gravity. However, the results of μCT showed that a substantial deterioration in micro-structure occurred in proximal tibial metaphyses of both the HU and ES animals and no significant difference in all of the micro-structural parameters between the HU and ES groups, except the significant higher trabecular spacing in the ES group. However, taking the body weight of rats into consideration, it was possible that the treatment effect of electrical stimulation had been influenced by other physiological and/or psychological factors. For instance, Campbell et al (2011) demonstrated that combined treatment with parathyroid hormone (PTH) and alendronate would enhance bone architecture compared to monotherapy but maintaining the state of surface mineralization in ovariectomized rats (201). This suggested the possibility that bone mineralization and micro-architecture could be affected differently by physiological and/or psychological factors.

Based on the results of the current study, direct electrical stimulation at DRG by implantable devices would preserve bone mineral density and bone micro-architecture in unloaded tibia by enhancing expression of CGRP+ neurons in DRG and CGRP+ fibers at proximal metaphysis. The

enhancement in CGRP+ fibers, in turn, suppressed activity of osteoclasts but enhanced activity of osteoblasts.

5.3 Limitations

In the current study, the stimulation voltage (0.25 V) was defined based on the results of an *in vivo* measurement experiment. However, other treatment parameters such as treatment current, period and frequency (61.3 µA, 90 µs, 150 Hz) as well as the rectangular stimulation waveform were adopted from the protocol of beep brain stimulation (DBS) developed by our team previously (146, 202). It would be possible that better treatment outcomes could be yielded if other values of treatment parameter had been applied. For instance, electrical stimulation with long pulse durations was more sensitive to the pulse's shape whereas rectangular pulses were most optimal for short pulse durations (203). Thus, further investigations with various treatment parameters would be needed in order to optimize treatment outcomes. Besides treatment parameters, further improvements on the physical size and shape of the implanted stimulator are required in order to minimize the trauma created to the animals. The current dimensions and weight of the IMES (dimensions: 25 mm x 20 mm x 8 mm, weight: 5.86 g) were reduced compared to the original prototype, which was designed for DBS (202). However, the size of the IMES was relatively large as compared to the body of rats and a smaller electrical stimulator would be expected to reduce the trauma as well as restriction in motion of the lumbar region after surgery.

The current study evaluated the treatment outcomes on the stimulated (right) side only. However, the systemic effects of electrical treatment at DRG were yet to be investigated. The treatment outcomes observed on the left DRGs and tibias as well as in spinal cords at the stimulated levels would provide a more comprehensive picture on the systemic treatment outcomes. In addition, the current study focused on the expression of CGRP. However, there were other potential transmitters of metabolic control of bone in the nervous system such as substance P, vasoactive intestinal peptide (VIP), and leptin (204). Further investigations on the impact of expressions of these potential neural peptides would provide more information on the action mechanism of the current treatment and the roles of nervous tissue in regulating bone biology.

In the evaluation of CGRP signals in DRGs, semi-quantified signal counting was applied to measure the level of CGRP expression, and this protocol has been widely used in previous research. However, quantification of real-time polymerase chain reaction (real-time PCR) would provide more precise quantification on CGRP expression.

In the current study, the biomechanical properties of tibia samples were evaluated by 3-point bending. However, the test reflected mainly the biomechanical properties of the diaphyseal region of the tibias but the treatment effects of current electrical stimulation treatment as well as hindlimb unloading were more pronounced at the proximal metaphysis. Hence, current mechanical tests could not reflect the treatment effects in terms of biomechanical properties precisely. Further investigations using micro- or nano-indentation would provide precise and

compartment-specific measurement on the impact of electrical stimulation at DRG and hindlimb unloading on biomechanical properties of unloaded tibias. Besides, the variation for mechanical testing could be large and larger sample size would help yielding accurate results. However, in the current study, only 4 tibia samples were available for mechanical testing while the other tibia samples were reserved for histological analysis. Hence, this was one of the limitations of the current study.

5.4 Implications of the current study

The current study demonstrated that direct electrical stimulation at DRG would increase CGRP+ neuron expression at DRG and proximal tibial metaphysis. The increased expression of CGRP+ neurons at proximal tibial metaphysis in turn enhanced the activity of osteoblasts and suppressed the activity of osteoclasts in the region leading to a reduced decline in bone mineral density and reduced deterioration in bone micro-architecture. However, the treatment effects in preserving bone micro-architecture appeared to be affected by other physiological and/or psychological factors such as depression and inflammation after prolonged periods. Further investigations on the potential impact of these factors on bone quality would help explain the decline in bone micro-architecture of ES animals after prolonged period. The findings of the current study expanded our knowledge on the impact of electrical stimulation on DRG and bone exposed to unloading as well as the potential action mechanism. More importantly, the current results proved the potential of *in vivo* electrical stimulation at DRG with IMES on preventing disuse bone loss upon unloading.

CHAPTER 6. SUMMARY OF FINDINGS AND CONCLUSION

As mentioned in Chapter 2, the aim of this study is to investigate the impact of electrical stimulation at dorsal root ganglia on disuse osteoporosis and the underlying mechanism. Based on this aim, the following objectives were addressed:

I. To investigate whether *in vivo* electrical stimulation at DRG can enhance CGRP expression in DRG.

II. To investigate the histomorphological change in tibias exposed to unloading with or without electrical stimulation at DRG.

III. To compare the difference in change in bone mineral density, bone micro-architectural parameters and biomechanical properties of unloaded tibias between electrical stimulated and non-stimulated animals.

IV. To investigate the prolonged effects of electrical stimulation at DRG on tibia quality in terms of histomorphology, bone mineral density, bone micro-architecture, and biomechanical properties.

6.1 Impact of *in vivo* electrical stimulation at DRG on CGRP expression in DRG

The results of the current study showed that expression of CGRP+ neuron in DRG could be enhanced by electrical stimulation generated by IMES suggesting the electro-excitability and neuroplasticity of CGRP positive sensory neurons. Also, by comparing the current treatment

parameters and those in previous studies, excitation of CGRP-positive neurons could be achieved in a wide range of stimulation parameters. The results of prolonged treatment demonstrated that the effects of electrical stimulation at DRG could be sustained after prolonged periods.

6.2 Histomorphological change in tibias exposed to unloading with or without electrical stimulation at DRG

Upon unloading, based on H&E staining, the number and thickness of trabeculae in proximal metaphyses of the HU and ES animals were decreased as compared to the cage control animals. Also, signs of bone resorption were found in diaphysis as well. After prolonged treatment, the osteoporotic features were more obvious in that button phenomenon of trabeculae was found in proximal tibial metaphyses of hindlimb unloaded animals including both the HU and ES groups. In addition, further resorption was observed in diaphyses of the HU and ES samples and intensive bone remodeling was likely to occur at the diaphyseal region as indicated by the occurrence of multiple cementing lines.

On the other hand, the expression of CGRP-immunoreactive neurons in proximal tibial metaphysis could be altered by unloading as well as electrical stimulation at DRG that the density of CGRP+ neurons in the hindlimb unloaded group was significantly lower than that of the cage control group. However, no difference in density of CGRP+ neurons could be found between the cage control and electrical stimulated groups indicating that the impact of unloading on expression of CGRP+ neurons would likely to be reduced by direct electrical

stimulation at DRG. Moreover, sustainable observation on expression of CGRP+ neurons could be found in proximal tibial metaphysis after prolonged treatment.

After 2 weeks of hindlimb unloading, the density of osteoclasts in proximal metaphysis of unloaded tibias as reflected by TRAP staining was significantly higher than that of the cage control and the electrical stimulated samples. However, the activity of osteoblasts indicated by the average proportion of ALP active areas in the proximal tibial metaphyses of the hindlimb unloaded only group was significantly lower than the CC and ES groups. However, the difference in TRAP and ALP activities between the cage control and electrical stimulated groups were not significant. These results indicate that unloading would increase osteoclastic activity but decrease osteoblastic activity. Direct electrical stimulation at DRG would counteract the impact of unloading by suppressing the increase in osteoclastic activity and reduce the decline in osteoblastic activity. Furthermore, the results of prolonged treatment further confirmed the treatment effects of direct electrical stimulation at DRG on the activities of osteoclasts and osteoblasts in unloaded proximal tibia to be sustainable.

6.3 Difference in bone mineral density of unloaded tibias between electrical stimulated and non-stimulated animals

The pQCT results of the HU group complied with findings reported in previous studies (157, 186) that a decrease of bone mineral density could be induced by hindlimb unloading and the effects were mainly in the trabecular bone while the results of the ES group demonstrated that *in vivo* electrical stimulation at DRG would reduce the decline in total BMC and BMD as well as

trabecular BMD in proximal metaphysis of unloaded tibias. This suggests the potential application of electrical stimulation at DRG on preventing bone loss in disuse bone loss cases.

On the other hand, the results of the 6-week treatment showed the impact of prolonged unloading on bone mineral content by hindlimb unloading in rats that a dramatic decline in BMC and BMD was observed, which occurred mainly in metaphysis. Moreover, the results confirmed the preventive potential of *in vivo* electrical stimulation at DRG on disuse bone loss after prolonged periods.

6.4 Difference in bone micro-architectural parameters of unloaded tibias between electrical stimulated and non-stimulated animals

After 2 weeks of hindlimb unloading, significant deterioration in bone micro-architecture was observed in the HU group as reflected by the substantial lower proportion of bone content, connectivity density, and trabecular number in the trabecular compartment of proximal tibial metaphysis compared to the control group. Also, the trabecular separation of proximal metaphyseal region in the HU group was significantly larger than that of the control group which further demonstrated the deterioration in bone micro-architecture in the trabecular compartment upon unloading. The SMI of the HU group was significantly larger than that of the control group suggesting the occurrence of conversion from plate elements to rod elements in trabeculae of the HU animals. In comparing the micro-structural parameters between the ES and CC groups, the trabeculae of the ES animals was significantly less connected than that of the control group and the SMI of the ES group was larger than that of

the CC group as well. These indicated that certain level of micro-architectural deterioration did occur in the metaphysis of tibias of the ES animals. However, no significant differences in other measured micro-structural parameters existed between the ES and CC groups. Thus, the deterioration in micro-architecture of tracbeculae at proximal tibial metaphysis in the ES group was less severe compared to the HU group. In diaphysis, no significant difference was observed among the three groups indicating that the impact of unloading exposure and electrical stimulation treatment was concentrated in the trabecular compartment but not in the cortical compartment during the 2-week treatment.

After 6 weeks of treatment, significant deterioration in bone micro-architecture was observed in both the HU and ES groups signified by a significant lower bone volume fraction, lower trabecular connectivity, and number were found as compared to the cage control group. In addition, a substantial increase in SMI in both the HU and ES groups was found. In the diaphysis, no significant difference in micro-structural parameters was observed between cage control and hindlimb unloaded only animals. However, the total volume and bone volume of the ES group were significantly less than those of the cage control group. However, no significant difference in bone volume fraction as well as mean density of total volume and bone volume existed among the treatment groups. Thus, the significant lower total volume and bone volume would be due to the smaller physical size of tibia samples in the ES animals, which could be reflected by the body weight of the animals. Further, based on the significant correlation between body weight and micro-architectural parameters, it was possible that

physiological and/or psychological conditions such as depression and/or inflammation occurred and adversely affected the body weight and bone micro-architecture of the animal after prolonged treatment.

The results of 2-week treatment showed that reduced deterioration in bone micro-architecture was observed in the trabecular compartment of proximal tibial metaphysis of electrical stimulated animals. The prolonged treatment results demonstrated that the treatment effect of electrical stimulation was attenuated and no significant difference in bone micro-structural parameters was observed between the HU and ES groups. However, it is important to realize that the metabolism of bone could be affected by various factors. After the prolonged treatment period, body weights of the HU and ES animals were significantly lower than that of the cage control animals and the ES rats were significantly lighter than the HU rats. Thus, it was possible that the μCT results of prolonged treatment might be influenced by other physiological and/or psychological factors.

6.5 Difference in biomechanical properties of unloaded tibias between electrical stimulated and non-stimulated animals

No significant difference in stiffness and ultimate load among all groups for both 2-week and 6-week treatment was observed. These results were consistent with the results of pQCT and μCT that no significant difference in change in bone mineral density and micro-structural parameters in diaphysis were observed among the treatment groups.

6.6 Conclusions

In conclusion, direct electrical stimulation at dorsal root ganglion via implanted stimulator was able to enhance the expression of CGRP+ neurons and this enhancement was likely to be associated with the increased expression of CGRP+ neurons at proximal metaphysis of unloaded tibias. Upon unloading, a decline in bone mineral density and deteriorated bone micro-structural occurred and the impact would be more obvious after prolonged periods. Moreover, the osteoporotic symptoms were concentrated in the trabecular compartment whereas the progress of bone loss in the cortical area occurred at a slower pace. Increased osteoclastic activity and lower osteoblastic activity were observed in hindlimb unloaded only animals. The altered activities of osteoclasts and osteoblasts led to disturbances in the balance between bone resorption and formation and would explain the decline in bone mineral density and deteriorated bone micro-architecture. In the ES animals, expression of CGRP+ neurons in DRG as well as at proximal tibial metaphysis was enhanced. The enhancement in CGRP+ neurons in proximal metaphysis probably altered the rates of bone formation and resorption by changing the activities of osteoblasts and osteoclasts respectively. Thus, a reduced decline in bone mineral density and bone micro-structure were observed in unloaded tibias of the ES animals compared to the HU group. After prolonged treatment, suppressed osteoclastic activity, enhanced osteoblastic activity and reduced decline in bone mineral density were observed in electrical stimulated animals as compared to the hindlimb unloaded

only group. These results demonstrate the prolonged efficacy of direct electrical stimulation at DRG on preserving bone density under exposure to micro-gravity.

Based on the results of the current study, *in vivo* electrical stimulation at DRG by IMES would likely preserve bone quality in unloaded tibias by enhancing expression of CGRP+ neurons in both DRG and proximal metaphysis. The enhancement in CGRP+ fibers expression in tibial metaphysis would be expected to suppress activity of osteoclasts but enhanced activity of osteoblasts and thus reduced bone loss and preserved bone micro-architecture. Further investigations on other potential transmitters of metabolic control of bone in the nervous system such as substance P, vasoactive intestinal peptide (VIP), and leptin would enhance our knowledge on the action mechanism of the current treatment and the roles of nervous tissue in regulating bone biology. In addition, further optimization on the physical size of IMES and treatment parameters would ensure safer treatment with reduced trauma but higher efficacy of treatment.

CHAPTER 7. EXTRA CHAPTER: Dorsal root ganglion electrical stimulation promoted inter-transverse process spinal fusion

7.1 Introduction

Lumbar spinal fusion is increasingly being used for treatment of degenerative spine disorders such as degenerative disc disease, spondylolisthesis, spondylosis, spinal stenosis, and scoliosis (205, 206). Traditionally, spinal fusion can be achieved by decortications of articular surface and packing the joint space with bone grafts or biological substitutes (205-207) such as synthesized hydroxyapatite and bone morphogenetic proteins (BMPs) (208).

The present study was to test a concept of electrical stimulation (ES) at dorsal root ganglion (DRG) via an implantable micro-electrical stimulator (IMES) to achieve an inter-transverse process fusion without bone grafting in a rat model. In DRG, there are neurons synthesizing and releasing calcitonin-gene-related peptide (CGRP) which is a sensory neuropeptide sharing the same gene complex encoding with calcitonin (10). Calcitonin is produced when the gene is expressed in C cells in the thyroid while the CGRP is produced when the same gene is expressed in sensory neurons located in the DRG and is transported peripherally. Numerous studies have proven the distribution of CGRP receptors on the membrane of osteoblasts (11, 132, 209). It was reported recently that CGRP stimulates BMP-2 expression and the differentiation of human osteoblast-like cells *in vitro* (210). CGRP-expressing nerves present in periosteum, bone, and endosteum (211, 212). Rapid proliferation of CGRP-expressing nerves

has been observed during healing of rat tibial fractures (14, 213, 214). The important role of CGRP in fracture healing has been evidenced by our findings that sciatic neurectomy in rats resulted in the absence of CGRP-expressing nerve fibers in fracture sites in tibiae and delayed fracture healing (215). Our group has also reported rapid growth of CGRP-expressing nerves in spinal fusion callus in rabbits (5, 6).

Recent studies further showed that secretion of CGRP could be triggered by ES at DRG (19, 209). We have recently developed an IMES which provides precise ES to target neurons in rats (146). The purpose of this study was to examine DRG stimulation via IMES for its promotion potential in spinal fusion enhancement in a rat model.

7.2 Materials and methods

7.2.1 Animals and experimental design

Sixteen Sprague-Dawley rats (3-month-old, weight: 420–450 g) were equally randomly allocated into 2 groups (n = 8 for each group), i.e. the cage control (CC) group and the ES group. ES was applied at the right DRGs at the vertebral level L4–L6 of rats in the ES group. The experiment duration was 6 weeks. DRG stimulation was provided via a set of IMES implanted at the L4–L6 transverse processes. Rats were housed individually in metal cages. They were allowed free access to tap water and standard rodent chew. The environment was kept with 12-hour day-night cycle at 24℃. All animal care and experimental protocols were approved by the Animal Ethics Committee of The Hong Kong Polytechnic University in Hong Kong SAR, China (Ref no. of animal experiment license: (10-57) in DH/HA&P/8/2/4 Pt.3).

7.2.2 Implantation of IMES and stimulation protocol

As described in Chapter 3, electrical stimulation was generated by an IMES developed by the School of Aerospace, Tsinghua University, China (146, 216). The implanted stimulation system consists of three parts: a body consisting of a circuit board and a button-type battery; three electrodes; and, wires connecting the body to the electrodes (figure 3.3). The body was connected to three coaxial electrodes. The outer layer of each electrode was a stainless steel tube serving as a reference pole. The core was fitted a stainless steel wire coated with a layer of parylene C. The uncoated tip of the core served as the stimulating pole of negativity polarity (figure 3.4). The implanted stimulator unit was controlled externally with a remote control unit.

The implantation protocol was identical to that of DRG stimulation as described in Chapter 3. Briefly, after anesthesia of the rat, right transverse processes of L4 to L6 were exposed through a dorsal incision and the periosteum was carefully preserved. A hole of 1 mm diameter was drilled at the location of DRG on each right transverse processes (figure 3.7) and an electrode of the IMES was inserted. Then, the muscle was sutured to cover the transverse processes and to fix the positions of the electrodes. The body of the stimulator was implanted subcutaneously at the left low back area such that to create least restriction on motion of the animal. The positions of electrodes and the stimulator were confirmed by X-ray. Two orthogonal views were necessary to demonstrate that the electrodes were in-situ in both medio-lateral (figure 3.8C) and dorso-ventral directions (figure 3.8A). The computed radiographic images were taken by a conventional X-ray unit (Model TF-6TL-6, Toshiba

Corporation, Tokoyo, Japan) with the use of a computed radiographic image processing unit (FCR 5000R, Fuji Photo Film Co Ltd., Japan). The X-ray beam was centered on the surgical site of electrodes placement. The exposure setting at 55 KVp, 5mAs and a source to image distance of 100 cm was used throughout the imaging study.

The electrical stimulation signal was in a rectangular pulse waveform and constant amplitude. The pulse width, frequency, current, and voltage of the electrical stimulation applied were 90 μs, 150 Hz, 61.3 μA, and 0.25 V. The stimulation voltage used in this study was defined as the maximum stimulation voltage applied without triggering visible contraction of the muscles innervated by motor neurons located at the level L4 to L6. Based on the observations, no muscle contraction was induced when stimulation voltage was 0.25 V but *in vivo* electrical signals were still detectable under this voltage (216). In the ES group, each animal was stimulated 20 minutes/day and 5 days/week for 6 weeks.

The animals were euthanized by CO_2 inhalation at the end of the experiment. The vertebrates at the vertebral level L4 to L6 along with the spinal cord and DRGs were harvested and kept frozen at –80°C in PBS-soaked gauze until further procedures.

7.2.3 Spinal fusion assessment

Using a mammographic X-ray unit (Siemens Mammommat 3000 Nova), high resolution magnification CR mammographic imaging at 20 lp/mm was used to demonstrate the bony details of each lumbar column. A dorso-ventral view was taken in each of the specimens using

Molybenum/Molybenum anode filter at 28 KVp, 14 mAs and a source to image distance of 65 cm.

Fusion of transverse processes was evaluated. Fusion was defined as complete and uninterrupted bony bridging between upper and lower transverse processes. The fusion rate of L4/L5 and L5/L6 was calculated.

7.2.4 Quantitative assessment of new bone formation / fusion mass

The bony tissue of L4–L6 vertebrates were examined with high resolution micro-computed tomography (μCT) scanner (μCT-40, SCANCO Medical AG, Switzerland) The setting of the scan was energy level 70 kV, current 114 μA, and integration time 170 ms. The L4–L6 vertebrates were scanned at a resolution with an isotropic voxel size of 19 μm. In order to suppress the noise in the results, all images were evaluated with a constrained 3D Gaussian filter (filter width: σ = 1.2; filter support: S = 2). A region of 200 slices before the mid-length was analyzed in each vertebrate with a threshold value of 467.1 mgHA/ccm. All scans were reconstructed with the same parameters for different portions. Bone volume fraction (BV/TV, given as %), total bone mass and bone mineral density (BMD) of ectopic bone as well as normal bone were evaluated for each portion using the software μCT Evaluation Program V6.0 (SCANCO Medical AG, Switzerland).

7.2.5 Immunohistochemistry

The harvested specimen of spinal cord and DRGs were rehydrated in 0.01 M phosphate-buffered saline (PBS) containing 20% sucrose for 5 hours at room temperature. Then, the DRG samples were sectioned at a thickness of 7 µm on a cryostat. The immunohistochemical staining was done according to an established protocol (152). Briefly, the DRG sections were treated in 0.5% horse serum (Gibco, USA) for 30 minutes at room temperature. The sections were then incubated with rabbit antibody to CGRP (1:50; Abcam, USA) for 24 hours at 4℃ followed by incubation with goat anti-rabbit Alexa Fluor 555 fluorescent antibody conjugate for visualization (1:1000; Invitrogen, USA). Finally, the sections were mounted with aqueous-based mounting agent with 4', 6-diamidino-2-phenylindole (DAPI; Vector Labs, USA). The sections were examined using fluorescence microscope (Nikon Eclipse 80i; Nikon, Japan) immediate after immunostaining. The fluorescent microscope was equipped with a mercury lamp and filters of various excitation ranges that red fluorescent signals of CGRP could be detected within the excitation range of 550 to 590 nm whereas the DAPI produced blue fluorescent signals with excitation at about 360 nm (154).

The captured images of labeled DRG sections were further analyzed using ImageJ version 1.46r (NIH, USA) as described. The area of CGRP fibers was defined as the region of interest (ROI) and the total area was quantitatively measured. The intensity of the signals and the number of pixels within the ROI were generated using the built-in histogram function of the software. The actual area of the ROI was estimated from the proportion of the number of pixels within the

ROI and the total number of pixels captured. Intense signals were defined as signals with an intensity higher than the mean intensity within the ROI at 2 times of the standard deviation. The density of intense signals was estimated.

7.2.6 Statistical analysis

Statistical analysis was performed using SPSS version 20 (IBM, New York, USA). The results were presented as mean and standard deviation. The differences in micro-structural parameters between fusion mass and normal bones were evaluated with Student-t test. Statistical significance was considered when $p < 0.05$.

7.3 Results

7.3.1 Implantation of IMES and stimulation to DRG

All animals tolerated the implants and electrical stimulation well. There was no post-implantation infection or edema at the surgery site and hindlimbs.

7.3.2 Spinal fusion assessment

In the ES group, the rate of radiographic fusion with complete and uninterrupted bony bridging was 100% (8/8) for the right L4/L5 transverse processes and was 75% (6/8) right L5/L6 transverse processes. In the other two rats, there was new bone formation in right L5/L6 transverse processes, but there was a cleft between the new bone mass on L5 and L6 and solid bony fusion was not yet achieved. Bony callus formations were absent in the left L4–L6

transverse processes in the ES group, as well as in bilateral L4–L6 transverse processes in the cage control group.

7.3.3 Quantitative assessment of new bone formation / fusion mass

Micro-structural analysis with µCT showed that bony callus formed transverse processes ipsilateral to the DRG stimulation side. Callus formation was spatially limited to the level of DRG stimulation between L4 and L6, posterior to transverse processes and pedicle (figures 7.1 and 7.2). The quantitative analysis of µCT image (table 7.1) revealed that the BMD of ectopic bone was significantly lower than that of normal bone, though there was no significant difference in bone volume fraction ($p = 0.057$) and total bone mass ($p = 0.114$) between the fusion callus and the normal bone tissue.

Figure 7.1 Ventro-dorsal radiograph of lumbar vertebrae L4–L6 Left: control group without electrical stimulation. Inter-transverse processes bony callus is absence in the lumbar vertebral region L4–L6; Right: ES group. Callus formation is spatially limited to the level of DRG stimulation between L4 and L6. There is a radiographic fusion with complete and uninterrupted bony bridging between L4 and L5. New bone formation is shown between right L5 and L6 transverse processes, but there is a cleft between the new bone mass on L5 and L6 transeverse processes and solid bony fusion is not yet achieved.

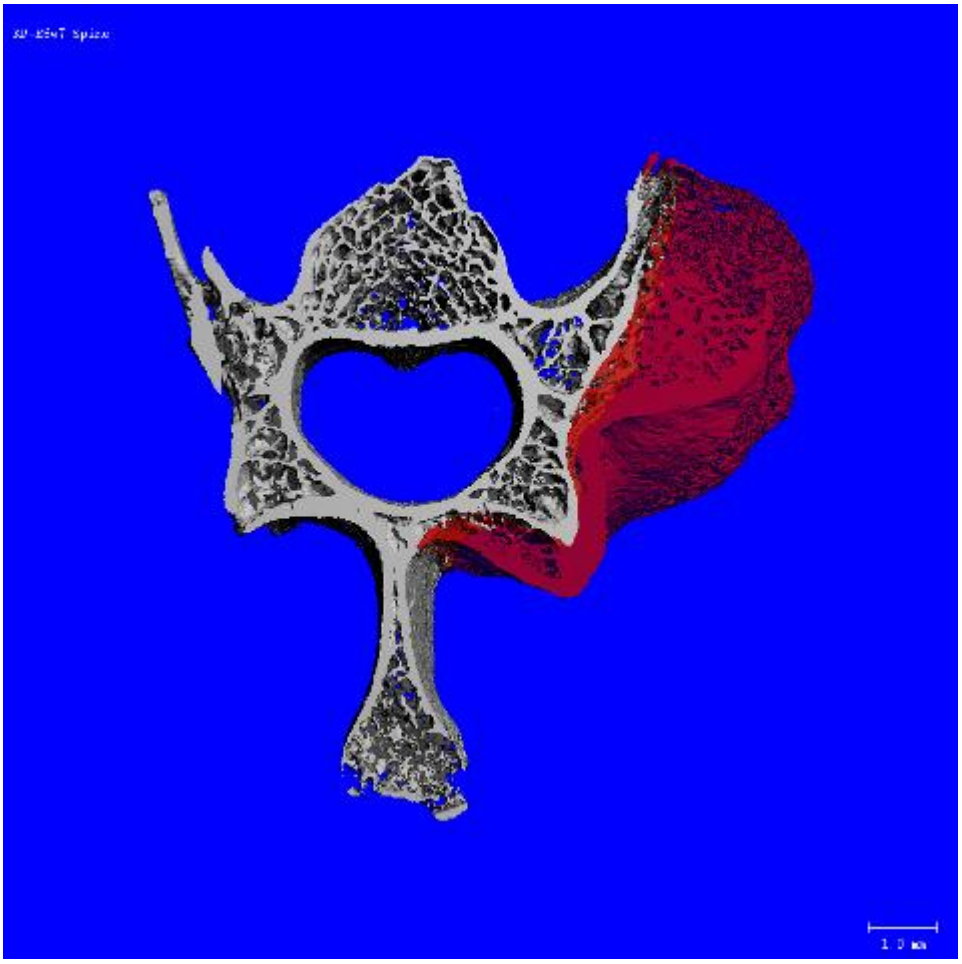

Figure 7.2 3D reconstruction of micro-CT images of a L5 vertebra
New bone callus (red) distributes on and covers the dorsal aspect of transverse process and pedicle.

Table 7.1 Comparison of micro-structural parameters between normal bone and callus

	Normal bone	Callus
BV/TV (%)	0.3196±0.0259	0.4394±0.1148
Total bone mass (mm3)	21.83±0.62	13.44±7.71
BMD (mgHA/ccm)	906.22±13.11	821.95±53.91*

* $P < 0.05$ against normal bone

7.3.4 Immunohistochemistry

CGRP-expressing neurons in DRG were visualized by immunohistochemistry (figure 4.2). By comparing the CGRP signals in the right DRG between the ES and CC groups, intense CGRP signals were observed only in the ES group but not in the non-stimulated cage control group (figure 4.2H). The average number of enhanced signals was 21.78±4.40/mm^2. The intense CGRP signals complied with the occurrence of DAPI signals (figure 4.2G–4.2I), where DAPI bound DNA and produced fluorescent signals upon excitation.

7.4 Discussion

In this study, we achieved a more than 75% solid fusion rate following 6 weeks electrical stimulation via IMES to the DRG without decortication and grafts. The IMES used in the current study was biocompatible and the parameters of ES were shown tolerable by animals. This result achieved in the present proof-of-concept study is very encouraging, as traditional posterolateral spinal fusion in rat models has reported a 40% fusion rate with decortication and an autogenous bone or demineralized bone matrix graft 6 weeks after surgery (217-219). Compared with traditional spinal fusion methods, IMES has the advantage that it needs only minimal invasive surgery to insert and fix the IMES units. To our knowledge, this is the first report on achieving posterolateral spinal fusion with electrical stimulation via IMES to the DRG without bone graft. Electrical stimulations are useful for enhancing fracture healing, including spinal fusion (220, 221). However, the methodology and underlying mechanisms of the electrical stimulation in the present study differed completely from those in previous studies.

All previously reported electrical stimulations for enhancing fracture healing were direct stimulations to the bony callus (221-223) based on the theory that electrical stimulation could promote proliferation of osteoblasts.

The current experimental study did not show callus formation at the left transverse process following electrical stimulation to the right DRG. The association between the enhanced CGRP expression and the presence of fusion callus suggested increased CGRP expression that is known to play an important role in inducing callus formation. *In vitro* studies have demonstrated that CGRP stimulates osteoblast proliferation and differentiation in both osteoblast cell lines (10, 224, 225) and bone marrow mesenchyme stromal cells (226). CGRP stimulates BMP-2 expression and differentiation of human osteoblast-like cells (210).

DRG electrical stimulation through IMES has recently been used in both animal (227-229) and humans (228) for relieving chronic pain. There was no report on inter-transverse process fusion following DRG stimulation. In these chronic pain intervention studies, electrodes were placed via an epidural approach, with access gained using the loss-of-resistance technique standard for this type of intervention, without creating injuries to the bony tissue. In the present study, a hole was drilled on each pedicle at the vertebral level L4–L6 which resulted in injuries to the periosteum, bone and endosteum of L4–L6 transverse processes. Callus formation and spinal fusion were found between L4 and L6 without spreading to other levels. This comparison suggested bony injury is essential for callus formation and electrical

stimulation to DRG can only augment new bone formation and thus achieve inter-transverse process fusion.

There is a more than 15 years of history of clinical application of IMES for deep brain stimulation (DBS). Safety of chronic stimulation to the nervous system and its effectiveness have been proven by both animal experiments and clinical practices. DBS has been approved in the United States by the Food and Drug Administration as a treatment for essential tremor, Parkinson's disease, and dystonia. Results of the present study suggest a potential new application of IMES in enhancing bone healing.

In conclusion, electrical stimulation at DRG through IMES promoted bone formation and achieved high inter-transverse process fusion rate and mass in this rat model, suggesting a potential application of IMES in enhancing spinal fusion. Furthermore, CGRP-expressing nerve fibers are widely distributed throughout bone. A high density of CGRP-expressing fibers in areas with high bone formation rates were found during both spinal fusion and fracture healing. Electrical stimulation to DRG may also promote healing of limb fractures.

CHAPTER 8. AWARD AND PUBLICATIONS

Award received

Special Innovation Award of 2nd World Cup of Computer Implemented Inventions (CIIs) on "Application of Implantable Micro-electrical Stimulator (IMES) on Reduction of Disuse Bone Loss".

Publications in peer reviewed journals

Roy Yuen-chi Lau and Xia Guo, ***A Review on Current Osteoporosis Research: With Special Focus on Disuse Bone Loss***, Journal of Osteoporosis, 2011; 2011: 293808. Epub 2011 Aug 16.

Yuen Chi Lau, Yau-Ming Lai, Kai-Ting Po, Xing Qian, Hong-Wei Hao, Hu-Cheng Zhao, Lu-Ming Li, Xia Guo, **Dorsal Root Ganglion Electrical Stimulation Promoted Intertransverse Process Spinal Fusion – A Proof-of-Concept Study**, The Spine Journal, 2014 Apr 12.

Roy YC Lau, Lu-ming Li, Kevin KT Po, Xing Qian, Xia Guo, **Electrical stimulation at the dorsal root ganglion preserves trabecular bone mass and microarchitecture of the tibia in hindlimb-unloaded rats**, Osteoporosis International (Accepted)

Roy YC Lau, Lu-ming Li, Kevin KT Po, Xing Qian, Xia Guo, **A proof-of-mechanism study on preventing disuse bone loss with electrical stimulation at the dorsal root ganglion**, Journal of Bone Mineral Research (Submitted)

Roy YC Lau, Xia Guo, Kevin Po, Lu-ming Li and Xing Qian, **Electrical Stimulation at Dorsal Root Ganglion Reduced Bone Mineral Loss due to Prolonged Hindlimb Suspension** (Prepared)

Conference papers

Roy YC Lau, Xia Guo, Kevin Po, **Implantable Micro-electrical Stimulator (IMES)**, in Challenges and Innovation International Conference, Kaohsiung, Taiwan, 24-27 August 2011

Roy YC Lau, Kevin Po, Xia Guo, Lu Ming Li, Hong Wei Hao, Hu Cheng Zhao, Xing Qing, **Design and Implantation of Implantable Micro-electrical Stimulator for Osteoporosis Prevention,** in Orthopaedic Reseach Society 2013 Annual Meeting, San Antonio, Texas, USA., 26-28 Jannuary, 2013

Roy YC Lau, Kevin Po, Xia Guo, Lu Ming Li, Hong Wei Hao, Hu Cheng Zhao, Xing Qing, **Electrical Stimulation at Dorsal Root Ganglion by Means of Implantable Micro-electrical Stimulator Preserves Bone Mineral Content in Hindimb Unloaded Rats,** in Orthopaedic Reseach Society 2013 Annual Meeting, San Antonio, Texas, USA., 26-28 Jannuary, 2013

APPENDICES

香港特別行政區政府
衞生署
香港灣仔皇后大道東213號
胡忠大廈17及21樓

THE GOVERNMENT OF THE HONG KONG SPECIAL ADMINISTRATIVE REGION
DEPARTMENT OF HEALTH,
WU CHUNG HOUSE, 17TH & 21ST FLOORS,
213 QUEEN'S ROAD EAST, WAN CHAI,
HONG KONG.

本署檔號 OUR REF.: (10-57) in DH/HA&P/8/2/4 Pt.3
來函檔號 YOUR REF.:
電 話 TEL.: 2961 8645
圖文傳真 FAX: 2127 7329

9 September 2010

LAU Yuen Chi
Department of Rehabilitation Sciences
The Hong Kong Polytechnic University

Dear Sir/Madam,

Animals (Control of Experiments) Ordinance
Chapter 340

I refer to your application dated 23 August 2010 and forward herewith the following licence(s) issued under the above Ordinance:-

Form 2 : Licence to Conduct Experiments

Your attention is drawn to regulations 4 and 5 of the Animals (Control of Experiments) Regulations as excerpted below:-

"4. Records
Every licensee shall keep up-to-date a book in the form set out as Form 6 in the Schedule in which he shall record the particulars therein indicated of all experiments performed by him.

5. Returns
Every licensee shall render to the Director of Health on or before the 1st day of January each year a return in the form set out as Form 7 in the Schedule of all experiments performed by him during the preceding twelve months."

Copies of Form 6 and Form 7 are enclosed for your convenience. Failure to comply with either regulation 4 or regulation 5 is an offence, each offence punishable by a fine of HK$500 and to imprisonment for 3 months. Conviction of an offence against either regulation 4 or regulation 5 or failure to comply with either regulation may result in your licence being cancelled.

/P.2.....

We are committed to providing quality client-oriented service

Please also be reminded that if you wish to continue your experiments after the specified periods as stated on the above licence / endorsements / teaching permit, you should renew them at least two months before the end-dates. On the other hand, if you have completed or stopped your experiments before the specified periods, you should inform us immediately.

Yours sincerely,

(Dr Jaime SIN)
for Director of Health

* *Remarks:-*

A "Code of Practice – Care and Use of Animals for Experimental Purposes" was prepared by the Agriculture, Fisheries and Conservation Department on the advice of the Animal Welfare Advisory Group.

Please visit the Agriculture, Fisheries and Conservation Department's website at <http://www.afcd.gov.hk/english/publications/publications_qua/files/code.pdf> for details of the Code of Practice.

Encl.

We are committed to providing quality client-oriented service

Form 2

Licence to Conduct Experiments

Name : LAU Yuen Chi [Ref No.: (10-57) in DH/HA&P/8/2/4 Pt.3]

Address : Department of Rehabilitation Sciences, The Hong Kong Polytechnic University

By virtue of section 7 of the Animals (Control of Experiments) Ordinance, Chapter 340, the above-named is hereby licensed to conduct the type of experiment(s), at the place(s) and upon the conditions, hereinafter mentioned.

Type of experiment(s)

Rats will be used in the experiment. The animals will be divided into groups. The hindlimbs of the animals will be unloaded by tail suspension to create a disuse bone loss model. Animals allowed to have free movement will be used as normal control. Animals in treatment groups will then be subjected to electrical stimulation (IMES) to dorsal root ganglion (DRG) through a subcutaneously implanted pulse generator.

1. *Disuse bone loss model.* The animals will be fixed with a tail harness to raise the hindlimbs above the ground and keep the animals in a head-down position.
2. *DRG stimulation by IMES.* Under anaesthesia, a pulse generator will be implanted subcutaneously into the animals. Electrodes will be connected through the leads to the generator and located at L4-L5 position for DRG stimulation. Electrical stimulation will be applied to the animals for treatment.

Throughout the experiment, the conditions and well-being of the animals will be monitored. At different time points, the animals will be sacrificed by overdose of anaesthetics. Tissues including tibia and spinal cord will be harvested for analyses, such as measurement of bone mineral density and mechanical properties, histomorphometry, immunohistochemistry and analysis of CGRP expression.

Place(s) where experiment(s) may be conducted

(a) Centralised Animal Facility, The Hong Kong Polytechnic University
(b) ST422, 4/F, Core S, The Hong Kong Polytechnic University

Conditions

1. Such experiment(s) may only be conducted for the following purposes-

To study the effects of electrical stimulation on CGRP secretion by sensory neurons at dorsal root ganglia and the efficacy on preventing bone loss in hindlimb unloaded animal model.

2. This licence is valid from 9 September 2010 to 8 September 2012

Dated 9 September 2010

DEPARTMENT OF HEALTH 衞生署 HONG KONG

Licensing Authority

康復治療科學系
Department of Rehabilitation Sciences

Application of Implantable Micro-electrical Stimulator (IMES) on Reduction of Disuse Bone Loss

Roy YC Lau, Xia Guo, Kevin Pao
Department of Rehabilitation Sciences, The Hong Kong Polytechnic University, Hong Kong SAR, China

Osteoporosis is one of the major health problems accounting for huge burden for healthcare systems and economies in different nations. It also poses adverse impact on quality of life of patients suffered as well as their families.

Physical inactivity has been shown to be associated with osteoporotic symptoms. People who have difficulties in performing physical exercises such as elderly and patients with physical disabilities are thus more susceptible to be suffered from osteoporosis.

Electrical stimulation enhances the secretion of calcitonin gene-related peptides (CGRPs), which plays important role in bone modeling and remodeling, in sensory nerves and this is expected to reduce osteoporotic symptoms. The implantable micro-electrical stimulator (IMES) is a compact device implanted at the dorsal root ganglion (DRG) producing electrical stimulations which frequency, duration and stimulation intensity are adjustable using a wireless external controller in order to suit the requirements of different treatment protocols. The IMES would provide a convenient treatment for reducing disuse bone loss.

Implantable Micro-electrical Stimulator (IMES)

Schematic illustration of structural organization of IMES

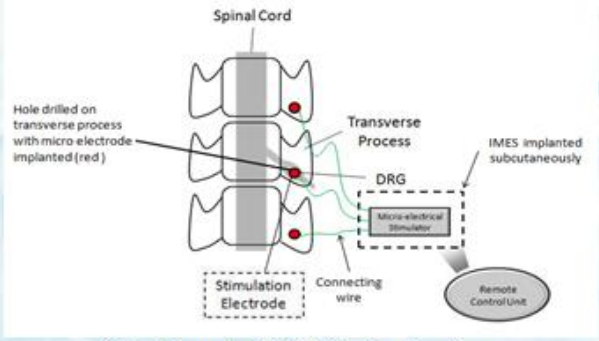

Implantation protocol of IMES in lumbar spine region

X-ray image of SD rat implanted with IMES

THE HONG KONG POLYTECHNIC UNIVERSITY
香港理工大學

www.rs.polyu.edu.hk

Touching lives, making an impact

Poster for Challenges and Innovation International Conference 2011

康復治療科學系
Department of Rehabilitation Sciences

清華大學
Tsinghua University

Design and Implantation of Implantable Micro-electrical Stimulator for Osteoporosis Prevention

Lu Ming Li[1], Hong Wei Hao[1], Hu Cheng Zhao[1], Xing Qing[1], Roy A. Lau[2], Kevin Po[2], Xia Guo[2]
[1]School of Aerospace, Tsinghua University, Beijing, China
[2]Department of Rehabilitation Sciences, The Hong Kong Polytechnic University, Hong Kong SAR

Introduction:
Chronic electrical stimulation (CES) by means of implantable micro-electrical stimulator (IMES) has been applied to treat disorders of central nervous system, e.g. Parkinson disease, but has not yet been used for peripheral nerve stimulation. Previous studies suggested that calcitonin gene-related peptide (CGRP) secreted by dorsal root ganglion (DRG) regulates bone metabolism by increasing bone formation rate and enhancing bone volume. It is reported that electrical stimulation at DRG could enhance expression of CGRP. Aim of this study was try to develop an IMES which is suitable to be used for peripheral nerve CES and to test the effect of CES in enhancing CGRP expression in DRG.

Methods:
A stimulation electrode was implanted at the position of DRG on the transverse processes of L5 vertebra whereas a recording electrode was implanted 2mm in front of the site of stimulation. Voltages generated at stimulation electrode were measured with an oscilloscope via recording electrode (Figure 2). By varying the input voltages of stimulation, multiple recordings were obtained and the difference between input and recorded signals was evaluated. The average voltage change between stimulation and recording electrodes at different input voltages was thus measured.

Figure 1. Implantable micro-electrical stimulator

Results:
Voltages generated by DRG stimulation were recorded. The average peak voltage recorded had a linear relationship with the stimulation voltage and this observation was consistent throughout the range of voltage tested. However, dramatic reduction of voltage was observed in the in vivo recorded signal (Table 1). Electrical stimulations at different voltages were tested and the corresponding muscular behaviors were observed and summarized. Two weeks after daily stimulation with stimulation voltage 0.3V, expression of CGRP at the DRG under stimulation was significantly increased in comparison with the control sample (Figure 3).

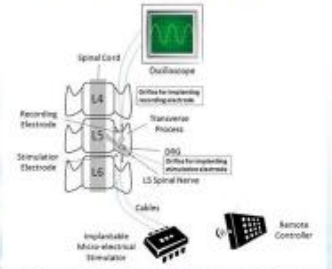

Figure 2. Experimental setup for electrical stimulation of DRG and in vivo measurement of voltage distribution

Discussion:
The results of this study showed that dramatic voltage drop occurred across stimulation and recording electrodes. This phenomenon was due to capacitance of the tissue medium. The proposed effect of DRG CES is to trigger the secretion of CGRP, which plays regulatory role in bone modeling and remodeling and hence to prevent bone loss. It is proved that this novel IMES is suitable to be used for CES and the DRG CES could effectively enhance CGRP expression.

Significance:
The current study demonstrated the implantation of IMES at DRG suggests the potential application of CES in prevention or treatment of peripheral nerve related bone diseases, such as disuse bone loss in elderly, astronaut or patients with mobility disability.

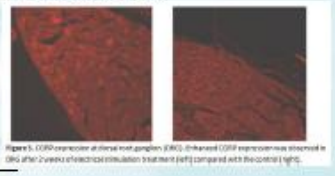

Acknowledgements:
This project is supported by NSFC/RGC Joint Research Scheme 2011 [RGC Ref.: N_PolyU537/10] and PolyU PhD stipend [NSFC Ref.: 51061160501]

Table 1. Average voltage reduction for different stimulation voltages.

Stimulation Voltage (V)	0.25	0.3	0.5	1	1.5	2	2.5
Average Peak Voltage Recorded (V)	0.0243	0.029	0.109	0.133	0.174	0.236	0.326
Average Voltage Reduction	90.28%	90.33%	78.30%	86.70%	88.40%	88.20%	86.96%

THE HONG KONG POLYTECHNIC UNIVERSITY
香港理工大學

www.rs.polyu.edu.hk

Touching lives, making an impact

Poster for Orthopaedic Reseach Society 2013 Annual Meeting - 1

康復治療科學系
Department of Rehabilitation Sciences

清華大學
Tsinghua University

Electrical Stimulation at Dorsal Root Ganglion by Means of Implantable Micro-electrical Stimulator Preserves Bone Mineral Content in Hindimb Unloaded Rats

Roy A. Lau[1], Kevin Po[1], Xia Guo[1], Lu Ming Li[2], Hong Wei Hao[2], Hu Cheng Zhao[2], Xing Qing[2]
[1]Department of Rehabilitation Sciences, The Hong Kong Polytechnic University, Hong Kong SAR
[2]School of Aerospace, Tsinghua University, Beijing, China

INTRODUCTION

Osteoporosis is a multifactorial skeletal disorder characterized by decreased bone mass and deteriorated micro-architecture that lead to increased risk of fracture. It has been reported that high dosage of Calcitonin gene-related peptide (CGRP) significantly inhibited bone resorption in rat suggesting that CGRP might serve as a local regulator of bone cell function. Besides, previous study demonstrated that electrical stimulation at dorsal horn could enhance secretion of CGRP. Hence, the purpose of this study is to investigate the effects of electrical stimulation at dorsal root ganglion (DRG) by using an implantable micro-electrical stimulator (IMES) on preventing bone loss in hindlimb unloaded animal model.

MATERIALS AND METHODS

18 Sprague-Dawley rats were randomly allocated into 3 groups namely 1) cage control (CC), 2) hindlimb unloaded (HU) and 3) hindlimb unloaded with electrical stimulation (ES). The hindlimbs of HU and ES rats were suspended by tail suspension. For the ES rats, right dorsal root ganglia (DRG) of L4 to L6 region were stimulated by electrical stimulation generated by implantable micro-electrical stimulators (IMES) implanted at L4 to L6 level of spinal region.

The pulse width and frequency of the electrical stimulation applied were respectively 90μs and 150Hz. The stimulation voltage used was 0.25V and each electrical stimulated animal was stimulated 20 minutes per day for 14 days.

Post-treatment immunohistochemistry was performed to detect the occurrence of CGRP in DRG. Besides, tomographic scans of epiphyseal and diaphyseal regions of tibias were performed both before and after treatment. The bone mineral content (BMC) and bone mineral density (BMD) in both cortical and trabecular compartments as well as total area were measured in epiphyseal region whereas cortical BMC and BMD were measured in diaphyseal region.

RESULTS

Enhanced CGRP signals were found in electrical stimulated DRG (figure 2D) but not in control sample (figure 2C). Total BMC and total BMD in the epiphyseal region of right hindlimb decreased 40% and 28% respectively in HU whereas that in ES were respectively 35.7% and 26% after 2 weeks unloading (figure 3A and 3B). In cortical compartment, percentage decrease in cortical BMD and BMC of HU was significantly greater than that of control sample in both hindlimbs. Such observation could not be found in ES samples (figure 3C and 3D). No significant difference was found among percentage change in epiphyseal trabecular BMC and BMD as well as cortical BMC and BMD in diaphyseal region.

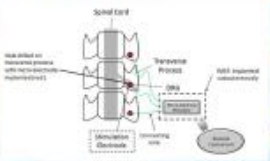

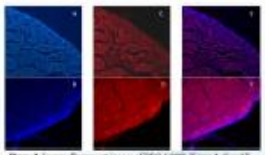

Figure 2. Immunofluorescent images of DRG (x200). Figure A, C and E show fluorescent signals in control DRG whereas figure B, D and F show signals in electrical stimulated DRG. DAPI labeled nuclei signals (A and B). CGRP immunoreactive signals (C and D). Combined images of DAPI and CGRP signals (E and F).

DISCUSSION

In this study, the use of implantable micro-electrical stimulator on stimulating expression of CGRP in DRG was demonstrated. Dramatic reduction in total BMD and BMC was observed in epiphyseal region of hindlimb unloaded animals. The electrical stimulation was applied only at the right DRG of spinal level L4 to L6, which innervated only the tibial region of right hindlimb. Thus, the bone parameters measured at right hindlimb reflected the effects of electrical stimulation. Significant percentage decrease in total BMD, cortical BMC and BMD were observed in HU compared with control samples but not in ES samples. Moreover, the percentage decrease in cortical BMC in electrical stimulated samples was significantly lower than those without electrical stimulation. These findings suggested that electrical stimulation at DRG could be effective in retaining bone quality. However, the enhancement of CGRP expression as well as the reduction in bone loss could be further improved by optimizing the treatment parameters and the duration of treatment.

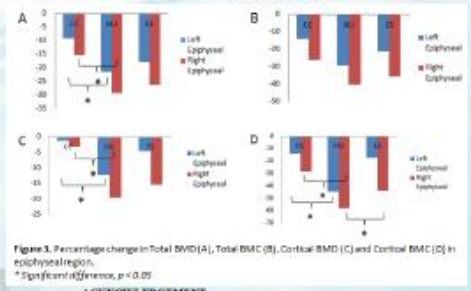

Figure 3. Percentage change in Total BMD (A), Total BMC (B), Cortical BMD (C) and Cortical BMC (D) in epiphyseal region.
* Significant difference, $p < 0.05$

ACKNOWLEDGEMENT

This project is supported by NSFC/RGC Joint Research Scheme 2011 [RGC Ref.: N_PolyU537/10] and PolyU PhD stipend [NSFC Ref.: 51061160501]

THE HONG KONG POLYTECHNIC UNIVERSITY
香港理工大學

www.rs.polyu.edu.hk

Touching lives, making an impact

Poster for Orthopaedic Reseach Society 2013 Annual Meeting – 2

REFERENCES

1. Roux W. Der Kampf der Teile im Organismus. Engelmann, Leipzig. 1881.

2. van der Meulen MC, Huiskes R. Why mechanobiology? A survey article. J Biomech. 2002;35(4):401-14.

3. Lam W, Guo X, Kwong K, Leung K. Effect of immobilization and neural influence on tibial fracture in rats. Bone. 2005;36:S367.

4. Lam W, Guo X, Kwong K, Leung K. Sciatic nerve section decreases callus response to low intensity pulsed ultrasound. Calcif Tissue Intern. 2007;80:S80-1.

5. Wang XY, Guo X, Qu SX, Weng J, Cheng CY. Temporal and spatial CGRP innervation in recombinant human bone morphogenetic protein induced spinal fusion in rabbits. Spine (Phila Pa 1976). 2009;34(22):2363-8.

6. Wang XY, Guo X, Cheng JC, Mi YL, Lai PY. Involvement of calcitonin gene-related peptide innervation in the promoting effect of low-intensity pulsed ultrasound on spinal fusion without decortication. Spine (Phila Pa 1976). 2010;35(26):E1539-45.

7. Wang Q, Zheng YP, Wang XY, Huang YP, Liu MQ, Wang SZ, et al. Ultrasound evaluation of site-specific effect of simulated microgravity on articular cartilage. Ultrasound Med Biol. 2010;36(7):1089-97.

8. Zaidi M, Bevis PJ, Girgis SI, Lynch C, Stevenson JC, MacIntyre I. Circulating CGRP comes from the perivascular nerves. Eur J Pharmacol. 1985;117(2):283-4.

9. Dambacher MA, Neff M, Kissling R, Qin L. Highly precise peripheral quantitative computed tomography for the evaluation of bone density, loss of bone density and structures. Consequences for prophylaxis and treatment. Drugs Aging. 1998;12 Suppl 1:15-24.

10. Zaidi M, Chambers TJ, Bevis PJ, Beacham JL, Gaines Das RE, MacIntyre I. Effects of peptides from the calcitonin genes on bone and bone cells. Q J Exp Physiol. 1988;73(4):471-85.

11. Imai S, Matsusue Y. Neuronal regulation of bone metabolism and anabolism: calcitonin gene-related peptide-, substance P-, and tyrosine hydroxylase-containing nerves and the bone. Microsc Res Tech. 2002;58(2):61-9.

12. Konttinen Y, Imai S, Suda A. Neuropeptides and the puzzle of bone remodeling. State of the art. Acta Orthop Scand. 1996;67(6):632-9.

13. Kuntz A, Richings C. Innervation of the bone marrow. J Comp Neurol. 2001;83:213-22.

14. Hukkanen M, Konttinen YT, Santavirta S, Paavolainen P, Gu XH, Terenghi G, et al. Rapid proliferation of calcitonin gene-related peptide-immunoreactive nerves during healing of rat tibial fracture suggests neural involvement in bone growth and remodelling. Neuroscience. 1993;54(4):969-79.

15. Madsen J, Wang J, Hukkanen M. Sensory nerve ingrowth during bone graft incorporation in the rat. Acta Orthop Scand. 2005;67:217-20.

16. Aro H, Eerola E, Aho AJ. Development of nonunions in the rat fibula after removal of periosteal neural mechanoreceptors. Clin Orthop Relat Res. 1985(199):292-9.

17. Dyck PJ, Stevens JC, O'Brien PC, Oviatt KF, Lais AC, Coventry MB, et al. Neurogenic arthropathy and recurring fractures with subclinical inherited neuropathy. Neurology. 1983;33(3):357-67.

18. Malcangio M, Bowery NG. Calcitonin gene-related peptide content, basal outflow and electrically-evoked release from monoarthritic rat spinal cord in vitro. Pain. 1996;66(2-3):351-8.

19. Brooks JW, Thompson SW, Rice AS, Malcangio M. (S)-AMPA inhibits electrically evoked calcitonin gene-related peptide (CGRP) release from the rat dorsal horn: reversal by cannabinoid receptor antagonist SR141716A. Neurosci Lett. 2004;372(1-2):85-8.

20. Hao H-w, Li L-m, Ma B-z, Chen Z-y, Liu F-j, Xue L, et al. A Programmable and Implantable Neuro-stimulator. Space Medicine and Medical Engineering. 2008;21(2):147-51.

21. Liu X, Demosthenous A, Donaldson N. Implantable stimulator failures: Causes, outcomes, and solutions. Conference Proceeding: Annual International Conference of the IEEEE Engineering in Medicine & Biology Society 2007: 5787-90. 2007.

22. McCarter GC, Reichling DB, Levine JD. Mechanical transduction by rat dorsal root ganglion neurons in vitro. Neurosci Lett. 1999;273(3):179-82.

23. Kanis JA, Melton LJ, Christiansen C, Johnston CC, Khaltaev N. The diagnosis of osteoporosis. J Bone Miner Res. 1994;9(8):1137-41.

24. Carter DR, Bouxsein ML, Marcus R. New approaches for interpreting projected bone densitometry data. J Bone Miner Res. 1992;7(2):137-45.

25. Marcus R. Fundamentals of Osteoporosis. Elsevier/Academic Press. 2010.

26. Bronckers AL, Gay S, Dimuzio MT, Butler WT. Immunolocalization of gamma-carboxyglutamic acid-containing proteins in developing molar tooth germs of the rat. Coll Relat Res. 1985;5(1):17-22.

27. Malone JD, Teitelbaum SL, Griffin GL, Senior RM, Kahn AJ. Recruitment of osteoclast precursors by purified bone matrix constituents. J Cell Biol. 1982;92(1):227-30.

28. Mundy GR, Poser JW. Chemotactic activity of the gamma-carboxyglutamic acid containing protein in bone. Calcif Tissue Int. 1983;35(2):164-8.

29. Lucas PA, Price PA, Caplan AI. Chemotactic response of mesenchymal cells, fibroblasts and osteoblast-like cells to bone Gla protein. Bone. 1988;9(5):319-23.

30. Price PA, Williamson MK, Lothringer JW. Origin of the vitamin K-dependent bone protein found in plasma and its clearance by kidney and bone. J Biol Chem. 1981;256(24):12760-6.

31. Brown JP, Delmas PD, Malaval L, Edouard C, Chapuy MC, Meunier PJ. Serum bone Gla-protein: a specific marker for bone formation in postmenopausal osteoporosis. Lancet. 1984;1(8386):1091-3.

32. Termine JD, Kleinman HK, Whitson SW, Conn KM, McGarvey ML, Martin GR. Osteonectin, a bone-specific protein linking mineral to collagen. Cell. 1981;26(1 Pt 1):99-105.

33. Otsuka K, Yao KL, Wasi S, Tung PS, Aubin JE, Sodek J, et al. Biosynthesis of osteonectin by fetal porcine calvarial cells in vitro. J Biol Chem. 1984;259(15):9805-12.

34. Maurer P, Mayer U, Bruch M, Jenö P, Mann K, Landwehr R, et al. High-affinity and low-affinity calcium binding and stability of the multidomain extracellular 40-kDa basement membrane glycoprotein (BM-40/SPARC/osteonectin). Eur J Biochem. 1992;205(1):233-40.

35. Bianco P, Silvestrini G, Termine JD, Bonucci E. Immunohistochemical localization of osteonectin in developing human and calf bone using monoclonal antibodies. Calcif Tissue Int. 1988;43(3):155-61.

36. Funk SE, Sage EH. The Ca2(+)-binding glycoprotein SPARC modulates cell cycle progression in bovine aortic endothelial cells. Proc Natl Acad Sci U S A. 1991;88(7):2648-52.

37. Lane TF, Sage EH. Functional mapping of SPARC: peptides from two distinct Ca+(+)-binding sites modulate cell shape. J Cell Biol. 1990;111(6 Pt 2):3065-76.

38. Riggs LB, Melton JL. Osteoporosis: etiology, diagnosis, and management. Lippincott-Raven. 1995;2nd Edition.

39. Butler WT. The nature and significance of osteopontin. Connect Tissue Res. 1989;23(2-3):123-36.

40. Kasugai S, Todescan R, Nagata T, Yao KL, Butler WT, Sodek J. Expression of bone matrix proteins associated with mineralized tissue formation by adult rat bone marrow cells in vitro: inductive effects of dexamethasone on the osteoblastic phenotype. J Cell Physiol. 1991;147(1):111-20.

41. Reinholt FP, Hultenby K, Oldberg A, Heinegård D. Osteopontin--a possible anchor of osteoclasts to bone. Proc Natl Acad Sci U S A. 1990;87(12):4473-5.

42. Helfrich MH, Nesbitt SA, Dorey EL, Horton MA. Rat osteoclasts adhere to a wide range of RGD (Arg-Gly-Asp) peptide-containing proteins, including the bone sialoproteins and fibronectin, via a beta 3 integrin. J Bone Miner Res. 1992;7(3):335-43.

43. Yoon K, Buenaga R, Rodan GA. Tissue specificity and developmental expression of rat osteopontin. Biochem Biophys Res Commun. 1987;148(3):1129-36.

44. McKee MD, Farach-Carson MC, Butler WT, Hauschka PV, Nanci A. Ultrastructural immunolocalization of noncollagenous (osteopontin and osteocalcin) and plasma (albumin and alpha 2HS-glycoprotein) proteins in rat bone. J Bone Miner Res. 1993;8(4):485-96.

45. van der Plas A, Aarden EM, Feijen JH, de Boer AH, Wiltink A, Alblas MJ, et al. Characteristics and properties of osteocytes in culture. J Bone Miner Res. 1994;9(11):1697-704.

46. Khosla S, Riggs BL, Atkinson EJ, Oberg AL, McDaniel LJ, Holets M, et al. Effects of sex and age on bone microstructure at the ultradistal radius: a population-based noninvasive in vivo assessment. J Bone Miner Res. 2006;21(1):124-31.

47. Kobayashi T, Kronenberg H. Minireview: transcriptional regulation in development of bone. Endocrinology. 2005;146(3):1012-7.

48. Chen S, Feng J, Zhang H, Jia M, Shen Y, Zong Z. Key role for the transcriptional factor, osterix, in spine development. Spine J. 2013.

49. Athanasou NA. Colour atlas of bone, joint and soft tissue pathology. Oxford University Press. 1999.

50. Roodman GD. Advances in bone biology: the osteoclast. Endocr Rev. 1996;17(4):308-32.

51. Kerby JA, Hattersley G, Collins DA, Chambers TJ. Derivation of osteoclasts from hematopoietic colony-forming cells in culture. J Bone Miner Res. 1992;7(3):353-62.

52. Blair HC, Schlesinger PH, Ross FP, Teitelbaum SL. Recent advances toward understanding osteoclast physiology. Clin Orthop Relat Res. 1993(294):7-22.

53. Vigorita VJ. Orthopaedic Pathology. Lippincott-Raven 1999.

54. BACHRA BN, TRAUTZ OR, McCONNELL D, FRAJOLA WJ, DEAMER DW. Carbonic anhydrase and the precipitation of apatite. Science. 1962;137(3527):337-8.

55. Ou-Yang H, Paschalis EP, Mayo WE, Boskey AL, Mendelsohn R. Infrared microscopic imaging of bone: spatial distribution of CO3(2-). J Bone Miner Res. 2001;16(5):893-900.

56. Carter DR, Hayes WC. The compressive behavior of bone as a two-phase porous structure. J Bone Joint Surg Am. 1977;59(7):954-62.

57. Morgan EF, Keaveny TM. Dependence of yield strain of human trabecular bone on anatomic site. J Biomech. 2001;34(5):569-77.

58. Howard A. Coding for bone diseases. F*or The Record.* 2011;23(9).

59. Rutherford O. The Role of Exercise in Prevention of Osteoporosis. P*hysiotherapy.* 1990;76(9):522-6.

60. Milliken LA, Wilhelmy J, Martin CJ, Finkenthal N, Cussler E, Metcalfe L, et al. Depressive symptoms and changes in body weight exert independent and site-specific effects on bone in postmenopausal women exercising for 1 year. J Gerontol A Biol Sci Med Sci. 2006;61(5):488-94.

61. Chan K, Qin L, Lau M, Woo J, Au S, Choy W, et al. A randomized, prospective study of the effects of Tai Chi Chun exercise on bone mineral density in postmenopausal women. Arch Phys Med Rehabil. 2004;85(5):717-22.

62. Feskanich D, Willett W, Colditz G. Walking and leisure-time activity and risk of hip fracture in postmenopausal women. JAMA. 2002;288(18):2300-6. doi: joc20730 [pii]. PubMed PMID: 12425707.

63. Robling AG, Castillo AB, Turner CH. Biomechanical and molecular regulation of bone remodeling. Annu Rev Biomed Eng. 2006;8:455-98.

64. Rittweger J, Simunic B, Bilancio G, De Santo NG, Cirillo M, Biolo G, et al. Bone loss in the lower leg during 35 days of bed rest is predominantly from the cortical compartment. Bone. 2009;44(4):612-8.

65. Rittweger J, Frost HM, Schiessl H, Ohshima H, Alkner B, Tesch P, et al. Muscle atrophy and bone loss after 90 days' bed rest and the effects of flywheel resistive exercise and pamidronate: results from the LTBR study. Bone. 2005;36(6):1019-29.

66. Rittweger J, Beller G, Armbrecht G, Mulder E, Buehring B, Gast U, et al. Prevention of bone loss during 56 days of strict bed rest by side-alternating resistive vibration exercise. Bone. 2010;46(1):137-47.

67. Garland DE, Stewart CA, Adkins RH, Hu SS, Rosen C, Liotta FJ, et al. Osteoporosis after spinal cord injury. J Orthop Res. 1992;10(3):371-8.

68. Kiratli BJ, Smith AE, Nauenberg T, Kallfelz CF, Perkash I. Bone mineral and geometric changes through the femur with immobilization due to spinal cord injury. J Rehabil Res Dev. 2000;37(2):225-33.

69. Smith EM, Comiskey CM, Carroll AM. A study of bone mineral density in adults with disability. Arch Phys Med Rehabil. 2009;90(7):1127-35.

70. Collet P, Uebelhart D, Vico L, Moro L, Hartmann D, Roth M, et al. Effects of 1- and 6-month spaceflight on bone mass and biochemistry in two humans. Bone. 1997;20(6):547-51.

71. Vico L, Collet P, Guignandon A, Lafage-Proust MH, Thomas T, Rehaillia M, et al. Effects of long-term microgravity exposure on cancellous and cortical weight-bearing bones of cosmonauts. Lancet. 2000;355(9215):1607-11.

72. Raisz L, Bilezikian J, Martin T. Pathophysiology of Osteoporosis. Pri*nciples of Bone Biology (Third Edition). 2*: Elsevier; 2008. p. 1635-47.

73. Ralston S. Genetic Determinants of Bone Mass and Osteoporotic Fracture. Principles of Bone Biology (Third Edition). 2: Elsevier; 2008. p. 1611-34.

74. Martin T, Rodan G. Coupling of Bone Resorption and Formation during Bone Remodeling. Osteoporosis (Second Edition)2001. p. 361-71.

75. Narducci P, Nicolin V. Differentiation of activated monocytes into osteoclast-like cells on a hydroxyapatite substrate: an in vitro study. Ann Anat. 2009;191(4):349-55.

76. Baron R, Neff L, Vignery A. Differentiation and functional characteristics of osteoclasts. Bone. 1985;6(5):414.

77. Horne W, Duong L, Sanjay A, Baron R. Regulating Bone Resorption: Targeting Integrins, Calcitonin Receptor, and Cathepsin K. Principles of Bone Biology (Third Edition): Elsevier; 2008. p. 221-36.

78. Khosla S. Minireview: the OPG/RANKL/RANK system. Endocrinology. 2001;142(12):5050-5.

79. Kimble RB, Matayoshi AB, Vannice JL, Kung VT, Williams C, Pacifici R. Simultaneous block of interleukin-1 and tumor necrosis factor is required to completely prevent bone loss in the early postovariectomy period. Endocrinology. 1995;136(7):3054-61.

80. Ammann P, Rizzoli R, Bonjour JP, Bourrin S, Meyer JM, Vassalli P, et al. Transgenic mice expressing soluble tumor necrosis factor-receptor are protected against bone loss caused by estrogen deficiency. J Clin Invest. 1997;99(7):1699-703.

81. Hughes DE, Dai A, Tiffee JC, Li HH, Mundy GR, Boyce BF. Estrogen promotes apoptosis of murine osteoclasts mediated by TGF-beta. Nat Med. 1996;2(10):1132-6.

82. Komori T, Yagi H, Nomura S, Yamaguchi A, Sasaki K, Deguchi K, et al. Targeted disruption of Cbfa1 results in a complete lack of bone formation owing to maturational arrest of osteoblasts. Cell. 1997;89(5):755-64.

83. Otto F, Thornell AP, Crompton T, Denzel A, Gilmour KC, Rosewell IR, et al. Cbfa1, a candidate gene for cleidocranial dysplasia syndrome, is essential for osteoblast differentiation and bone development. Cell. 1997;89(5):765-71.

84. D'Ippolito G, Schiller PC, Ricordi C, Roos BA, Howard GA. Age-related osteogenic potential of mesenchymal stromal stem cells from human vertebral bone marrow. J Bone Miner Res. 1999;14(7):1115-22.

85. Rosen CJ. Insulin-like growth factor I and bone mineral density: experience from animal models and human observational studies. Best Pract Res Clin Endocrinol Metab. 2004;18(3):423-35.

86. Sakata T, Wang Y, Halloran BP, Elalieh HZ, Cao J, Bikle DD. Skeletal unloading induces resistance to insulin-like growth factor-I (IGF-I) by inhibiting activation of the IGF-I signaling pathways. J Bone Miner Res. 2004;19(3):436-46.

87. Bikle DD, Sakata T, Halloran BP. The impact of skeletal unloading on bone formation. Gravit Space Biol Bull. 2003;16(2):45-54.

88. Lau RY, Guo X. A review on current osteoporosis research: with special focus on disuse bone loss. J Osteoporos. 2011;2011:293808.

89. Fleisch H, Russell RG, Straumann F. Effect of pyrophosphate on hydroxyapatite and its implications in calcium homeostasis. Nature. 1966;212(5065):901-3.

90. Barnett B, Strickland L. Structure of disodium dihydrogen 1-hydroxyethyldiene-diphosphonate tetrahydrate: A bone growth regulator. Acta Crystallographica Section B. 1979;35:1212-4.

91. Leu CT, Luegmayr E, Freedman LP, Rodan GA, Reszka AA. Relative binding affinities of bisphosphonates for human bone and relationship to antiresorptive efficacy. Bone. 2006;38(5):628-36.

92. Fleisch H. Bisphosphonates: mechanisms of action. Endocr Rev. 1998;19(1):80-100.

93. Cosman F, Nieves J, Walliser J, Lindsay R. Postmenopausal osteoporosis: patient choices and outcomes. Maturitas. 1995;22(2):137-43.

94. Davis S, Sachdeva A, Goeckeritz B, Oliver A. Approved treatments for osteoporosis and what's in the pipeline. Drug Benefit Trends. 2010;22(4):121-4.

95. Coetzee M, Kruger MC. Osteoprotegerin-receptor activator of nuclear factor-kappaB ligand ratio: a new approach to osteoporosis treatment? South Med J. 2004;97(5):506-11.

96. Poole KE, Reeve J. Parathyroid hormone - a bone anabolic and catabolic agent. Curr Opin Pharmacol. 2005;5(6):612-7.

97. Kearns AE, Khosla S, Kostenuik PJ. Receptor activator of nuclear factor kappaB ligand and osteoprotegerin regulation of bone remodeling in health and disease. Endocr Rev. 2008;29(2):155-92.

98. Reeve J, Hesp R, Williams D, Hulme P, Klenerman L, Zanelli JM, et al. Anabolic effect of low doses of a fragment of human parathyroid hormone on the skeleton in postmenopausal osteoporosis. Lancet. 1976;1(7968):1035-8.

99. Cranney A, Papaioannou A, Zytaruk N, Hanley D, Adachi J, Goltzman D, et al. Parathyroid hormone for the treatment of osteoporosis: a systematic review. CMAJ. 2006;175(1):52-9.

100. Cummings SR, San Martin J, McClung MR, Siris ES, Eastell R, Reid IR, et al. Denosumab for prevention of fractures in postmenopausal women with osteoporosis. N Engl J Med. 2009;361(8):756-65.

101. Perrone M. FDA clears Amgen's bone-strengthening drug Prolia. BioScience Technology. 2010.

102. Davey RA, Findlay DM. Calcitonin: physiology or fantasy? J Bone Miner Res. 2013;28(5):973-9.

103. Chambers TJ, Magnus CJ. Calcitonin alters behaviour of isolated osteoclasts. J Pathol. 1982;136(1):27-39.

104. Downs RW, Bell NH, Ettinger MP, Walsh BW, Favus MJ, Mako B, et al. Comparison of alendronate and intranasal calcitonin for treatment of osteoporosis in postmenopausal women. J Clin Endocrinol Metab. 2000;85(5):1783-8.

105. Das S, Crockett JC. Osteoporosis - a current view of pharmacological prevention and treatment. Drug Des Devel Ther. 2013;7:435-48.

106. Lin C, Jiang X, Dai Z, Guo X, Weng T, Wang J, et al. Sclerostin mediates bone response to mechanical unloading through antagonizing Wnt/beta-catenin signaling. J Bone Miner Res. 2009;24(10):1651-61.

107. Spatz JM, Ellman R, Cloutier AM, Louis L, van Vliet M, Suva LJ, et al. Sclerostin antibody inhibits skeletal deterioration due to reduced mechanical loading. J Bone Miner Res. 2013;28(4):865-74.

108. Saftig P, Hunziker E, Wehmeyer O, Jones S, Boyde A, Rommerskirch W, et al. Impaired osteoclastic bone resorption leads to osteopetrosis in cathepsin-K-deficient mice. Proc Natl Acad Sci U S A. 1998;95(23):13453-8.

109. Gelb BD, Shi GP, Chapman HA, Desnick RJ. Pycnodysostosis, a lysosomal disease caused by cathepsin K deficiency. Science. 1996;273(5279):1236-8. PubMed PMID: 8703060.

110. Gauthier JY, Chauret N, Cromlish W, Desmarais S, Duong lT, Falgueyret JP, et al. The discovery of odanacatib (MK-0822), a selective inhibitor of cathepsin K. Bioorg Med Chem Lett. 2008;18(3):923-8.

111. Pérez-Castrillón JL, Pinacho F, De Luis D, Lopez-Menendez M, Dueñas Laita A. Odanacatib, a new drug for the treatment of osteoporosis: review of the results in postmenopausal women. J Osteoporos. 2010;2010.

112. Mishima S. The effect of long-term pulsing electromagnetic field stimulation on experimental osteoporosis of rats. J UOEH. 1988;10(1):31-45.

113. Tabrah F, Hoffmeier M, Gilbert F, Batkin S, Bassett CA. Bone density changes in osteoporosis-prone women exposed to pulsed electromagnetic fields (PEMFs). J Bone Miner Res. 1990;5(5):437-42.

114. Zati A, Gnudi S, Mongiorgi R, Giardino R, Fini M, Valdrè G, et al. Effects of pulsed magnetic fields in the therapy of osteoporosis induced by ovariectomy in the rat. Boll Soc Ital Biol Sper. 1993;69(7-8):469-75.

115. Shen WW, Zhao JH. Pulsed electromagnetic fields stimulation affects BMD and local factor production of rats with disuse osteoporosis. Bioelectromagnetics. 2010;31(2):113-9.

116. Renno AC, de Moura FM, dos Santos NS, Tirico RP, Bossini PS, Parizotto NA. Effects of 830-nm laser, used in two doses, on biomechanical properties of osteopenic rat femora. Photomed Laser Surg. 2006;24(2):202-6.

117. Xu M, Deng T, Mo F, Deng B, Lam W, Deng P, et al. Low-intensity pulsed laser irradiation affects RANKL and OPG mRNA expression in rat calvarial cells. Photomed Laser Surg. 2009;27(2):309-15.

118. Flieger J, Karachalios T, Khaldi L, Raptou P, Lyritis G. Mechanical Stimulation in the Form of Vibration Prevents Postmenopausal Bone Loss in Ovariectomized Rats. Calcified T*issue International. 1998;63:5*10-4.

119. Oxlund BS, Ørtoft G, Andreassen TT, Oxlund H. Low-intensity, high-frequency vibration appears to prevent the decrease in strength of the femur and tibia associated with ovariectomy of adult rats. Bone. 2003;32(1):69-77.

120. Wu S, Kawahara Y, Manabe T, Ogawa K, Matsumoto M, Sasaki A, et al. Low-intensity pulsed ultrasound accelerates osteoblast differentiation and promotes bone formation in an osteoporosis rat model. Pathobiology. 2009;76(3):99-107.

121. McElhaney JH, Stalnaker R, Bullard R. Electric fields and bone loss of disuse. J Biomech. 1968;1(1):47-52.

122. Martin RB, Gutman W. The effect of electric fields on osteoporosis of disuse. Calcif Tissue Res. 1978;25(1):23-7.

123. Stein RB. Functional electrical stimulation after spinal cord injury. J Neurotrauma. 1999;16(8):713-7.

124. Creasey GH, Ho CH, Triolo RJ, Gater DR, DiMarco AF, Bogie KM, et al. Clinical applications of electrical stimulation after spinal cord injury. J Spinal Cord Med. 2004;27(4):365-75.

125. Clark JM, Jelbart M, Rischbieth H, Strayer J, Chatterton B, Schultz C, et al. Physiological effects of lower extremity functional electrical stimulation in early spinal cord injury: lack of efficacy to prevent bone loss. Spinal Cord. 2007;45(1):78-85.

126. Kundu B, Khare SK, Singh G. Role of polypeptides in the treatment and diagnosis of osteoporosis. Peptides. 1999;20(4):523-37.

127. Bevis PJ, Zaidi M, MacIntyre I. A dual effect of calcitonin gene-related peptide on plasma calcium levels in the chick. Biochem Biophys Res Commun. 1990;169(3):846-50.

128. Zhang WZ, Yu SF, Zheng LF. Effects of calcitonin gene-related peptide on bone resorption mediated by interleukin-1. Chin Med J (Engl). 1994;107(5):351-4.

129. Owan I, Ibaraki K. The role of calcitonin gene-related peptide (CGRP) in macrophages: the presence of functional receptors and effects on proliferation and differentiation into osteoclast-like cells. Bone Miner. 1994;24(2):151-64.

130. Garcia L, Pinçon-Raymond M, Romey G, Changeux JP, Lazdunski M, Rieger F. Induction of normal ultrastructure by CGRP treatment in dysgenic myotubes. FEBS Lett. 1990;263(1):147-52.

131. Changeux JP. Compartmentalized transcription of acetylcholine receptor genes during motor endplate epigenesis. New Biol. 1991;3(5):413-29.

132. Ballica R, Valentijn K, Khachatryan A, Guerder S, Kapadia S, Gundberg C, et al. Targeted expression of calcitonin gene-related peptide to osteoblasts increases bone density in mice. J Bone Miner Res. 1999;14(7):1067-74.

133. Yoo YM, Kwag JH, Kim KH, Kim CH. Effects of neuropeptides and mechanical loading on bone cell resorption in vitro. Int J Mol Sci. 2014;15(4):5874-83.

134. Valentijn K, Gutow AP, Troiano N, Gundberg C, Gilligan JP, Vignery A. Effects of calcitonin gene-related peptide on bone turnover in ovariectomized rats. Bone. 1997;21(3):269-74.

135. Malcangio M, Bowery NG. Calcitonin gene-related peptide content, basal outflow and electrically-evoked release from monoarthritic rat spinal cord in vitro. Pain. 1996;66(2-3):351-8.

136. Schaible HG, Freudenberger U, Neugebauer V, Stiller RU. Intraspinal release of immunoreactive calcitonin gene-related peptide during development of inflammation in the joint in vivo--a study with antibody microprobes in cat and rat. Neuroscience. 1994;62(4):1293-305.

137. Benemei S, Nicoletti P, Capone JG, Geppetti P. CGRP receptors in the control of pain and inflammation. Curr Opin Pharmacol. 2009;9(1):9-14.

138. Kondo T, Oshima T, Koseki J, Hattori T, Kase Y, Tomita T, et al. Effect of Rikkunshito on the expression of substance P and CGRP in dorsal root ganglion neurons and voluntary movement in rats with experimental reflux esophagitis. Neurogastroenterol Motil. 2014.

139. Yu D, Liu F, Liu M, Zhao X, Wang X, Li Y, et al. The inhibition of subchondral bone lesions significantly reversed the weight-bearing deficit and the overexpression of CGRP in DRG neurons, GFAP and Iba-1 in the spinal dorsal horn in the monosodium iodoacetate induced model of osteoarthritis pain. PLoS One. 2013;8(10):e77824.

140. Colman RJ, Lane MA, Binkley N, Wegner FH, Kemnitz JW. Skeletal effects of aging in male rhesus monkeys. Bone. 1999;24(1):17-23.

141. Umemura Y, Ishiko T, Tsujimoto H, Miura H, Mokushi N, Suzuki H. Effects of jump training on bone hypertrophy in young and old rats. Int J Sports Med. 1995;16(6):364-7. doi: 10.1055/s-2007-973021.

142. Willie BM, Birkhold AI, Razi H, Thiele T, Aido M, Kruck B, et al. Diminished response to in vivo mechanical loading in trabecular and not cortical bone in adulthood of female C57Bl/6 mice coincides with a reduction in deformation to load. Bone. 2013;55(2):335-46.

143. Morey-Holton ER, Globus RK. Hindlimb unloading rodent model: technical aspects. J Appl Physiol. 2002;92(4):1367-77.

144. Ren JC, Fan XL, Song XA, Zhao XH, Chen MX, Shi L. Prolonged hindlimb unloading leads to changes in electrophysiological properties of L5 dorsal root ganglion neurons in rats after 14 days. Muscle Nerve. 2012;45(1):65-9.

145. Zerath E, Canon F, Guezennec CY, Holy X, Renault S, André C. Electrical stimulation of leg muscles increases tibial trabecular bone formation in unloaded rats. J Appl Physiol. 1995;79(6):1889-94.

146. Qian X, Hao H, Ma B, Wen X, Hu C, Li L, et al. Programmable and implantable neurostimulator with novel stimulus waveforms for rat models. Electronics letters. 2012;48(17):1036-8.

147. Greene EC. Anatomy of the rat. Hafner. 1963.

148. Zhang JM, Homma Y, Ackerman WE, Brull SJ. Topical application of acidic bupivacaine to the lumbar ganglion induces mechanical hyperalgesia in the rat. Anesth Analg. 2001;93(2):466-71, 4th contents page.

149. Miocinovic S, Lempka SF, Russo GS, Maks CB, Butson CR, Sakaie KE, et al. Experimental and theoretical characterization of the voltage distribution generated by deep brain stimulation. Exp Neurol. 2009;216(1):166-76.

150. Kurtis MM, San Luciano M, Yu Q, Goodman RR, Ford B, Raymond D, et al. Clinical and neurophysiological improvement of SGCE myoclonus-dystonia with GPi deep brain stimulation. Clin Neurol Neurosurg. 2010;112(2):149-52.

151. Butson CR, McIntyre CC. Tissue and electrode capacitance reduce neural activation volumes during deep brain stimulation. Clin Neurophysiol. 2005;116(10):2490-500.

152. Nelson BR, Claes K, Todd V, Chaverra M, Lefcort F. NELL2 promotes motor and sensory neuron differentiation and stimulates mitogenesis in DRG in vivo. Dev Biol. 2004;270(2):322-35.

153. Sugama S, Fujita M, Hashimoto M, Conti B. Stress induced morphological microglial activation in the rodent brain: involvement of interleukin-18. Neuroscience. 2007;146(3):1388-99.

154. Florijn RJ, Slats J, Tanke HJ, Raap AK. Analysis of antifading reagents for fluorescence microscopy. Cytometry. 1995;19(2):177-82.

155. Reineke T, Jenni B, Abdou MT, Frigerio S, Zubler P, Moch H, et al. Ultrasonic decalcification offers new perspectives for rapid FISH, DNA, and RT-PCR analysis in bone marrow trephines. Am J Surg Pathol. 2006;30(7):892-6.

156. Nomura T, Aoyama M, Waguri-Nagaya Y, Goto Y, Suzuki M, Miyazawa K, et al. Tumor necrosis factor stimulates osteoclastogenesis from human bone marrow cells under hypoxic conditions. Exp Cell Res. 2013.

157. Bloomfield SA, Allen MR, Hogan HA, Delp MD. Site- and compartment-specific changes in bone with hindlimb unloading in mature adult rats. Bone. 2002;31(1):149-57.

158. Tuukkanen J, Koivukangas A, Jämsä T, Sundquist K, Mackay CA, Marks SC. Mineral density and bone strength are dissociated in long bones of rat osteopetrotic mutations. J Bone Miner Res. 2000;15(10):1905-11.

159. Utvåg SE, Grundnes O, Reikerås O. Graded exchange reaming and nailing of non-unions. Strength and mineralisation in rat femoral bone. Arch Orthop Trauma Surg. 1998;118(1-2):1-6.

160. Hildebrand T, Rüegsegger P. Quantification of Bone Microarchitecture with the Structure Model Index. Comput Methods Biomech Biomed Engin. 1997;1(1):15-23.

161. Bikson M, Rahman A, Datta A, Fregni F, Merabet L. High-resolution modeling assisted design of customized and individualized transcranial direct current stimulation protocols. Neuromodulation. 2012;15(4):306-15.

162. Tilton FE, Degioanni JJ, Schneider VS. Long-term follow-up of Skylab bone demineralization. Aviat Space Environ Med. 1980;51(11):1209-13.

163. Vico L, Novikov VE, Very JM, Alexandre C. Bone histomorphometric comparison of rat tibial metaphysis after 7-day tail suspension vs. 7-day spaceflight. Aviat Space Environ Med. 1991;62(1):26-31.

164. Vico L, Bourrin S, Genty C, Palle S, Alexandre C. Histomorphometric analyses of cancellous bone from COSMOS 2044 rats. J Appl Physiol. 1993;75(5):2203-8.

165. Ivanusic JJ. Size, neurochemistry, and segmental distribution of sensory neurons innervating the rat tibia. J Comp Neurol. 2009;517(3):276-83.

166. Offley SC, Guo TZ, Wei T, Clark JD, Vogel H, Lindsey DP, et al. Capsaicin-sensitive sensory neurons contribute to the maintenance of trabecular bone integrity. J Bone Miner Res. 2005;20(2):257-67.

167. Maayan C, Becker Y, Gesundheit B, Girgis SI. Calcitonin gene related peptide in familial dysautonomia. Neuropeptides. 2001;35(3-4):189-95. doi: 10.1054/npep.2001.0863.

168. Hukkanen M, Konttinen YT, Rees RG, Gibson SJ, Santavirta S, Polak JM. Innervation of bone from healthy and arthritic rats by substance P and calcitonin gene related peptide containing sensory fibers. J Rheumatol. 1992;19(8):1252-9.

169. Judex S, Carlson KJ. Is bone's response to mechanical signals dominated by gravitational loading? Med Sci Sports Exerc. 2009;41(11):2037-43.

170. Nakamura H, Aoki K, Masuda W, Alles N, Nagano K, Fukushima H, et al. Disruption of NF-κB1 prevents bone loss caused by mechanical unloading. J Bone Miner Res. 2013;28(6):1457-67.

171. Boudignon BM, Bikle DD, Kurimoto P, Elalieh H, Nishida S, Wang Y, et al. Insulin-like growth factor I stimulates recovery of bone lost after a period of skeletal unloading. J Appl Physiol (1985). 2007;103(1):125-31.

172. Kodama Y, Dimai HP, Wergedal J, Sheng M, Malpe R, Kutilek S, et al. Cortical tibial bone volume in two strains of mice: effects of sciatic neurectomy and genetic regulation of bone response to mechanical loading. Bone. 1999;25(2):183-90.

173. Squire M, Donahue LR, Rubin C, Judex S. Genetic variations that regulate bone morphology in the male mouse skeleton do not define its susceptibility to mechanical unloading. Bone. 2004;35(6):1353-60.

174. Dehority W, Halloran BP, Bikle DD, Curren T, Kostenuik PJ, Wronski TJ, et al. Bone and hormonal changes induced by skeletal unloading in the mature male rat. Am J Physiol. 1999;276(1 Pt 1):E62-9.

175. Halloran BP, Bikle DD, Wronski TJ, Globus RK, Levens MJ, Morey-Holton E. The role of 1,25-dihydroxyvitamin D in the inhibition of bone formation induced by skeletal unloading. Endocrinology. 1986;118(3):948-54.

176. Lueken SA, Arnaud SB, Taylor AK, Baylink DJ. Changes in markers of bone formation and resorption in a bed rest model of weightlessness. J Bone Miner Res. 1993;8(12):1433-8.

177. Vico L, Chappard D, Alexandre C, Palle S, Minaire P, Riffat G, et al. Effects of a 120 day period of bed-rest on bone mass and bone cell activities in man: attempts at countermeasure. Bone Miner. 1987;2(5):383-94.

178. David V, Lafage-Proust MH, Laroche N, Christian A, Ruegsegger P, Vico L. Two-week longitudinal survey of bone architecture alteration in the hindlimb-unloaded rat model of bone loss: sex differences. Am J Physiol Endocrinol Metab. 2006;290(3):E440-7.

179. Sakai A, Nakamura T. Changes in trabecular bone turnover and bone marrow cell development in tail-suspended mice. J Musculoskelet Neuronal Interact. 2001;1(4):387-92.

180. Basso N, Jia Y, Bellows CG, Heersche JN. The effect of reloading on bone volume, osteoblast number, and osteoprogenitor characteristics: studies in hind limb unloaded rats. Bone. 2005;37(3):370-8.

181. Tamma R, Colaianni G, Camerino C, Di Benedetto A, Greco G, Strippoli M, et al. Microgravity during spaceflight directly affects in vitro osteoclastogenesis and bone resorption. FASEB J. 2009;23(8):2549-54.

182. Vico L, Collet P, Guignandon A, Lafage-Proust MH, Thomas T, Rehaillia M, et al. Effects of long-term microgravity exposure on cancellous and cortical weight-bearing bones of cosmonauts. Lancet. 2000;355(9215):1607-11.

183. Bucaro MA, Zahm AM, Risbud MV, Ayyaswamy PS, Mukundakrishnan K, Steinbeck MJ, et al. The effect of simulated microgravity on osteoblasts is independent of the induction of apoptosis. J Cell Biochem. 2007;102(2):483-95.

184. Dai ZQ, Wang R, Ling SK, Wan YM, Li YH. Simulated microgravity inhibits the proliferation and osteogenesis of rat bone marrow mesenchymal stem cells. Cell Prolif. 2007;40(5):671-84.

185. Wang L, Shi X, Zhao R, Halloran BP, Clark DJ, Jacobs CR, et al. Calcitonin-gene-related peptide stimulates stromal cell osteogenic differentiation and inhibits RANKL induced NF-kappaB activation, osteoclastogenesis and bone resorption. Bone. 2010;46(5):1369-79.

186. Lecoq B, Potrel-Burgot C, Granier P, Sabatier JP, Marcelli C. Comparison of bone loss induced in female rats by hindlimb unloading, ovariectomy, or both. Joint Bone Spine. 2006;73(2):189-95.

187. Allen MR, Bloomfield SA. Hindlimb unloading has a greater effect on cortical compared with cancellous bone in mature female rats. J Appl Physiol. 2003;94(2):642-50.

188. Laib A, Barou O, Vico L, Lafage-Proust MH, Alexandre C, Rügsegger P. 3D micro-computed tomography of trabecular and cortical bone architecture with application to a rat model of immobilisation osteoporosis. Med Biol Eng Comput. 2000;38(3):326-32.

189. LeBlanc AD, Spector ER, Evans HJ, Sibonga JD. Skeletal responses to space flight and the bed rest analog: a review. J Musculoskelet Neuronal Interact. 2007;7(1):33-47.

190. Levine JP. Identification, diagnosis, and prevention of osteoporosis. Am J Manag Care. 2011;17 Suppl 6:S170-6.

191. Yang P, Jia B, Ding C, Wang Z, Qian A, Shang P. Whole-body vibration effects on bone before and after hind-limb unloading in rats. Aviat Space Environ Med. 2009;80(2):88-93.

192. Wu Y, Liu J, Guo H, Luo Q, Yu Z, Liao E, et al. Establishment of OPG Transgenic Mice and the Effect of OPG on Bone Microarchitecture. Int J Endocrinol. 2013;2013:125932.

193. Zuckerman-Levin N, Hochberg Z, Latzer Y. Bone health in eating disorders. Obes Rev. 2014;15(3):215-23.

194. Erez HB, Weller A, Vaisman N, Kreitler S. The relationship of depression, anxiety and stress with low bone mineral density in post-menopausal women. Arch Osteoporos. 2012;7(1-2):247-55.

195. Yu H, Watt H, Kesavan C, Johnson PJ, Wergedal JE, Mohan S. Lasting consequences of traumatic events on behavioral and skeletal parameters in a mouse model for post-traumatic stress disorder (PTSD). PLoS One. 2012;7(8):e42684.

196. Miller AH. Depression and immunity: a role for T cells? Brain Behav Immun. 2010;24(1):1-8.

197. Shelton RC, Miller AH. Eating ourselves to death (and despair): the contribution of adiposity and inflammation to depression. Prog Neurobiol. 2010;91(4):275-99.

198. Miller AH, Maletic V, Raison CL. Inflammation and its discontents: the role of cytokines in the pathophysiology of major depression. Biol Psychiatry. 2009;65(9):732-41.

199. Dantzer R. Cytokine, sickness behavior, and depression. Immunol Allergy Clin North Am. 2009;29(2):247-64.

200. Capuron L, Fornwalt FB, Knight BT, Harvey PD, Ninan PT, Miller AH. Does cytokine-induced depression differ from idiopathic major depression in medically healthy individuals? J Affect Disord. 2009;119(1-3):181-5.

201. Campbell GM, Bernhardt R, Scharnweber D, Boyd SK. The bone architecture is enhanced with combined PTH and alendronate treatment compared to monotherapy while maintaining the state of surface mineralization in the OVX rat. Bone. 2011;49(2):225-32.

202. Qian X, Hao H, Ma B, Wen X, Li L. Study on DBS device for small animals. Conf Proc IEEE Eng Med Biol Soc. 2011;2011:6773-6.

203. Krouchev NI, Danner SM, Vinet A, Rattay F, Sawan M. Energy-optimal electrical-stimulation pulses shaped by the least-action principle. PLoS One. 2014;9(3):e90480.

204. Jones KB, Mollano AV, Morcuende JA, Cooper RR, Saltzman CL. Bone and brain: a review of neural, hormonal, and musculoskeletal connections. Iowa Orthop J. 2004;24:123-32.

205. Rajaee SS, Bae HW, Kanim LE, Delamarter RB. Spinal fusion in the United States: analysis of trends from 1998 to 2008. Spine (Phila Pa 1976). 2012;37(1):67-76.

206. Ma Y, Passias P, Gaber-Baylis LK, Girardi FP, Memtsoudis SG. Comparative in-hospital morbidity and mortality after revision versus primary thoracic and lumbar spine fusion. Spine J. 2010;10(10):881-9.

207. Reid JJ, Johnson JS, Wang JC. Challenges to bone formation in spinal fusion. J Biomech. 2011;44(2):213-20.

208. Cooper GS, Kou TD. Risk of cancer after lumbar fusion surgery with recombinant human bone morphogenic protein-2 (rh-BMP-2). Spine (Phila Pa 1976). 2013;38(21):1862-8.

209. Zaidi M, Chambers TJ, Bevis PJ, Beacham JL, Gaines Das RE, MacIntyre I. Effects of peptides from the calcitonin genes on bone and bone cells. Q J Exp Physiol. 1988;73(4):471-85.

210. Tian G, Zhang G, Tan YH. Calcitonin gene-related peptide stimulates BMP-2 expression and the differentiation of human osteoblast-like cells in vitro. Acta Pharmacol Sin. 2013;34(11):1467-74. doi: 10.1038/aps.2013.41.

211. Bjurholm A, Kreicbergs A, Brodin E, Schultzberg M. Substance P- and CGRP-immunoreactive nerves in bone. Peptides. 1988;9(1):165-71.

212. Hill EL, Elde R. Distribution of CGRP-, VIP-, D beta H-, SP-, and NPY-immunoreactive nerves in the periosteum of the rat. Cell Tissue Res. 1991;264(3):469-80.

213. Irie K, Hara-Irie F, Ozawa H, Yajima T. Calcitonin gene-related peptide (CGRP)-containing nerve fibers in bone tissue and their involvement in bone remodeling. Microsc Res Tech. 2002;58(2):85-90.

214. Madsen JE, Hukkanen M, Aspenberg P, Polak J, Nordsletten L. Time-dependent sensory nerve ingrowth into a bone conduction chamber. Acta Orthop Scand. 2000;71(1):74-9.

215. Lam WL, Guo X, Leung KS, Kwong KS. The role of the sensory nerve response in ultrasound accelerated fracture repair. J Bone Joint Surg Br. 2012;94(10):1433-8.

216. Lau Y, Li L, Hao H. Design and implantation of implantable micro-electrical stimulator for osteoporosis prevention. Poster No. 0695. in Orthopaedic Reseach Society 2013 Annual Meeting. 26-28 Jannuary, 2013;San Antonio, Texas, USA.

217. Grauer JN, Bomback DA, Lugo R, Troiano NW, Patel TC, Friedlaender GE. Posterolateral lumbar fusions in athymic rats: characterization of a model. Spine J. 2004;4(3):281-6. doi: 10.1016/j.spinee.2003.10.001.

218. Wang JC, Kanim LE, Yoo S, Campbell PA, Berk AJ, Lieberman JR. Effect of regional gene therapy with bone morphogenetic protein-2-producing bone marrow cells on spinal fusion in rats. J Bone Joint Surg Am. 2003;85-A(5):905-11.

219. Shi D, Yang B, Tae G. Enhanced spinal fusion using a biodegradable porous mesh cotainer in a rat posterolateral spinal fusion model. . Spine J 2013 (In press).

220. Griffin M, Bayat A. Electrical stimulation in bone healing: critical analysis by evaluating levels of evidence. Eplasty. 2011;11:e34.

221. Tian NF, Wu YS, Zhang XL, Mao FM, Xu HZ, Chi YL. Efficacy of electrical stimulation for spinal fusion: a meta-analysis of fusion rate. Spine J. 2013. doi: 10.1016/j.spinee.2013.06.056.

222. Mooney V. A randomized double-blind prospective study of the efficacy of pulsed electromagnetic fields for interbody lumbar fusions. Spine (Phila Pa 1976). 1990;15(7):708-12.

223. Kahanovitz N. Electrical stimulation of spinal fusion: a scientific and clinical update. Spine J. 2002;2(2):145-50.

224. Kawase T, Howard GA, Roos BA, Burns DM. Diverse actions of calcitonin gene-related peptide on intracellular free Ca2+ concentrations in UMR 106 osteoblastic cells. Bone. 1995;16(4 Suppl):379S-84S.

225. Kawase T, Okuda K, Burns DM. Immature human osteoblastic MG63 cells predominantly express a subtype 1-like CGRP receptor that inactivates extracellular signal response kinase by a cAMP-dependent mechanism. Eur J Pharmacol. 2003;470(3):125-37.

226. Wang YS, Wang YH, Zhao GQ, Li YB. Osteogenic potential of human calcitonin gene-related peptide alpha gene-modified bone marrow mesenchymal stem cells. Chin Med J (Engl). 2011;124(23):3976-81.

227. Seagrove LC, Suzuki R, Dickenson AH. Electrophysiological characterisations of rat lamina I dorsal horn neurones and the involvement of excitatory amino acid receptors. Pain. 2004;108(1-2):76-87.

228. Deer TR, Grigsby E, Weiner RL, Wilcosky B, Kramer JM. A prospective study of dorsal root ganglion stimulation for the relief of chronic pain. Neuromodulation. 2013;16(1):67-71

229. Ding L, Tao S, Yi C. Transcutaneous electrical nerve stimulation (TENS) improves the diabetic cytopathy (DCP) via up-regulation of CGRP and cAMP. Plos One. 2013;8:e57477.